ISSN 2667-9787
ISSN 2720-8087 (online)
Reviewed Scientific Journal

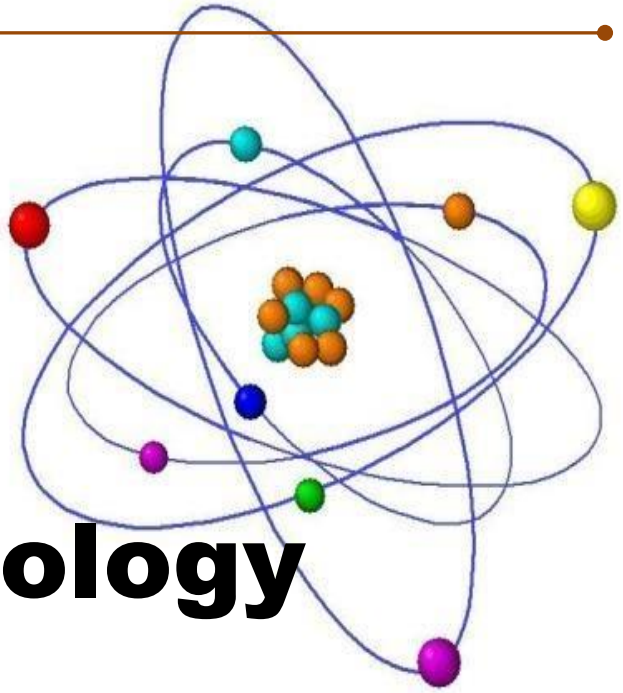

Radiobiology and Radiation safety

The journal "Radiobiology and Radiation Safety" publishes scientific articles reflecting the results of studies of radiation and nuclear effects and various issues related to radiation safety problems

Vol.5,№6
2025

Editorial office: 14 Levan Gotua St, Rooms-913; 931, Tbilisi, Georgia, 0160

Tel: (+995) 032 237-03-00/911. **Mob**. (+99532)555-10-17-90

E-mail: radiobiologia2020@gmail.com

Website:https://radiobiology.ge

TABLE OF CONTENTS

THE EFFECT OF IONIZING RADIATION ON HIPPOCAMPAL NA,K-ATPASE ACTIVITY

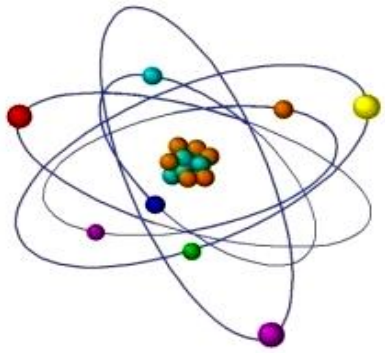

[1,2]Gvanca Chkadua*., [1]Eka Nozadze., [1]LeilaTsakadze., [1]Lia Shioshvili, [1]Nana Arutinova., [1]Marine Leladze., [1]Sophio Dzneladze

[1]Laboratory of Membranology, Iv.Beritashvili Center of Experimental Biomedicine, Georgia
[2]Georgian National University

https://doi.org/10.63465/rrs520258976 *Correspondingauthor: gvantsas@hotmail.com

ABSTRACT: *Ionizing radiation (IR) exposure initiates the rapid generation of reactive oxygen species (ROS), leading to oxidative stress and cellular damage. While ROS serve as critical signaling molecules under physiological conditions, excessive levels can disrupt membrane integrity via lipid peroxidation and impair membrane-bound enzymes such as Na^+,K^+-ATPase. In this context, our study investigates the dual effect of IR-induced ROS and endogenous ouabain on Na^+,K^+-ATPase activity. We demonstrate that different doses of IR (1 Gy and 5 Gy) initially enhance enzyme activity through reversible redox modification of thiol groups of the Na^+,K^+-ATPase complex. Simultaneously, IR stimulates the release of endogenous ouabain, which not only binds to Na^+,K^+-ATPase but also activates intracellular signaling cascades that further augment mitochondrial ROS production. This positive feedback loop—termed the "Na^+,K^+-ATPase oxidant amplification loop"—ultimately leads to irreversible oxidative modifications and enzyme inhibition under sustained oxidative stress. These findings highlight a redox-dependent biphasic regulation of Na^+,K^+-ATPase in response to IR, implicating both reversible and irreversible oxidative mechanisms in radiation-induced cellular effects.*

Keywords: Na,K-ATPase, gamma irradiation, enzyme activity, thiol groups

INTRODUCTION

Oxidative stress describes a physiological condition in which the balance between the production of reactive oxygen species (ROS) and the body's antioxidant defenses is disrupted, leading to an excess of ROS. This state reflects an imbalance in cellular oxidation processes, where tissues experience heightened exposure to molecular oxygen or its reactive derivatives. Normally, oxygen is used in metabolism to produce energy, generating byproducts like superoxide, hydrogen peroxide, and hydroxyl radicals. When ROS levels exceed the antioxidant defenses, they can damage lipids, proteins, and DNA, potentially leading to cell dysfunction or death. This stress plays a key role in aging and chronic diseases like Parkinson's, atherosclerosis, cancer, diabetes, and eye disorders [1-3]. Diets rich in antioxidants (e.g., polyphenols, vitamin C, carotenoids) are linked to lower disease risk. Measuring oxidative damage and total antioxidant capacity helps us understand how oxidative stress contributes to pathology and how dietary antioxidants might protect against it [4 -5]. To study oxidative stress, researchers often measure (i) free radicals, (ii) damage they cause to lipids, proteins, or DNA,

and (iii) antioxidant levels or enzyme activity. Free radicals are unstable molecules naturally formed during metabolism and immune responses. While they play beneficial roles, excessive levels can damage cells by oxidizing lipids, proteins, and DNA [6]. The body counters this with antioxidant defenses, including enzymes (like SOD, catalase) and molecules (like vitamins C and E). An imbalance between radicals and antioxidants contributes to aging and diseases such as cancer and Parkinson's.

Free radicals come from two main sources Endogenous: Formed inside the body during normal metabolic processes, enzyme activity, or metal ion reactions Exogenous: Generated from environmental exposures such as radiation, heavy metals, smoking, pollution, and poor diet. Recent studies have focused on how ionizing radiation affects the brain, suggesting that the damage involves a mix of vascular and neurodegenerative changes [6-7]. In rats, whole-brain irradiation (25 Gy) led to cognitive decline and brain tissue changes one year later, resembling accelerated brain aging seen in diseases like Alzheimer's [7]. Notably, cognitive issues have also been observed in patients receiving radiotherapy outside the brain, such as breast cancer patients, even months after treatment [8]. Radiation effects have been widely studied in whole-body or targeted treatments, but less is known about changes in distant tissues. Studies have shown that irradiating the mediastinal area in rats caused right ventricular hypertrophy and reduced cardiac Na^+,K^+-ATPase activity [9], essential for sodium balance. The enzyme's function also declined in the kidneys, likely due to increased oxidative stress in the blood [10]. Since Na^+,K^+-ATPase is sensitive to oxidative stress, its impaired activity may result from changes in its sodium and ATP binding sites. Brain tissue is especially vulnerable to ROS due to its high oxidative metabolism, abundance of polyunsaturated fatty acids in membrane lipids, presence of iron ions, and relatively low antioxidant enzyme capacity [12-13]. Studies have shown that both lethal and sublethal doses of radiation can affect sodium-potassium transport systems in neural and glial cell-enriched fractions as well as in cortical slices from rats [14]. Na^+,K^+-ATPase is essential for maintaining ion balance across the plasma membrane, supporting the resting membrane potential crucial for muscle function [15]. Skeletal muscles, which contain the most immense amount of this enzyme, rely heavily on it for normal excitability and contraction. Among its isoforms, α2 is dominant in adult muscle and adapts to activity, helping resist fatigue. This isoform is found mainly in transverse tubules and at neuromuscular junctions. Na^+,K^+-ATPase also binds cardiotonic steroids like ouabain, which at low physiological levels may act as a hormone [16-18]. Ouabain, a plant-derived cardiotonic steroid, is believed to be synthesized naturally in the adrenal cortex and hypothalamus [19]. Endogenous ouabain typically circulates at subnanomolar levels, though its concentration can rise under different physiological and pathological conditions [20-22]. While high levels of ouabain are toxic, low concentrations show potential in regulating inflammation, blood pressure, and neural activity [23-24]. This study examined whether whole-body irradiation in mice alters Na^+,K^+-ATPase activity in the brain, specifically in the hippocampus.

MATERIALS AND METHODS

Experiments were conducted on age- and weight-matched male and female mice (10 weeks old). The animals underwent a single session of total-body ionizing radiation (IR). Two experimental groups were established: one group (n = 6) received a 1 Gy dose, while another

group (n = 6) was exposed to a 5 Gy dose. A third group, which did not undergo radiation exposure, served as the control. Post-irradiation, animals were housed separately based on group and monitored.

Hippocampal tissue was extracted from each group and utilized for analysis. Tissue homogenization followed the protocol recommended by Gislaine Rezin [25]. The activity of Na^+,K^+-ATPase was assessed by quantifying the ouabain-sensitive component of total ATPase activity. The assay for total ATPase activity utilized an incubation medium comprising 140 mM NaCl, 5 mM KCl, and 50 mM Tris-HCl buffer (pH 7.7). Mg-ATPase activity was evaluated in the presence of 1 mM ouabain using a medium containing 145 mM KCl and 50 mM Tris-HCl buffer (pH 7.7). The difference between the two assays was used to calculate the activity of the Na,K-ATPase. Protein concentration was standardized to 0.014 mg/mL for all enzymatic assays.

Incubations were carried out at 37°C for 15 minutes. Enzymatic activity was determined based on the hydrolysis of ATP, with the amount of inorganic phosphate (Pi) released expressed per mg protein per hour. The liberated Pi was quantified according to the method described by Chan et al. [26]. Na,K^+-ATPase activity was calculated in nanomoles of Pi released per minute per mg of protein. Protein concentrations were measured using the Lowry method [27], employing bovine serum albumin as the reference standard.

All experimental data were statistically analyzed. Results are reported as arithmetic means ± standard error (SE). Statistical significance between two groups was determined using an unpaired, two-tailed Student's t-test, with p-values less than 0.05 considered significant.

No animals showed signs of distress prior to decapitation. All procedures were reviewed and approved by the Institutional Animal Care and Use Committee of the Ivane Beritashvili Center of Experimental Biomedicine.

RESULTS

Our previous study has shown [28], that IR influences ATPase activity from brain synaptic membranes. This study focused on hippocampal fraction and investigated Na,K-ATPase activity after one and two weeks of total-body IR (1Gy and 5 Gy). Fig.1 demonstrates the effect of 1Gy irradiation on Na,K-ATPase activity after 1 and 2 weeks. From Fig.1, it is clear that 1Gy irradiation increases enzyme activity after 1 week by 45%. No statistical changes occur after 2 weeks ($P>0.05$) compared with one week group, and activity remains elevated by 36% compared to the control group (Fig.1). For 5Gy irradiated groups after 1 week Na,K-ATPase activity is increased by 129% compared to the control group, and after the 2-week activity is decreased compared to 1week group by 19% but still is elevated by 87% compared to the control group (Fig.2). Various external and internal factors can lead to specific alterations in the structure and function of Na^+,K^+-ATPase, resulting in changes to its enzymatic activity [29-32]. Among these factors are ROS, a class of chemically reactive molecules formed through the incomplete reduction of molecular oxygen. These free radicals have the potential to change Na,K-ATPase activity [29]. IR possesses enough energy to remove electrons from atoms, resulting in ionization and facilitating the production of ROS. ROS primarily targets cysteine (Cys) residues within proteins, which are key sites for diverse thiol-based modifications. To test whether IR affects Cys within the enzyme, we have studied the influence of IR on p-

chloromercuribenzoic acids (PCMB) affinity. PCMB interacts with protein thiol groups, inducing conformational changes that can either activate or inhibit specific proteins, depending on their structure and function [33]. From Fig.3 it is clear, that 1Gy IR does not change the maximal velocity (V_{max}) of the enzyme. For the control group V_{max}=0.285± 0.0013; after 1 week of 1Gy irradiation V_{max}=0.286±0.0014; after 2 weeks V_{max}=0.283±0.001. PCMB inhibition constant (K_i) remained the same after 1 week but deeply increased after 2 weeks of IR. Ki = 2.69±0.12 for the control group; Ki = 2.55±0.23 after 1 week and Ki = 3.72 ±0.18 after 2 weeks; 5Gy IR also does not change the V_{max} of the enzyme after 1 (V_{max}=0.284±0.0034) and 2 weeks (V_{max}=0.293±0.0016) but increases the K_i after 2 weeks (Fig.4). Ki = 2.09±0.13 after 1 week and Ki = 3.72 ±0.18 after 2 weeks.

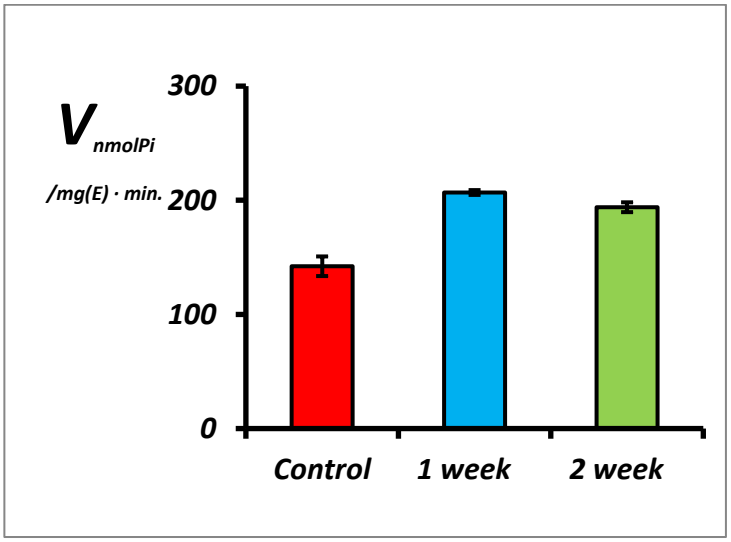

Fig.1 Dependence of hippocampal Na, K-ATPase activity on IR (1Gy). The reaction medium was [MgATP]=1.69mM; [Mg_f^{2+}]=[ATP_f]=0.31mM. (P < 0.001 vs control)

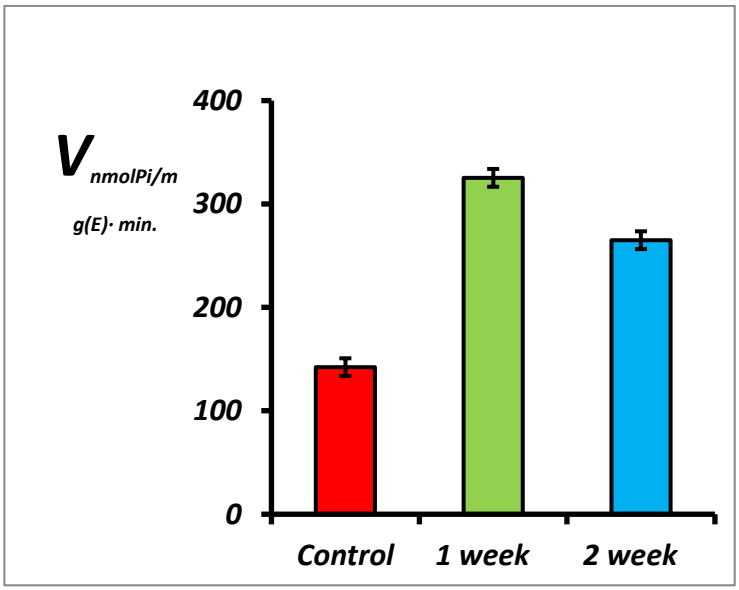

Fig.2 Dependence of hippocampal Na,K-ATPase activity on IR (5 Gy). The reaction medium was [MgATP]=1.69mM; [Mg_f^{2+}]=[ATP_f]=0.31mM.(P < 0.001 vs control)

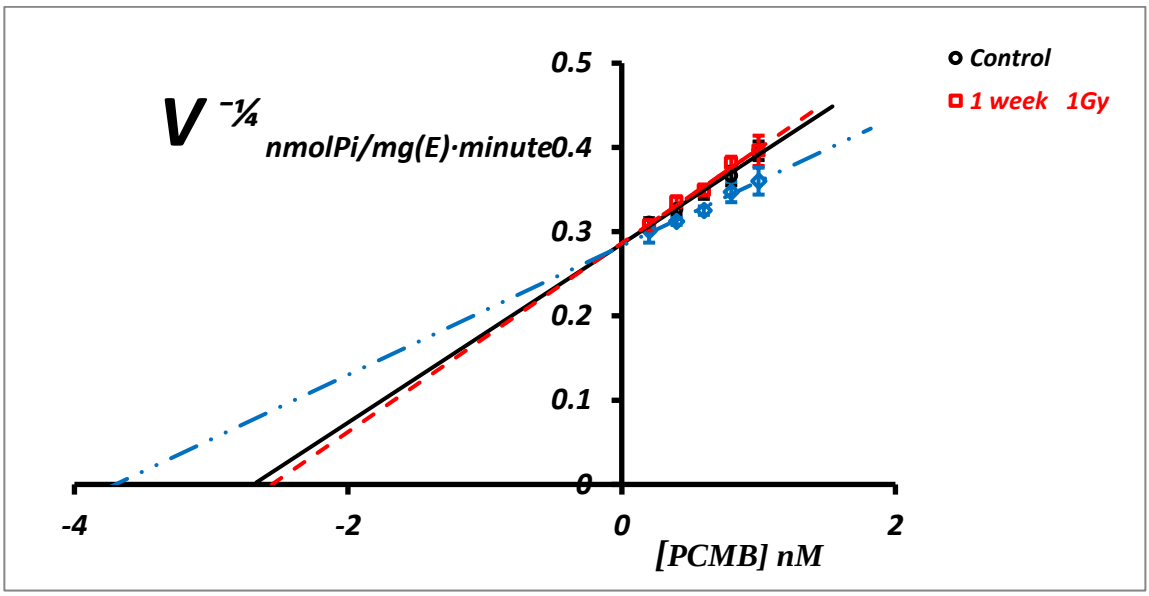

Fig.3. Dependence of hippocampal Na, K-ATPase activity on PCMB concentrations in the $V^{-1/4}$=f(PCMB) coordinate system. The reaction medium was [MgATP]=1.69mM; $[Mg_f^{2+}]=[ATP_f]\leq 0.31$mM. (P < 0.01vs control; n = 3).IR=1Gy
I -Control $V^{-1/4}$=0.106x + 0.285 Ki = 2.69±0.12 V_{max}=0.285± 0.0013 x=[PCMB]
II- 1week $V^{-1/4}$=0.112x +0.286 Ki = 2.55±0.23 V_{max}=0.286±0.0014
III –2 week $V^{-1/4}$=0.076x + 0.283 Ki = 3.72 ±0.18 V_{max}=0.283±0.001

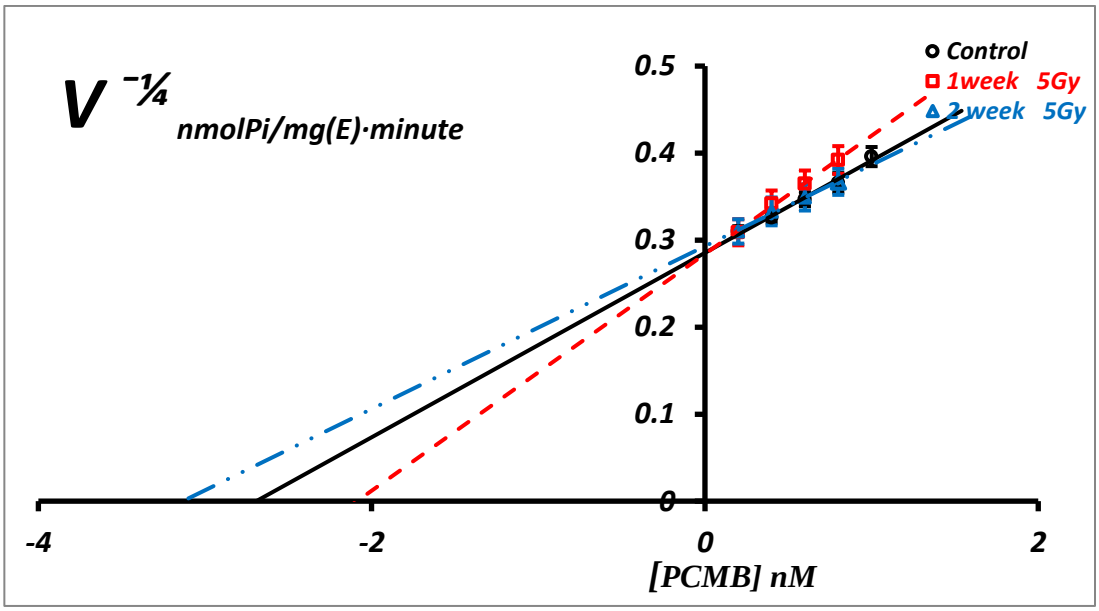

Fig.4 Dependence of hippocampal Na, K-ATPase activity on PCMB concentrations in the $V^{-1/4}$=f(PCMB) coordinate system. The reaction medium was [MgATP]=1.69mM; $[Mg_f^{2+}]=[ATP_f]\leq 0.31$mM. (P < 0.01vs control; n = 3).IR=5Gy
I -Control $V^{-1/4}$=0.106x + 0.285 Ki = 2.69± 0.12; V_{max}=0.285± 0.0013 x=[PCMB]
II- 1week $V^{-1/4}$=0.136x +0.284 Ki = 2.09±0.13 V_{max}=0.284±0.0034
III –2 week $V^{-1/4}$=0.093x + 0.293 Ki = 3.15 ±0.11 V_{max}=0.293±0.0016

DISCUSSION

It is well established that exposure to IR immediately triggers the generation of free radicals, initiating the production of ROS and subsequently leading to cellular damage. Under normal physiological conditions, ROS act as important signaling mediators [34], and their levels are tightly regulated by endogenous antioxidant systems, such as thiol-containing molecules. These antioxidants neutralize excess radicals, preventing oxidative damage. However, IR-induced elevation in free radical production disrupts this balance, promoting lipid peroxidation—a process that compromises membrane integrity [6]. Alterations in the oxidative state and lipid composition of membranes can profoundly impact the functional activity of membrane-bound enzymes such as Na^+,K^+-ATPase [29]. Notably, a rise in lipid peroxidation byproducts has been directly associated with the suppression of Na^+,K^+-ATPase activity [29]. Additionally, IR exposure has been shown to elevate levels of endogenous ouabain [35], a cardiotonic steroid known for its high-affinity interaction with Na^+,K^+-ATPase. While ouabain is classically recognized as an inhibitor of the enzyme, at physiologically relevant (low) concentrations—comparable to endogenously released levels—it may also exert activating effects on the pump [36–38]. Endogenous ouabain is synthesized from cholesterol in the zona glomerulosa of the adrenal cortex [17]. The stress response induced by IR activates both the sympathetic nervous system and the hypothalamic–pituitary–adrenal axis, thereby modulating ouabain synthesis and secretion [17]. Interestingly, while ROS typically suppress Na^+,K^+-ATPase function, they are also implicated in a self-perpetuating oxidative stress signaling cascade [17]. The binding of ouabain to Na^+,K^+-ATPase can initiate multiple intracellular signaling pathways, including those that stimulate mitochondrial ROS production—thereby creating a feedback loop that further modulates Na^+,K^+-ATPase function [17].

This redox-based signaling involves the reversible covalent modification of cysteine residues located in the catalytic or regulatory domains of proteins. ROS-induced oxidation of these cysteines leads to the formation of disulfide bonds (R–S–S–R) through a sulfenic acid (R–SOH) intermediate in a biologically reversible manner [39]. These disulfides may be intramolecular, intermolecular, or occur between a protein thiol and glutathione (S-glutathionylation). Redox-regulating proteins such as thioredoxins (Trx) and glutaredoxins (Grx) catalyze the reduction of these disulfide bonds, allowing for controlled signal transduction. However, further oxidation by hydrogen peroxide (H_2O_2) can irreversibly convert sulfenic acids into sulfinic ($R–SO_2H$) and sulfonic ($R–SO_3H$) acids [39].

At early stages following 1 Gy and 5 Gy IR exposure, increased ROS production and elevated endogenous ouabain levels may initially stimulate Na^+,K^+-ATPase activity via reversible redox modification of cysteine residues in its subunits (Fig. 1; Fig. 2). These early effects appear to enhance enzyme function. However, as oxidative pressure intensifies, ouabain-induced activation of signaling pathways further amplifies mitochondrial ROS production, perpetuating the so-called "Na^+,K^+-ATPase oxidant amplification loop." This continued oxidative modification leads to irreversible thiol oxidation and subsequent enzymatic inhibition (Fig. 1).

Na^+,K^+-ATPase is a heterotrimeric protein complex composed of three subunits: the large catalytic α subunit (100–113 kDa), responsible for ion transport and ATP hydrolysis; the β

subunit (~55 kDa), which plays a regulatory and structural role; and the FXYD family of small regulatory proteins (7–11 kDa), expressed in a tissue-specific manner [40]. Each of these subunits contains cysteine residues susceptible to redox modification. In particular, the β subunit includes a single accessible thiol group located at the membrane interface, which transitions in and out of the membrane during enzyme cycling [40]. The FXYD subunit possesses two reactive thiols [40], while the α subunit contains 23–24 thiol groups, depending on the isoform [40]. These residues represent prime candidates for ROS-mediated redox regulation. The changes in pCMB affinity induced by IR confirm the involvement of regulatory thiols in this mechanism (Fig.3; Fig.4).

Therefore, our experimental findings suggest that IR-induced ROS formation and ouabain elevation initially lead to enhanced Na^+,K^+-ATPase activity via reversible thiol oxidation. However, sustained oxidative stress results in irreversible enzyme inhibition.

REFERENCE

[1]. Kregel, K.C. & Zhang, H.J. (2007). An integrated view of oxidative stress in aging: basic mechanisms, functional effects, and pathological considerations. Am. J. Physiol. Regul. Integr. Comp. Physiol., 292,R18–36.

[2]. Fearon, I.M. & Faux, S.P. (2009). Oxidative stress and cardiovascular disease: novel tools give (free) radical insight. J. Mol. Cell Cardiol., 47,372–381.

[3]. Ceriello, A. & Motz, E. (2004). Is oxidative stress the pathogenic mechanism underlying insulin resistance, diabetes, and cardiovascular disease? The common soil hypothesis revisited. Arterioscler. Thromb. Vasc. Biol., 24,816–823.

[4]. Laval, J. (1996). Role of DNA repair enzymes in the cellular resistance to oxidative stress. Pathol. Biol., 44,14-24.

[5]. Halliwell, B. & Whiteman, M. (2004). Measuring reactive species and oxidative damage in vivo and in cell culture: how should you do it and what do the results mean? Br. J. Pharmacol., 142(2),231-255.

[6]. Wilson, J. (1997). Antioxidant defense of the brain: a role for astrocytes (review). Can. J. phys. Pharmacol., 75,1149–1163.

[7]. Loganovsky, K., Perchuk, I., Marazziti, D. (2016). Workers on transformation of the shelter object of the Chernobyl nuclear power plant into an ecologically-safe system show qEEG abnormalities and cognitive dysfunctions: a follow-up study. World J Biol Psychiatry, 17,600-607.

[8]. Loganovskaja, T. (2016). Ionizing radiation: brain effects and related neuropsychiatric manifestations. Probl Radiac Med Radiobiol., 21,64-90.

[9]. Shibayama, O., Yoshiuchi, K., Inagaki, M., et al. (2014). Association between adjuvant regional radiotherapy and cognitive function in breast cancer patients treated with conservation therapy. Cancer Med., 3,702-709.

[10].Mezesova, L., Vlkovicova, J., Kalocayova, B. et al. (2014). Effects of g-irradiation on Na,K-ATPase in cardiac sarcolemma. Mol Cell Biochem., 388,241-247.

[11].Novaes, L.S., Dos Santos, N.B., Dragunas, G., et al. (2018). Repeated restraint stress decreases Na,K-ATPase activity via oxidative and nitrosative damage in the frontal cortex of rats. Neuroscience, 393,273-283.

[12].Bogdanova, A., Petrushanko, I.Y., Hernansanz-Agustin, P., Martinez-Ruiz, A. (2016). “Oxygen Sensing” by Na, K-ATPase: these miraculous thiols. Front Physiol.,7,314. doi: 10.3389/fphys.2016.00314

[13].Xie, Z., Jack-Hays, M., Wang, Y., et al. (1995). Different oxidant sensitivities of the alpha 1 and alpha 2 isoforms of Na^+/K^+-ATPase expressed in baculovirus-infected insect cells. Biochem Biophys Res Commun., 207,155-159.

[14]. Shainskaya, A.M., Dvoretsky, A.I. (1990). Mechanism of radiation injury in the ion transport systems of nervous tissue. Acta Physiol Hung.,76:295-299.

[15]. Clausen, T. (2013). Quantification of Na^+,K^+ pumps and their transport rate in skeletal muscle: Functional significance. J. Gen. Physiol., 142,327–345.

[16].Lingrel, J.B. (2010). The physiological significance of the cardiotonic steroid/ouabain-binding site of the Na,K-ATPase. Annu. Rev. Physiol., 72,395–412.

[17].Bagrov, A.Y., Shapiro, J.I., Fedorova, O.V. (2009). Endogenous cardiotonic steroids: Physiology, pharmacology, and novel therapeutic targets. Pharmacol. Rev., 61,9–38.

[18].Tverskoi, A.M., Poluektov, Y.M., Klimanova, E.A., Mitkevich, V.A., Makarov, A.A., Orlov, S.N., Petrushanko, I.Y., Lopina, O.D. (2021). Depth of the Steroid Core Location Determines the Mode of Na,K-ATPase Inhibition by Cardiotonic Steroids. Int. J. Mol. Sci., 22,13268.

[19].Blaustein, M.P., Hamlyn, J.M. (2020). Ouabain, endogenous ouabain and ouabain-like factors: The Na^+ pump/ouabain receptor, its linkage to NCX, and its myriad functions. Cell Calcium**.,** 86,102159.

[20].Bauer, N., Müller-Ehmsen, J., Krämer, U., Hambarchian, N., Zobel, C., Schwinger, R.H., Neu, H., Kirch, U., Grünbaum, E.G., Schoner, W. (2005). Ouabain-Like compound changes rapidly on physical exercise in humans and dogs: Effects of β-blockade and angiotensin-converting enzyme inhibition. Hypertension**,** 45,1024–1028.

[21].Khalaf, F.K., Dube, P., Mohamed, A., Tian, J., Malhotra, D., Haller, S.T., Kennedy, D.J. (2018). Cardiotonic steroids and the sodium trade balance: New insights into trade-off mechanisms mediated by the Na^+/K^+-ATPase. Int. J. Mol. Sci., 19,2576.

[22].Lichtstein, D., Ilani, A., Rosen, H., Horesh, N., Singh, S.V., Buzaglo, N., Hodes, A. (2018). Na^+,K^+-ATPase Signaling and Bipolar Disorder. Int. J. Mol. Sci., 19, 2314.

[23].Kravtsova, V.V., Bouzinova, E.V., Matchkov, V.V., Krivoi, I.I. (2020). Skeletal muscle Na,K-ATPase as a target for circulating ouabain. Int. J. Mol. Sci., 21,2875.

[24].Kravtsova, V.V., Paramonova, I.I., Vilchinskaya, N.A., Tishkova, M.V., Matchkov, V.V., Shenkman, B.S., Krivoi, I.I. (2021). Chronic Ouabain Prevents Na,K-ATPase Dysfunction and Targets AMPK and IL-6 in Disused Rat Soleus Muscle. Int. J. Mol. Sci., 22,3920.

[25].Rezin, G.T., Scaini, G., Goncalves, C.L., Ferreira, G.K., Cardoso, M.R., Ferreira A.G.K., Cunha, M.J., Schmitz, F., Varela, R.B., Quevedo, J., Wyse, A.T.S., Streck, E.L. (2014). Evaluation of Na+, K+ -ATPase activity in the brain of young rats after acute administration of fenproporex. Revista Brasileira de Psiquiatri. 36,138–142. https://doi.org/10.1590/1516-4446-2012-0956

[26].Chan, K.M., Delfert, D., Junger, K.D. (1986). A Direct Calorimetric Assay for Ca2+-Stimulated ATPase Activity. Anal Biochem.,157,375-380. https://doi.org/10.1016/0003-2697(86)90640-8

[27].Lowry, O., Rosenbrough, N., Randall, R. (1951). Protein measurement with the folin phenol reagent. Journal of Biological Chemistry. 193(1),265-275. doi:10.1016/S0021-9258(19)52451-6.

[28].Chkadua, G., Nozadze, E., Tsakadze, L., Shioshvili, L., Arutinova, N., Leladze, M., Dzneladze, S., Javakhishvili, M., Jariashvili, T. (2023). Effect of ionizing radiation on ATPases. Journal of Radiobiology and Radiation Safety, Vol.3, No4.

[29]. Chkadua, G., Nozadze, E., Tsakadze, L., Shioshvili, L., Arutinova, N., Leladze, M., Dzneladze, S., Javakhishvili, M. (2022). Effect of H2O2 on Na,K-ATPase. Journal of Bioenergetics and Biomembranes, 54:241–249. https://doi.org/10.1007/s10863-022-09948-1.

[30]. Chkadua, G., Nozadze, E., Tsakadze, L., Shioshvili, L., Leladze, M., Arutinova, N., Dzneladze, S., Javakhishvili, M., Kupradze, S. (2022). Some Kinetic Features of Na,K-ATPase and Sensitivity to Noradrenalione. Cell Biochemistry and Biophysics, 80(1),23-29. doi:10.1007/s12013-021-01032-6.

[31]. Hernandez, J. (1992). Na,K-ATPase regulation by neurotransmitters. Neurochemistry Int., 20(1),1-10. doi: 10.1016/0197-0186(92)90119-c.

[32]. Chkadua, G., Nozadze, E., Tsakadze, L., Shioshvili, L., Arutinova, N., Leladze, M., Dzneladze, S., Javakhishvili, M., Jariashvili, T., Petriashvili, E. (2024). The effect of cytochrome c on Na,K ATPase. Journal of Bioenergetics and Biomembrane, 56,221-231. https://doi.org/10.1007/s10863-024-10012-3

[33]. Santos, K.L., Vento, M.A., Wright, J.W., Speth, R.C. (2013). The effects of para-chloromercuribenzoic acid and different oxidative and sulfhydryl agents on a novel, non-AT_1, non-AT_2 angiotensin binding site identified as neurolysin. Regul. Pept., 184,104–114. doi: 10.1016/j.regpep.2013.03.021.

[34]. Rhee, S.G., Kang, S.W., Jeong, W., Chang, T.S., Yang, K.S., Woo, H. A. (2005). Intracellular messenger function of hydrogen peroxide and its regulation by peroxiredoxins. CurrOpinCell Biol., 17,183–189. doi: 10.1016/j.ceb.2005.02.004.

[35]. Violetta, V., Kravtsova, A., Fedorova, M.V., Tishkova, A. A., Livanova, O. V., Vetrovoy, A. G., Markov, V. V., Matchkov I. I. (2022). Chronic Ouabain Prevents Radiation-Induced Reduction in the α2 Na,K-ATPase Function in the Rat Diaphragm Muscle. Int. J. Mol. Sci., 23,10921.

[36]. Holthouser, K.A., Mandal, A., Merchant, M.L., Schelling, J.R., Delamere, N.A., Valdes, R.R., Jr. Tyagi, S.C., Lederer, E.D., Khundmiri, S.J.(2010). Ouabain stimulates Na-K-ATPase through a sodium/hydrogen exchanger-1 (NHE-1)-dependent mechanism in human kidney proximal tubule cells. Am. J. Physiol. Ren. Physiol., 299,F77–F90.

[37]. Ketchem, C.J., Conner, C.D., Murray, R.D., Du Plessis, M., Lederer, E.D., Wilkey, D., Merchant, M., Khundmiri, S.J. (2016). Low dose ouabain stimulates Na-K ATPase α1 subunit association with angiotensin II type 1 receptor in renal proximal tubule cells. Biochim. Biophys. Acta., 1863,2624– 2636.

[38]. Klimanova, E.A., Tverskoi, A.M., Koltsova, S.V., Sidorenko, S.V., Lopina, O.D., Tremblay, J.M., Hamet, P., Kapilevich, L.V., Orlov, S.N. (2017). Time- and dose-dependent actions of cardiotonic steroids on transcriptome and intracellular content of Na+ and K+: A comparative analysis. Sci. Rep., 7,45403.

[39]. Petrushanko, I. Y., Mitkevich, V. A., Lakunin, V. A., Anashkina, A. A., Spirin, P. V., Rubtsov, P. M., Prassolov, V. S., Bogdanov, N. B., Hänggi, P., Fuller, W., Makarov, A. A., Bogdanova, A. (2017). Cysteine residues 244 and 458–459 within the catalytic subunit of Na,K-ATPase control the enzyme's hydrolytic and signaling function under hypoxic conditions. Redox Biology, 13,310–319. https://doi.org/10.1016/j.redox.2017.05.021. [40]. Bogdanova, A., Petrushanko, I., Boldyrev, A., Gassmann, M. (2006). Oxygen- and Redox-Induced Regulation of the Na/K ATPase. Curr. Enzyme Inhibit.,2,37–59. doi:10.2174/157340806775473490.

LIFETIME ATTRIBUTABLE BREAST CANCER RISK ASSOCIATED WITH RADIATION EXPOSURE FROM CHEST COMPUTED TOMOGRAPHY IN FEMALE COVID-19 PATIENTS IN GEORGIA

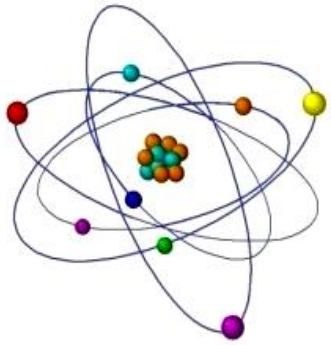

[1,2,3]Tamar Sanikidze, [4]Levan Ratiani, [5,2,3]Giorgi Gavashelishvili, [1]Alla. Zedginidze, [1,2,3]Sophio Kalmaxelidze, [4]Nino. Ormotsadze, [2]Maka. Korkelia, [1,2,3]Giorgi Ormotsadze*

[1] Iv.Beritashvili Center of Experimental Biomedicine, Georgia
[2] Tbilisi State Medical University Georgia
[3] Georgian Association of Medical Physics and Radiaton Protection, Georgia
[4] The First University clinic of Tbilisi State Medical University, Georgia
[5] Radiation Medicine Center, Georgia

https://doi.org/10.63465/rrs520258977 *Correspondingauthor: g.ormotsadze@lifescience.org.ge

ABSTRACT**:** *The study aimed to assess the lifetime attributable risk of breast cancer associated with chest computed tomography (CT) exposure in female COVID-19 patients in Georgia. Data was obtained from the National Center for Disease Control and Public Health of Georgia (NCDCG), concerning COVID-19 morbidity, hospitalization, and mortality rates for the general population during the period 2020–2021. Additionally, information on the age distribution of breast cancer incidence among the female population in Georgia from 2015 to 2023, as well as demographic data from the National Statistical Office of Georgia for the years 2017 to 2019, was used. Furthermore, data from the First University Clinic in 2020, detailing the age and sex distribution of hospitalized patients and survival-mortality indicators, was also incorporated into the analysis. Population doses were modeled using the Log-Normal distribution with mean 14.16 mGr and median 12.82 mGr for adults and for children 4.58 mGr and 4.47 mGr respectively. Age structure of study population were evaluated using a Bayesian approach. A competing risk methodology was employed to estimate both age-conditional and lifetime baseline risks (LBR) of breast cancer development. These estimates were calculated using the United States National Cancer Institute's DevCan software (version 6.9.0). To determine the age-conditional and lifetime attributable risk (LAR) of radiogenic breast cancer, the methodology outlined in the 2006 report by the Biological Effects of Ionizing Radiation (BEIR) VII Committee of the National Academies of Sciences was applied. Risk computations were performed using the National Cancer Institute's RadRAT software and the LARisk R package. Monte Carlo simulation techniques were used to estimate uncertainties in risk and subjective uncertainties under various assumptions.*

It was shown that the lifetime attributable risk for Breast cancer in female COVID patients in Georgia, related to chest computed tomography in one year is low - 12.77 [90% UR 3.20 - 29.90], and is only 0.2% of the lifetime baseline risk (LBR) for breast cancer. However, for the population under 40 years of age, this ratio is already 2.2%. Overall, the projected number of future breast cancer cases that could be attributed to a chest CT scan performed in one year is 20.06 [90% UR 5.02 - 46.96] cases. Given the cumulative effects of ionizing radiation and the potential risk of multiple or repeated scanning, further improvements in methods for predicting the long-term effects of medical radiation exposure appear necessary.

Keywords: Lifetime attributable breast cancer risk, chest computed tomography

INTRODUCTION

The unique diagnostic efficacy of computed tomography has led to a dramatic increase in the frequency of its use - over the past two decades, the number of CT scans in the United States increased from 57 million to 90 million [1,2]. Accordingly, the dose burdens associated with medical imaging on populations have increased dramatically.

To correctly assess the carcinogenic risks in the range of low doses of radiation and to solve the tasks of regulatory control, the National Research Council of the United States developed a population-specific, age- and sex-dependent methodology for assessing the carcinogenic risks [3], which, with various modifications and for different purposes, is currently widely used by both international and national regulatory organizations [4,5,6]. The World Health Organization used this methodology to assess and predict the medical consequences of the Fukushima incident [7]. Based on this methodology, it was shown in 2007 that approximately 1.5–2% of the total cancer incidence in the United States could be associated with computed tomography [8]. The prognostic values of the cancer risk associated with CT imaging were estimated according to the scanning zones; it has been shown that of the total number of associated with CT scans cancers (78 million scans) performed in the United States in 2007 (n=29,000 (95% UR, 15,000-45,000)), the most contributed were abdomen and pelvis (n = 14,000) (95% UR, 6,900-25,000) and chest (n = 4,100) (95% UR, 1,900-8,100) [9]. In subsequent years, large-scale epidemiological studies conducted in different countries [10-13] quantitatively verified and confirmed theoretical estimates of carcinogenic risks associated with CT. Among them, we would like to highlight a study by British scientists, where 178,604 patients were retrospectively analyzed, and it was revealed that compared with patients who received a dose of less than 5 mGy, the relative risk of leukaemia for patients who received a cumulative dose of at least 30 mGy was 3·18 (95% CI 1·46–6·94) and the relative risk of brain cancer for patients who received a cumulative dose of 50–74 mGy was 2·82 (1·33–6·03) [13].

The carcinogenic risk associated with medical imaging has received particular attention during and after the COVID-19 pandemic, which has been linked to a dramatic increase in chest CT scans in infected patients. For example, a multicenter study of 42,028 chest computed tomography scans found that total radiation exposure increased by 573% in patients screened in 2019, with the highest increase seen in the 20–29 age group (18.6-fold) [14]. Numerous studies, both international and national, have examined the radiation doses to the breast and lungs from chest CT scans using different protocols in populations and their prognostic values for carcinogenic risk in children, adults, and the elderly [15–22]. International expert organizations and regulatory bodies have been developing recommendations for minimizing doses and risks in chest CT by “justifying” and “optimizing” the procedures, taking into account the epidemiological situation, clinical situation, patient category, etc. [23-28].

In Georgia, prognostic assessments of the increase in oncological morbidity associated with the Covid-pandemic are not found in the literature available to us, while the aforementioned information seems to us to be very relevant, both in terms of identifying priority areas of the National Cancer Control Strategy in Georgia, In Georgia, prognostic assessments of the increase in oncological morbidity associated with the Covid-pandemic are not found in the literature available to us, while the aforementioned information seems to us to be very relevant, both in terms of identifying priority areas of the National Cancer Control Strategy in Georgia, as well as in terms of further refining the theoretical foundations of “justification” – “optimization” in computed tomography and regulatory control. In our earlier studies, radiogenic carcinogenic risk projection models for breast and lung sites were developed for the Georgian population based on the BEIR VII methodology [29]. This paper will present and discuss prognostic estimates of the increase in cancer incidence associated with the COVID-19 pandemic in the Georgian female population.

MATERIALS AND METHODS

Data was obtained from the National Center for Disease Control and Public Health of Georgia (NCDCG), concerning COVID-19 morbidity, hospitalization, and mortality rates for the general population during the period 2020–2021. Additionally, information on the age distribution of breast cancer incidence among the female population in Georgia from 2015 to 2023, as well as demographic data from the National Statistical Office of Georgia for the years 2017 to 2019, was used. Furthermore, data from the First University Clinic in 2020, detailing the age and sex distribution of hospitalized patients and survival-mortality indicators, was also incorporated into the analysis.

Organ (Breast) radiation dose in chest CT was evaluated from imaging protocols using the software CT-Expo V 2.8. Population doses were modeled using the Log-Normal distribution with mean 14.16 mGr and median 12.82 mGr for adults and for children 4.58 mGr and 4.47 mGr respectively. Age structure of study population were evaluated using a Bayesian approach. A competing risk methodology was employed to estimate both age-conditional and lifetime baseline risks (LBR) of breast cancer development. These estimates were calculated using the United States National Cancer Institute's DevCan software (version 6.9.0). To determine the age-conditional and lifetime attributable risk (LAR) of radiogenic breast cancer, the methodology outlined in the 2006 report by the Biological Effects of Ionizing Radiation (BEIR) VII Committee of the National Academies of Sciences was applied [3,4]. Risk computations were performed using the National Cancer Institute's RadRAT software and the LARisk R package. Monte Carlo simulation techniques were used to estimate uncertainties in risk and subjective uncertainties under various assumptions [30,31,32].

RESULTS

Before proceeding directly to the discussion of the results, we consider it appropriate to emphasize a few important points for further discussion clarification. The modern standard of quantitative hazard characteristics (quantitative risk characterization) imposes qualitatively new requirements on its content and accuracy. "Health risk assessment" is considered as a "process that includes determining (estimating) the health risk associated with the harmful effects of an external factors including the identification of attendant uncertainties [33]. The concept of "uncertainties" is fundamentally different from the classical "errors", namely, when measuring any quantity, it is necessary to indicate the conditions and circumstances under which the measurement is carried out, the full realization of which is in principle impossible, since it requires infinitely large amounts of information. Therefore, there always remains an area of subjective interpretation (informational uncertainty). This component may be, or may not be, of minimal importance, but its indication is considered necessary [32], especially when objects of high potential danger are characterized [34,35]. The modern standard considers the "uncertainty" of measurement (evaluation) as the sum of two types of uncertainty (Type A and Type B). Type A uncertainty - a random statistical error, for the evaluation of which standard statistical procedures are used, Type B uncertainty - does not decrease with an increase in the number of repeated measurements, and is evaluated by scientific judgment based on all of the available information on the possible variability of the measurand (in particular, the results obtained in earlier studies, expert assessments, etc.).

The main stages of uncertainty assessment according to Joint Committee for Guides in Metrology [30,31,32] are a) formulation (defining the input and output quantities, developing a model relating input and output quantities, on the basis of available knowledge assign probability density function (PDF) to each individual input), b) propagation (propagating PDF input data through the model to produce PDF output data) and c) summary.

Formulation:

First, it should be noted that, since the present study belongs to uncontrolled and unstructured observational studies, only B-type uncertainty is considered. As mentioned above, the study aimed to estimate the The population-averaged lifetime attributable risk (LAR) of Breast Cancer $((LAR)\bar{}\_P\hat{}Breast)$ and the age structure of the increase in cancer incidence ($N\_D\hat{}P\ (e)$) in the population infected with COVID-19 in Georgia irradiated in 2021 (Output quantities).

Our analysis of these characteristics is based on the BEIR VII methodology modified by the US EPA [3,4]. In the BEIR VII approach, the lifetime attributable risk (LAR) for each cancer site is the main measure of risk. It represents the lifetime probability of developing cancer in a hypothetical (100,000 people) exposed cohort and depends on 1) the demographic age-sex structure, 2) the age-sex structure of mortality, and 3) the age-sex structure of the background cancer incidence rate. Accordingly, it is specific for each population, including the Georgian population.

In the case of breast cancer, it has the following form:

$$\begin{aligned}&\langle\!\langle \boldsymbol{LAR} \rangle\!\rangle\ \hat{}\boldsymbol{Breast}\ (\boldsymbol{D},\boldsymbol{e})\\&\quad=\boldsymbol{D}*\boldsymbol{\beta}\int\_(\boldsymbol{e}+\boldsymbol{L})\hat{}\boldsymbol{100}\ \langle\!\langle \boldsymbol{exp}\,[(\boldsymbol{\gamma}(\boldsymbol{e}-\boldsymbol{25}))/\boldsymbol{10}]\ (\boldsymbol{a}/\boldsymbol{50})\hat{}\boldsymbol{\eta}*(\boldsymbol{S}(\boldsymbol{a}))\\&\quad/\ (\boldsymbol{S}(\boldsymbol{e}))*\boldsymbol{da}\ \ (\boldsymbol{1})\rangle\!\rangle\end{aligned}$$

Where D is the radiation dose, e is the age at exposure, a is the attained age, and β is the coefficient, which reflects the radiosensitivity of the study population (in this approach, the difference in radiosensitivity between populations is ignored). S(a) is the probability of surviving to age a, and L is the minimum latency period of developing cancer.

The following parameter values are recommended by the US EPA for breast cancer: β = 10; γ = -0.50; η= 3.5 for a < 50 and 1,1 for a > 50. These values are universal for all populations, the difference is only in the mortality curve S(a). From equation (1), by simple transformations, we can obtain $(LAR)\bar{}\_P\hat{}Breast$ and $N\_D\hat{}P\ (e)$:

$$\begin{aligned}&(\boldsymbol{LAR})\bar{}\boldsymbol{\_P\hat{}Breast}\\&\quad=\boldsymbol{D}\\&\quad/(\boldsymbol{N\_D\hat{}P}\ )\int\_\boldsymbol{0\hat{}100}\ \langle\!\langle \boldsymbol{N\_D\hat{}P}\ (\boldsymbol{e})\ \ \langle\!\langle \boldsymbol{LAR} \rangle\!\rangle\ \hat{}\boldsymbol{Breast}\ (\boldsymbol{D},\boldsymbol{e})\boldsymbol{de}\rangle\!\rangle\ \ (\boldsymbol{2})\end{aligned}$$

$$\boldsymbol{N\_P\hat{}Breast}\ (\boldsymbol{e},\boldsymbol{D})=\boldsymbol{D}\int_{\boldsymbol{e}}^{\boldsymbol{100}}\boldsymbol{N\_D\hat{}P}(\boldsymbol{e})[(\ \langle\!\langle \boldsymbol{LAR} \rangle\!\rangle\ \hat{}\boldsymbol{Breast}\ (\boldsymbol{D},\boldsymbol{e}))/\boldsymbol{100000}]\boldsymbol{de}\quad(\boldsymbol{3})$$

In this equations $N\_D\hat{}P\ (e)$ - the age structure of the irradiated in 2021 COVID-19 patients, and $N\_D\hat{}P=\int\_0\hat{}100\ \langle\!\langle N\_D\hat{}P\ (e)de\rangle\!\rangle$ - is their total number.

Equation (3) represent the models that relating the output quantities ($(LAR)\bar{}_P\hat{}Breast$and $N\_P\hat{}Breast\ (e,D)$), with input quantities, which in our case are considered: 1) $\langle\!\langle LAR \rangle\!\rangle\ \hat{}Breast\ (D,e)$ - lifetime attributable risk of developing breast cancer in a population irradiated with a dose D on the age of e, 2) $N\_D\hat{}P\ (e)$ - the age structure of the irradiated population and 3) D - the radiation dose, the value of which depends on a number of factors (the model of the CT scanner, the protocols used, the qualifications of the radiologists, the clinical status of the patient, etc.), these quantities are random variables, so the next stage of the study was the assessment of their probability density functions (PDF).

We described the PDF of the lifetime risk of developing breast cancer for each age group by a normal (Gaussian) distribution:

$$\langle\!\langle \boldsymbol{LAR} \rangle\!\rangle\ \hat{}\boldsymbol{Breast}\ (\boldsymbol{D}=\boldsymbol{10mGr},\boldsymbol{e}=\boldsymbol{e\_i})=\mathbf{N}\left(\boldsymbol{\mu}_{\boldsymbol{e_i}},\boldsymbol{\sigma}_{\boldsymbol{e_i}}\right)\ \ (\boldsymbol{4})$$

The mean values ($\boldsymbol{\mu_{e_i}}$) and standard deviation ($\boldsymbol{\sigma_{e_i}}$), for each $\boldsymbol{e_i}$age group were taken from our earlier work [29], where the age-dependent lifetime attributable risk of Breast Cancer (number of cancer cases per 100,000 persons) for the Georgian female population irradiated with a dose D = 10 mGy was estimated (Figure 1).

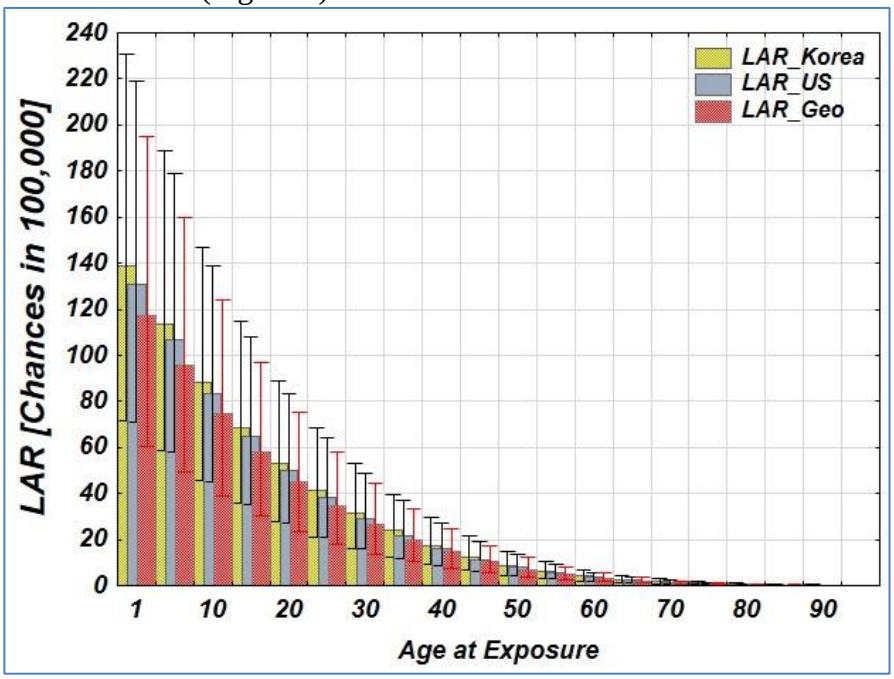

Figure 1. Distributions of lifetime attributable risk for female populations of Georgia, the United States, and Korea irradiated at a dose of 10 mGy. Whiskers – 95% uncertainty range

As for the age structure of the exposed population and the probability distribution functions of radiation doses, at the moment, the quantitative characteristics of the dose loads associated with the COVID-19 pandemic in the population of Georgia, as well as the age structure of the exposed population are not available to us, therefore, the assessment of these distributions seems possible only on the basis of indirect data and analysis of literature data; From this position, we consider it appropriate to first analyze the available information on the criteria for categorizing infected patients, the use of CT imaging in different categories of patients, imaging protocols and dose selection criteria.

The following classifiers proposed by the Fleischner Society provide general ideas about these criteria (criteria for "justifying" the diagnostic procedure) [23].

Severity of respiratory disease (*Mild: no evidence of significant pulmonary dysfunction or damage (eg, absence of hypoxemia, no or mild dyspnea), Moderate to severe: evidence of significant pulmonary dysfunction or damage (eg, hypoxemia, moderate-to-severe dyspnea)*

Pretest probability (*Based on background prevalence of disease as estimated by observed transmission patterns. May be further modified by individual's exposure risk. Subcategorized as: Low: sporadic transmission, Medium: clustered transmission, High: community transmission).*

Risk factors for disease progression (*Present: clinical judgment regarding combination of age .65 years and presence of comorbidities (eg, cardiovascular disease, diabetes, chronic respiratory disease, hypertension, immune-compromised).*

Resource constraints *(Limited access to personnel, personal protective equipment, COVID-19 testing ability (including swabs, reagent, or personnel), hospital beds, and/or ventilators with the need to rapidly triage patients).*

In addition to these criteria in terms of "justification" of the procedure, an important factor is considered the informative value of computed tomography in terms of diagnosing the disease, severity of the course, development of complications and prognosis of lethal outcome. The analysis of a number of clinical studies revealed that CT imaging has low specificity - Imaging findings are nonspecific and share commonalities with other infections such as influenza, H1N1, (SARS-CoV-1) and MERS-CoV [38], along with this, because the risk of infection transmission across imaging personnel and other patients, without known or suspected COVID-19 infections, is high [45], the United States Center for Disease Control and Prevention (CDC) does not recommend using chest radiographs or CT scans as a screening method or first-line diagnostic tool for COVID-19 [24],. Similarly, the American College of Radiology (ACR) advises against using CT scans for screening or diagnosing COVID-19, stating that such imaging should only be performed in specific cases involving hospitalized, symptomatic patients [25]. The Fleischner Society also shared this position. According to these recommendations, CT imaging is recommended only for monitoring complications of COVID-19 in hospitalized patients and for special case indications [23].

Somewhat different principles are observed in the approaches of Chinese specialists [26,27], who believe that although RT-PCR is the gold standard for diagnosis, high false negative results, which delay patient isolation and treatment initiation, increase the risk of persistent transmission of infection and the risk of complications Taking these circumstances into account, Chinese experts recommend the use of CT imaging in unconfirmed cases (screening, diagnosis), in cases of high Pretest probability and probable false negative test results. Pediatric cases require a separate discussion. Children are more vulnerable than adults to the effects of radiation dose, therefore, chest CT in children must only be performed when RT-PCR and immunoassays are not available and/or urgent information is needed in children with severe disease. [23]. As for the practice of using radiological imaging methods in COVID-19 patients in Georgia, it is regulated by the National Guidelines for the Clinical Management of Infection Caused by the Novel Coronavirus (SARS-CoV-2) (COVID-19) in Adult and Pediatric Patients [https://sms.tsmu.edu/ssms/cme/img/ax_co_ga_inf.pdf], according to which chest radiological examination (radiography, computed tomography) is recommended for adult hospitalized patients with both possible and confirmed COVID-19, although the study protocol is not specified. In children with lung damage caused by COVID-19, chest X-ray is considered necessary, and if this study is uninformative, computed tomography is recommended. Based on the above, with a high degree of certainty, the population of hospitalized COVID-19 patients in Georgia can be considered as a irradiated contingent.

The National Center for Disease Control and Public Health of Georgia registered 908,908 infected and 157,047 hospitalized patients of both sexes in 2021, but the literature available to us does not provide information on the age distribution of hospitalized patients by sex. Statistical reports reflect only the age structure of patients discharged from the clinic without gender details (Figure 2), while the age structure of hospitalized patients of different sexes may differ significantly, as indicated by the 2020 data of the First University Clinic of Tbilisi State Medical University on the sex and age structure of hospitalized patients (Figure 3)

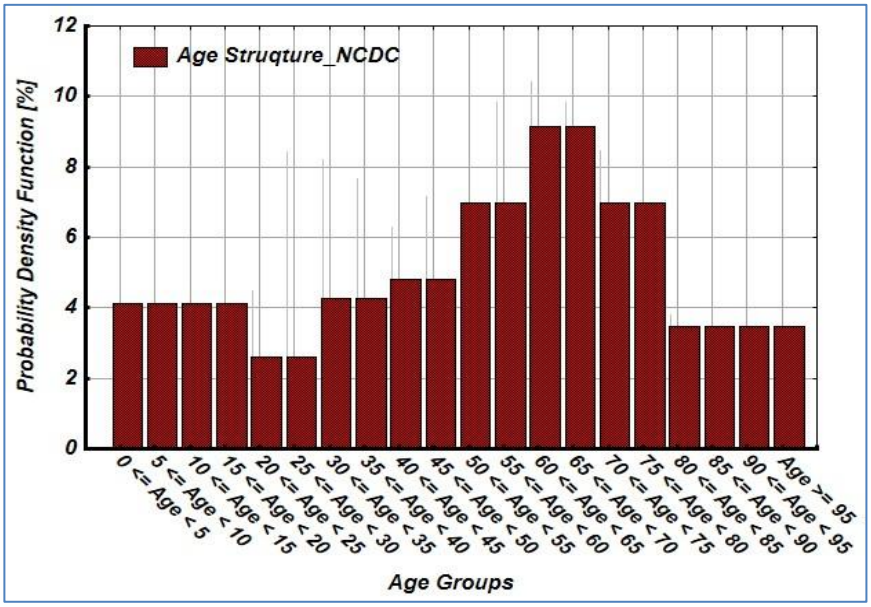

Figure 2. Age structure of patients discharged from clinics in 2021 across Georgia (NCDCG)

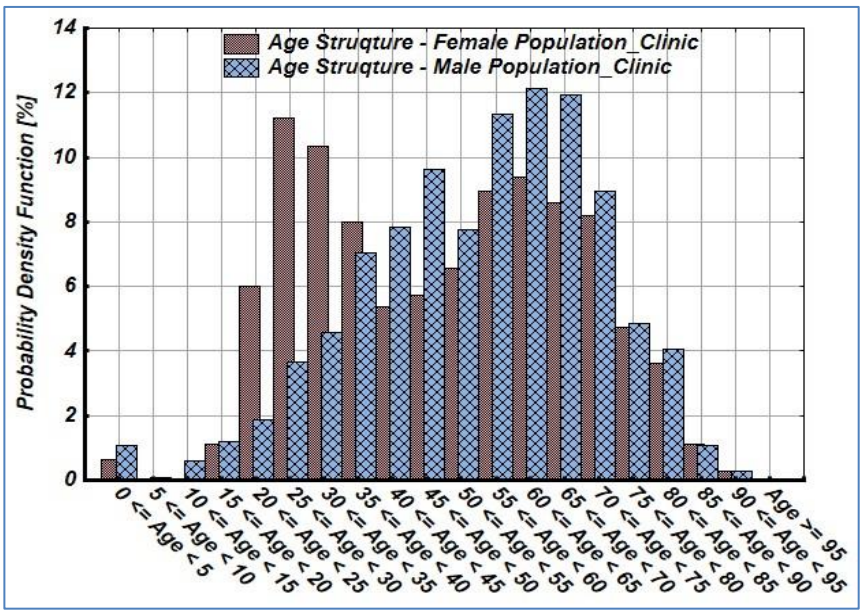

Figure 3. Age and sex structure of patients hospitalized at the First University Clinic of Tbilisi State Medical University in 2020

As can be seen from Figure 2 and Figure 3, the clinic data on the age structure of the female population, which is a bimodal distribution with maxima in the age ranges τ=25-35 and τ=60-70 years, qualitatively differs from the NCDCG data, which is an asymmetric bell-shaped function with a maximum in the age ranges τ=60-70 years. The reason for the identified difference, as we see it, is related to the uncertainties of the clinic and NCDCG data, the first of which is related to sampling error, while in relation to NCDC it should be associated with the insufficient quality of discretization by age and the averaging of data by sex. A literature review on the age structure of hospitalized patients of different sexes (Figure 4) partially coincide with the data of both the clinic and the NCDCG (therefore, they do not have additional information value).

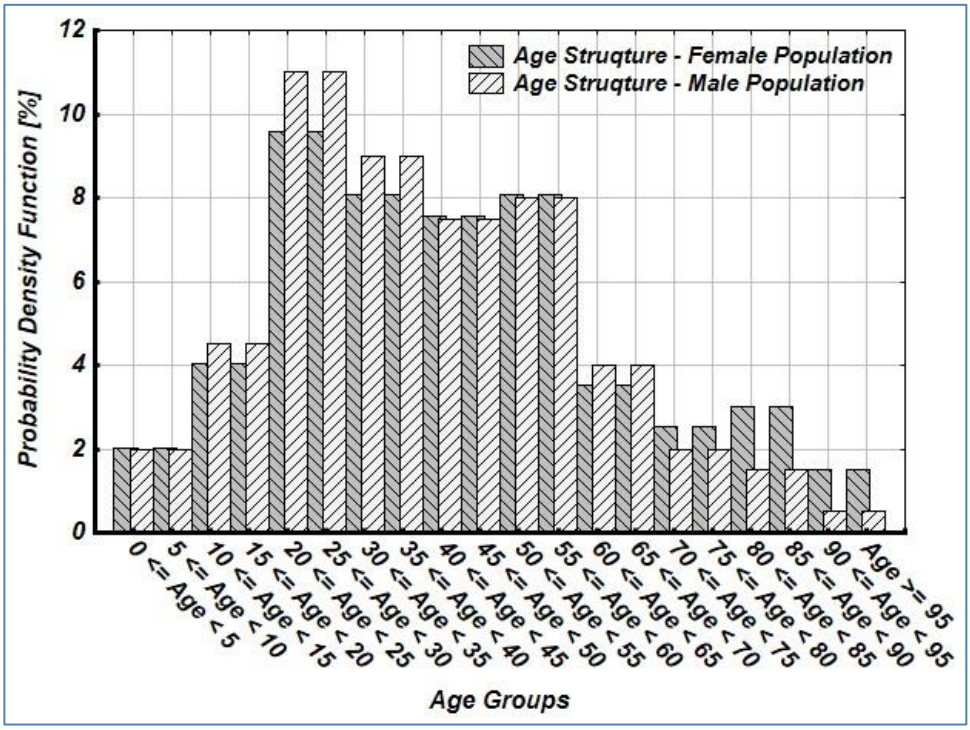

Figure 4. Age and sex structure of COVID-19 infected patients. (German population 2021, patient status unknown) [39]

Given the above stated, for the optimal use of the available information on the age and sex structure of the exposed population, it was considered appropriate to use the Bayesian approach, which allows integrating estimates obtained from various sources, including experiential estimates, which classical, frequency-based probability and statistics cannot provide. The approach is based on Bayes theorem of conditional probability, which is expressed in the following mathematical formula:

$$\boldsymbol{P(A|B) = \frac{P(B|A)\cdot P(A)}{P(B)}} \quad . . \quad .(\mathbf{4})$$

Where:
P(A|B) – the probability of event A occurring, given event B has occurred (posterior)
P(B|A) – the probability of event B occurring, given event A has occurred (likelihood)
P(A) – the probability of event A (prior)
P(B) – the probability of event B
In essence, the above theorem specifies the probability P(A) of the realization of some event (A), if occurring some event (B), independent of it. This makes it possible to integrate information obtained from various sources, including "expert estimation" into the study of a specific problem, which significantly reduces the "uncertainties" associated with the estimates and increases the degree of "reliability" of the results. All these factors add high flexibility and efficiency to the research, which is why the use of this methodology in research is recommended by the U.S. Food and Drug Administration [36,37].

Concerning our problem, quantity A is the probability (p_i) of a patient falling into some $\boldsymbol{\tau_i \div \tau_{i+1}}$ age group. The above-mentioned NCDCG data on the age structure of hospitalized patients (Figure 2) provide some, although incomplete, information on the distribution of $\boldsymbol{p_i}$; therefore, $\boldsymbol{P^{NCDCG}(p_i)}$ can be considered as the a posteriori distribution of $\boldsymbol{p_i}$.
In the case of known p_i, in any random sample of the study cohort, in our case in the cohort of patients hospitalized in the first university clinic ($\boldsymbol{N^{clinic}}$), the probability of a patient falling into the age group

$\boldsymbol{\tau_i \div \tau_{i+1}}$, $P(\boldsymbol{n_f^{clinic}} \mid \boldsymbol{p_i}, \boldsymbol{N^{clinic}})$ can be considered as a "likelihood Function". By integrating these two probabilities in (4), we obtain the age structure of COVID-19-infected and hospitalized female patients in Georgia:

$$\boldsymbol{P(p_i \mid n_f^{clinic}, n_i^{NCDCG}, N^{clinic}, N^{NCDCG}) \propto P(n_f^{clinic} \mid p_i, N^{clinic}) * P^{NCDCG}(p_i)} \quad (5)$$

The distribution of $\boldsymbol{p_i}$ is usually described by a beta-distribution, since the range of definition of this function is [0 1], in our variables it will have the following form:

$$\boldsymbol{P^{NCDCG}(p_i) = \left[\frac{1}{B(n_i^{NCDCG},\ N^{NCDC})}\right] \cdot \left[(p_i)^{(n_i^{NCDCG}-1)} \cdot (1-p_i)^{(N^{NCDCG}-1)}\right]} \ldots (6)$$

Here, $\boldsymbol{N^{NCDCG}}$ - NCDCG data on the total number of COVID-19 hospitalized patients in 2021 (157047 patients), $\boldsymbol{n_i^{NCDCG}}$ - NCDCG data on the age structure of COVID-19 hospitalized patients in 2021 (Figure 2). $\boldsymbol{B(n_i^{NCDC},\ N^{NCDC})}$- is the normalization coefficient in the beta distribution.

In the case of known $\boldsymbol{p_i}$, the number of patients in the age group (likelihood) $\boldsymbol{\tau_i \div \tau_{i+1}}$is described by the binomial statistical distribution:

$$\boldsymbol{P(n_f^{clinic} \mid p_i, N^{clinic}) = \binom{N^{clinic}}{p_i} \cdot p_i^{N^{clinic}} \left(1 - p_i^{N^{clinic}}\right)^{N^{clinic} - n_f^{clinic}}} \ldots (7)$$

By inserting expressions (6) and (7) into expression (5) and further simplifying, we obtain the expression for calculating the posterior distribution:

$$\boldsymbol{P(p_i \mid n_f^{clinic}, n_i^{NCDCG}, N^{clinic}, N^{NCDCG}) \propto p_i^{(n^{clinic} + n^{NCDCG} - 1)} * (1-p_i)^{(N^{clinic} - n_f^{clinic} + N^{NCDCG} - n_i^{NCDCG})}} \quad (8)$$

Using the expression (8), we obtain the distribution functions of patients $\boldsymbol{p_i}$, for a separate $\boldsymbol{\tau_i \div \tau_{i+1}}$ age group of patients (Figure 5), based on which the mean value of the probability, standard deviation, and 95% range of uncertainty were calculated for a separate $\boldsymbol{\tau_i \div \tau_{i+1}}$ age group (Figure 6).

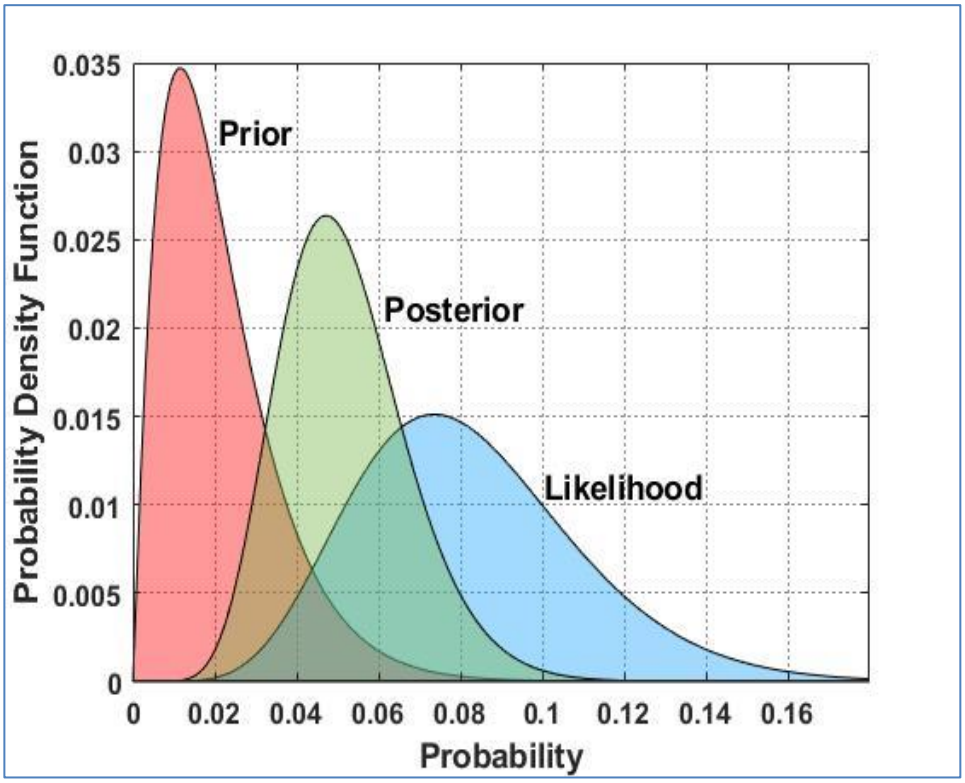

Figure 5. Prior, posteriori, and likelihood distribution functions of hospitalized female COVID-19 patients aged 35-40 years

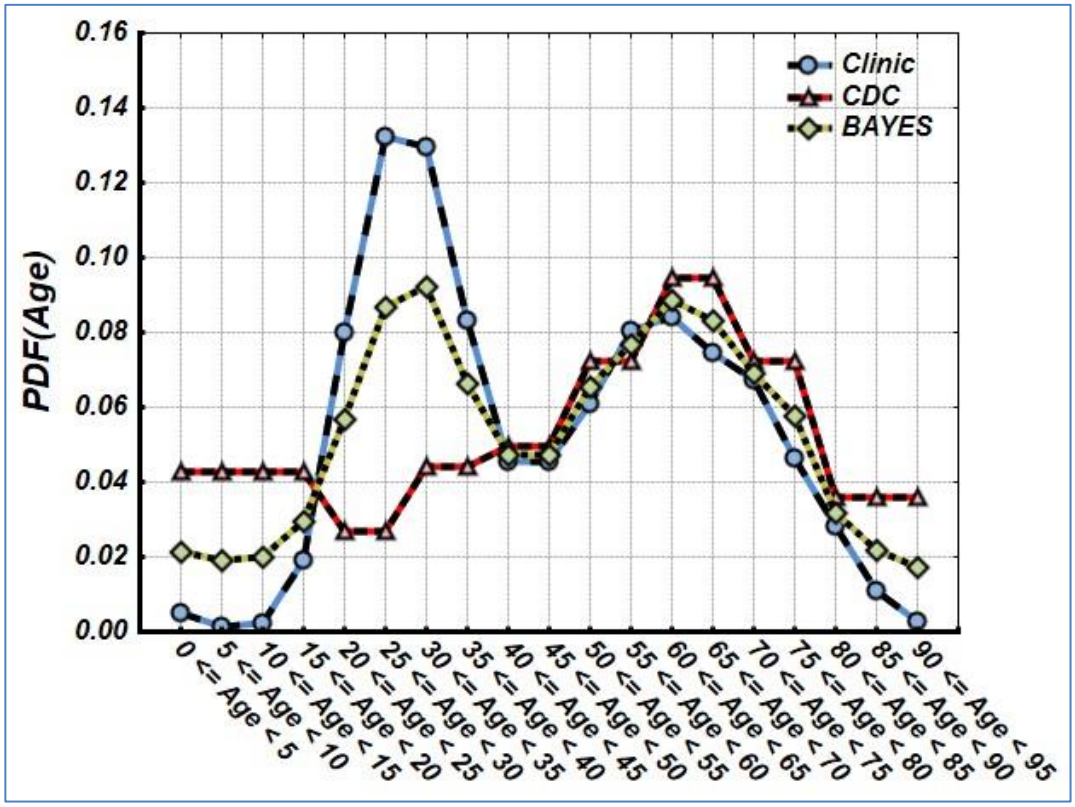

Figure 6. Age distribution of hospitalized women with COVID-19 based on clinic data (circles), NCDCG data (triangles), and estimated using a Bayesian approach (rhombuses)

Scanning techniques (protocols) in COVID-19 patients and doses used

The following general trends emerge regarding recommended CT imaging protocols in COVID-19 patients [23]:

in suspected or known COVID-19 pneumonia report a single-phase, non-contrast chest CT without the need for contrast injection or post-contrast series.

In subjects with suspected pulmonary embolism or necrotizing pneumonia from superimposed bacterial infection, direct post-contrast arterial phase CT can be performed.

There is no evidence to support the use of routine multiphase chest CT in patients with COVID-19 pneumonia.

A webinar [16,17] was organized by the International Atomic Energy Agency (IAEA) to monitor and optimize the dose rates used in medical imaging of COVID-19 patients, with the participation of 62 health care sites from 34 countries on 5 continents. Information on the local prevalence of COVID-19 infection, diagnostic methods, specific protocols and doses was discussed. It was found that than one-half of the health care sites used CT for initial diagnosis of COVID-19 pneumonia and three-fourths used CT for assessing disease severity, approximately 20% of participants used reduced-dose noncontrast chest CT with radiation dose less than the routine or general chest CT

protocol. Approximately 71% of cases used a single examination, 29% used two or more examinations, and approximately 20% used 2 or more phased examinations. There were no significant differences in the doses used between countries, while the doses used at different healthcare providers in the same country varied significantly. There were eightfold variations in median CTDIvol and 10-fold variations in median DLP across multiple participating health care providers from the same country. The medians of the CTDIvol and DLP distributions used varied between 7–11 mGy and 280–439 mGy *cm (absorbed dose of the breast 11.2 – 17.6 mGr*), with a pronounced right-skewed asymmetry (mean/median ≈ 1.106). (Organ (Breast) dose in chest CT was evaluated from imaging protocols using the software CT-Expo V 2.8)

Detailed information on the dose burden associated with CT imaging in COVID patients is presented in a systematic review article [18], which analyzed the results of 81 studies in different countries (China 66.3%, Italy 7.0%; France -4.7%, Iran-3.5%, the United States2.3%). It was found that 23% of CT examinations were used for screening purposes, Regarding the number of CT scans, 14858 patients, 267 patients, and 447 patients had one, two, and three or more CT examinations, respectively. The regimens used varied widely (CTDIvol range 2.3 – 12.6 mGr, (absorbed dose of the breast 4 – 20.8 mGr*), it should be noted that, as presented above, there is no significant difference in the protocols and doses used between different countries. Similar results are observed in other, numerous, international, or national studies [19]. Considering the high dose burden on the population during the COVID pandemic, especially young and pediatric patients, several healthcare providers have developed low-dose chest CT protocols for COVID-19 subjects. Some studies reported an 88–91% reduction in effective dose without compromising the diagnostic image information (CTDIvol 1÷3.5 mGr, DLP 20.4 ÷ 112, kVp 80÷100, mA 10÷50, Pitch 1÷1.7, absorbed dose of the breast 1.6 – 5.6 mGy*), [17, 22]. The most common technical parameters manipulated in low-dose protocols were tube potential and most importantly, tube current (mA).

In Georgia, when modeling the dose burden associated with chest CT in COVID-19 patients, we primarily proceeded from the fact established by the International Atomic Energy Agency that chest CT dose burdens in COVID-infected patients do not differ significantly across countries, while There were eightfold variations in median CTDIvol and 10-fold variations in median DLP across multiple participating health care providers**.** Accordingly, in the absence of a complete data of chest CT dose burdens in Georgia, it was considered more reliable to extrapolate the dose burdens adopted in international practice to the Georgian population**.** Based on the above, we used the asymmetric log-normal distribution to model the Breast absorbed dose during chest CT imaging in COVID-infected patients in Georgia:

$$\boldsymbol{P^{Breast}(D) = Lognormal(\mu, \delta^2)}$$

For the mean value of the normal distribution (μ) associated with the log-normal distribution, a dose of 14.8 mGy was considered optimal, and the value of δ was estimated taking into account the condition Mean (D_{Breast}) /Median (D_{Breast})=1.1 (Figure 7). This approach allows us to assume with a high degree of confidence that the proposed model correctly reflects the central tendencies in the Breast absorbed dose distributions, while the asymmetry of the distribution qualitatively characterizes the share of low-dose protocols and two or more multiple and phased gamma scans in the total dose loads. Similarly, were selected dose parameters for pediatric scanning.

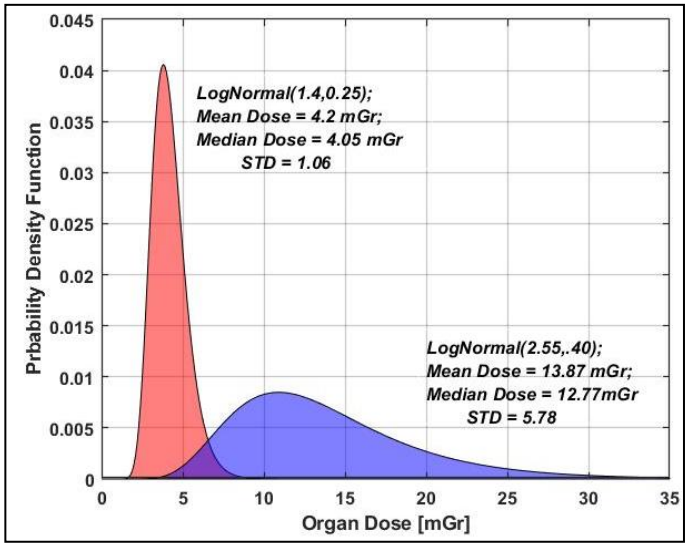

Figure 7. Breast absorbed dose distributions associated with chest CT in the COVID-19 pediatric and adult female patients in Georgia

b) Propagation:

Typically, when the output variables are a complex, nonlinear function of the input variables, the PDF of which cannot be determined analytically, Monte Carlo methods are used to estimate the uncertainty. The principle of MCM is to generate the random numbers by the probability density function of input variables, their assignment in the measurement model and calculation probability function of output variables. For each iteration of the Monte Carlo process, a set of random values for the model parameters are generated.

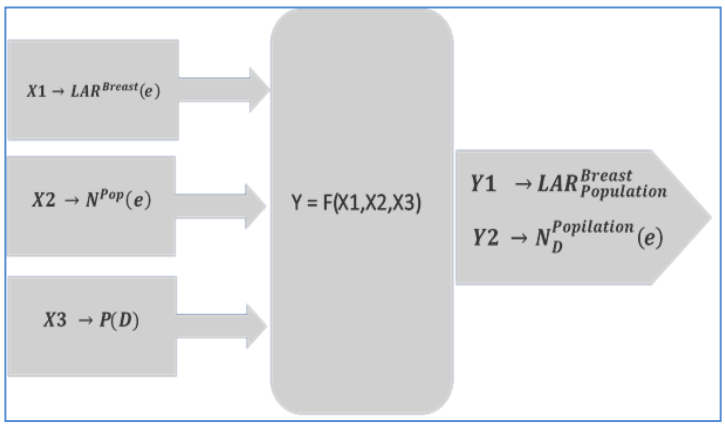

Figure 8. Illustrations of the methodologies. Propagation of uncertainties and resulting distributions

For Each input quantity X1, X2 and X3 generates M random vectors $X1_j, X2_j \; and \; X3_j$ j = 1, . . . , M according to the density of distribution of uncertainties.Thus generated $M \cdot 3$ numbers. Where the value of M was chosen from the condition $\boldsymbol{M \geq \frac{10^4}{(1-p)}}$, 100*p - represents the output variables coverage probability. We have coverage probability 90%, so p = 0,90 and M should be at least 200,000. The measurement model j-th element corresponds **X1j ,X2j, X3j** random numbers according to the uncertainty distribution density. The values **Yj, j = 1, . . . , *M*** must be sorted in the form of a histogram, the bin of which is determined by the required accuracy of the estimates. This ordered model represents a discrete distribution function **Y**, on the basis of which standard statistical indicators are calculated.

Figure 9. presents the Probability of developing radiation induced cancer as a function of age-at-exposure in a hypothetical population of women exposed to 10 mGr (rhombuses) and modeled (squares) doses. Colored area on the graphs correspond to mean ± standard deviation values.

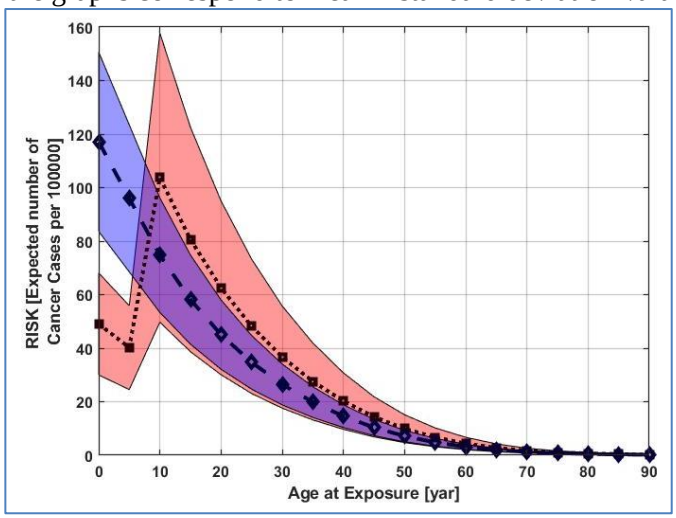

Figure 9. Probability of developing radiation induced cancer (number of additional cases per 100,000 exposed persons) as a function of age-at-exposure in a hypothetical population of women exposed to 10 mGr (rhombuses) and modeled (squares) doses. Colored area on the graphs correspond to mean ± standard deviation values

As can be seen from the graph, the colored area on the graph, corresponding to the modeled doses significantly exceeds the area corresponding to the fixed dose, which is due to the additional uncertainties associated with dose modeling.

According to our estimates, the projected number of future breast cancer cases, associated with chest CT examination of hospitalized in 2021 female COVID-19 patients is 20.06 [90% UR 5.02 - 46.96] cases, moreover, the largest number of cases is observed in the age group 10-35 at the time of exposure (Figure 10)

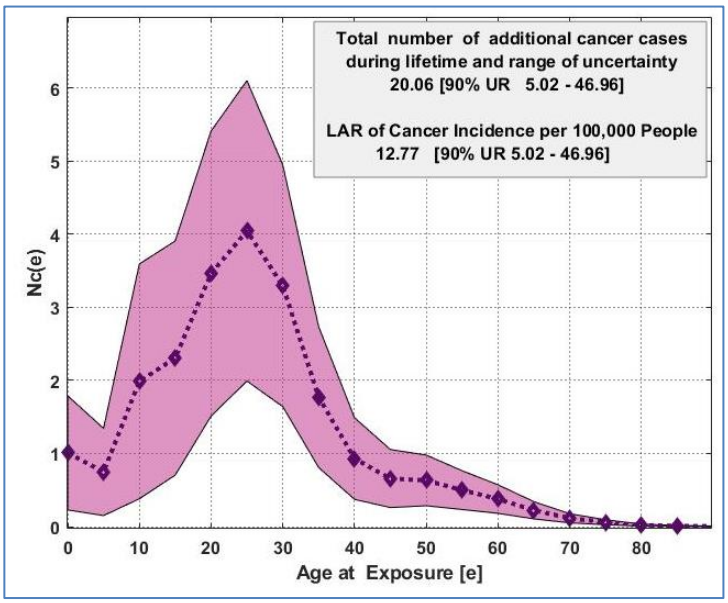

Figure 10. Prognostic values radiation-induced breast cancer cases during lifetime as a function of age at exposure, in hospitalized in 2021 female COVID-19 patients in Georgia. Colored area on the graph represents to 90% range of uncertainty.

Estimated value of the lifetime attributable risk (LAR) for Breast cancer in female COVID patients, related to chest computed tomography in one year is - 12.77 [90% UR 3.20 - 29.90] cases per 100,000 persons. In our earlier study [29], it was shown that the lifetime baseline risk of breast cancer (LBRgeo) in the Georgian female population is 6200 (UR 6500 – 6900) cases per 100,000 person, hence the risk associated with Chest CT causes a slight increase in the baseline risk for the entire population (≈0,2%), However, for the female population under 40 years of age, the ratio LAR and age-conditional baseline risk is approximately 2.2%, which is not a negligible value, considering the annual frequency of CT examinations and the cumulative effect of radiation.

DISCUSSION

The biological effects of low dose radiation and the prediction of their medical consequences have long been a subject of interest, and not only in relation to medical exposure. The intensification of research in this direction was driven by the sharp increase in the frequency of chest CT scans and, accordingly, dose loads on populations during the Covid pandemic. Studies have focused on estimating the prognostic values of CT doses and their associated carcinogenic risk in different countries and populations: In work [17] by searching various online databases: Medline, PubMed, Web of Science, Scopus, ResearchGate, medRxiv, bioRxiv and Google scholar, an extensive literature review was conducted regarding the protocols used, the dose loads and the associated carcinogenic risks in COVID-19 infected patients. Both low-dose, standard, and high-resolution protocols were discussed. It was found that the CTDIvol for standard and high-resolution protocols varied in the range of 6.8–13 mGy, DLP – in the range of 240–650 (mGy.cm), and the LAR estimated by the BEIR VII methodology varied in the range of 15–150 (cases/100,000 persons). The CTDIvol for low-dose protocols varied in the range of 1–3.5 mGy, DLP – in the range of 20–65 (mGy.cm), and the LAR estimated by the BEIR VII methodology varied in the range of 1.5–7 (cases/100,000 persons).

In the works of Italian scientists [40] The average CTDIvol, SSDE and DLP were 6.8 mGy, 8.7 mGy, 239 mGy cm respectively. The average LAR of all solid cancers was 21 cases per 100,000 patients, with breast and lung cancer localizations at the highest risk in the female population; approximately 25 cases per 100,000 patients. Relatively small risks were observed in the publication of Iranian researchers - The average LAR for all cancer types was 10.30 ± 6.03 cases per 100,000 patients. The average CTDIvol and DLP for females was 3.70 ± 6.63 mGy and 105.50 ± 48.51 mGy.cm respectively. In females, the highest equivalent doses were recorded for the lung (4.58 ± 0.60 mSv) and breast (4.06 ± 0.54 mSv).

The results obtained in our study are consistent with the literature estimates within the margin of error and for the population as a whole. the contribution of radiation exposure for 1 year is insignificant (0.2% of the LBR of breast cancer), However, for the female population under 40 accounts for 2.2% of the age-conditional probability of developing cancer.

As can be seen from the above, the increase in cancer incidence directly associated with the Covid pandemic should not be considered a cause for particular concern, but it demonstrates the need to predict the dose loads and risks associated with diagnostic radiology in the long-term (10-20 years) perspective and the relevance of assessing their share in global trends in cancer incidence in the population (permanent increase in incidence, rejuvenation of the contingent) [41-43]. The further adaptation of the BEIR VII methodology to the specifics of specific populations is a subject of separate discussion. As is known, the cancer risk estimates under BEIR VII are based on a linear no-threshold model and data collected from populations of Japan atomic bomb survivors and are thus an extrapolation. In addition, the methodology does not take into account possible interpopulation differences in radiosensitivity and for interpopulation risk transfer, a mixture of EAR and ERR risk models is used in varying proportions for different cancer sites. For breast cancer, the 100% EAR model was used, However, in recent years, strong evidence has emerged that questions the validity of using the EAR model to estimate breast cancer risk [44], in particular,

the incidence of breast cancer in the Japanese population has been steadily increasing. As a result, in the Life Span Study (LSS) of Japanese A-bomb Survivors, the ERR model currently predicts similar dose-dependent increases across age cohorts, whereas the EAR model predicts different dose-dependent increases across age cohorts. Problems with risk estimation have also been identified in a large-scale study, which, based on 111.6 million adult patients who underwent CT scans, found a plausible dose-dependent increase in cancer risk in exposed patients but highlighted the need for further development of the methodology for quantitative LAR estimates [19].

CONCLUSION

The lifetime attributable risk for Breast cancer in female COVID-19 patients in Georgia, related to chest computed tomography in one year is low - the LAR is only 0.2% of the LBR for breast cancer. However, the highest increase was seen in the 10-35 age group - for the population under 40 years old, it is 2.2% of the age-conditional probability of developing cancer. Given the cumulative effects of ionizing radiation and the potential risk of multiple or repeated scanning, further improvements in methods for predicting the long-term effects of medical radiation exposure in the population appear necessary.

REFERENCES

[1]. Davenport, M.S.; Chu, P.; Szczykutowicz, T.P.; Smith-Bindman, R. Comparison of Strategies to Conserve Iodinated Intravascular Contrast Media for Computed Tomography During a Shortage. JAMA 2022, 328, 476–478

[2]. Miglioretti, D.L.; Johnson, E.; Williams, A. Pediatric computed tomography and associated radiation exposure and estimated cancer risk. JAMA Pediatr. 2013, 167, 700–707.]

[3]. National Research Council. 2006. Health Risks from Exposure to Low Levels of Ionizing Radiation: BEIR VII Phase 2. Washington, DC: The National Academies Press.

[4]. EPA Radiogenic Cancer Risk Models and Projections for the U.S. Population, U.S. Environmental Protection Agency Office of Radiation and Indoor Air, April 2011, 1200 Pennsylvania Ave., NW Washington, DC 20460

[5]. Radiation Protection in Medicine, ICRP PUBLICATION 105, Annals of the ICRP, 2007

[6]. Amy Berrington de Gonzalez at all, RadRAT: A Radiation Risk Assessment Tool for Lifetime Cancer Risk Projection, J Radiol Prot. 2012 September ; 32(3):

[7]. Health risk assessment from the nuclear accident after the 2011 Great East Japan Earthquake and Tsunami based on a preliminary dose estimation. World Health Organization; 2013. (http://www. who.int/ionizing_radiation/pub_meet/fukushima_risk_assessment_ 2013/en)

[8]. Brenner DJ, Hall EJ. Computed tomography—an increasing source of radiation exposure. N Engl J Med. 2007; 357(22):2277–2284.]

[9]. Amy Berrington de González, Projected Cancer Risks from Computed Tomographic Scans Performed in the United States in 2007

[10]. childhood or adolescence: data linkage study of 11 million Australians, BMJ 2013;346:f2360.

[11]. Yu-Hsuan Shao at all, Exposure to Tomographic Scans and Cancer Risks. JNCI Cancer Spectrum (2020) 4(1):

[12]. Jae-Young Hong at all, Association of Exposure to Diagnostic Low-Dose Ionizing Radiation With Risk of Cancer Among Youths in South Korea, JAMA Network Open. 2019;2(9):e1910584

[13]. Mark S Pearce at all, Radiation exposure from CT scans in childhood and subsequent risk of leukaemia and brain tumours: a retrospective cohort study, Lancet 2012; 380: 499–505

[14]. Mehmet Coşkun, Did radiation exposure increase with chest computed tomography use among different ages during the COVID-19 pandemic? A multi-center study with 42028 chest computed tomography scans, Diagn Interv Radiol 2023; DOI: 10.5152/dir.2022.211043
[15]. Fatemeh Homayounieh at all, Variations in CT Utilization, Protocols, and Radiation Doses in COVID-19 Pneumonia: Results from 28 Countries in the IAEA Study, Radiology 2021; 298:E141–E151
[16]. Mannudeep K. Kalra at all, Chest CT practice and protocols for COVID-19 from radiation dose management perspective, European Radiology (2020) 30:6554–6560
[17]. Mandeep Garg at all, Radiation Exposure and Lifetime Attributable Risk of Cancer Incidence and Mortality from Low- and Standard-Dose CT Chest: Implications for COVID-19 Pneumonia Subjects, Diagnostics 2022, 12, 3043.
[18]. Jong Hyuk Lee, MD1 at all, CT Examinations for COVID-19: A Systematic Review of Protocols, Radiation Dose, and Numbers Needed to Diagnose and Predict, J Korean Soc Radiol 2021;82(6):1505-1523
[19]. Chun-Feng Cao at all, CT Scans and Cancer Risks: A Systematic Review and Dose-response Meta-analysis, BMC Cancer (2022) 22:1238
[20]. Nissren Tamam at all, Assessment of breast dose and cancer risk for young females during CT chest and abdomen examinations, Applied Radiation and Isotopes,Volume 190, December 2022, 110452
[21]. Mohammad Hossein Jamshidi at all, Estimation of Lifetime Attributable Risk (LAR) of Cancer Associated with Chest Computed Tomography Procedures in Children, Frontiers in Biomedical Technologies Vol. 10, No. 4 (Autumn 2023) 441-448
[22]. Joël Greffier at all, Ultra-low-dose chest CT performance for the detection of viral pneumonia patterns during the COVID-19 outbreak period: a monocentric experience, Quantitative Imaging in Medicine and Surgery, Vol 11, No 7 July 2021
[23]. Geoffrey D. Rubin at all, The Role of Chest Imaging in Patient Management during the COVID-19 Pandemic: A Multinational Consensus Statement from the **Fleischner Society,** Radiology: Volume 296: Number 1—July 2020.
[24]. Centers for Disease Control and Prevention. Interim Clinical Guidance for Management of Patients with Confirmed Coronavirus Disease (COVID-19). https://www.cdc.gov/ coronavirus/2019-ncov/hcp/clinical-guidance-managementpatients.html
[25]. ACR recommendations for the use of Chest Radiography and Computed Tomography (CT) for Suspected COVID-19 Infection. https://www.acr.org/Advocacy-and-Economics/ACR-PositionStatements/Recommendations-for-Chest-Radiography-and-CTfor-Suspected-COVID19-Infection].
[26]. Li Fan, ShiYuan Liu, CT and COVID-19: Chinese experience and recommendations concerning detection, staging and follow-up, European Radiology (2020) 30:5214–5216
[27]. Diagnosis and treatment protocols of COVID-19 infection (trial version 5). The National Health Commission of the People's Republic of China [EB/OL]
[28]. Mannudeep K. Kalra at all, Chest CT practice and protocols for COVID-19 from radiation dose management perspective, European Radiology (2020) 30:6554–6560
[29]. Giorgi Ormotsadze, Tamar Sanikidze, Alla Zedginidze, Levan Ormotsadze, radiogenic breast cancer risk projection for the Georgian female population, Journal of Radiobiology and Radiation Safety Vol.4, №5, 2024
[30]. International standard iso 31000, Risk management **— Guidelines**, Second edition 2018-02;

[31]. Joint Committee for Guides in Metrology (JCGM), Guide to the Expression of Uncertainty in Measurement (GUM) 100-208, "Evaluation of measurement data — Guide to the expression of uncertainty in measurement"],

[32]. Joint Committee for Guides in Metrology (JCGM), "Evaluation of measurement data — Supplement 1 to the "Guide to the expression of uncertainty in measurement" —Propagation of distributions using a Monte Carlo method",

[33]. IPCS risk assessment terminology. Part 1: IPCS/OECD key generic terms used in chemical hazard/risk assessment. Part 2: IPCS glossary of key exposure assessment terminology. Geneva, World Health Organization, International Programme on Chemical Safety (Harmonization Project Document No.)

[34]. Kemeny, J. et al., Report of the President's Commission on the Accident at Three Mile Island, Washington, DC, 1979;

[35]. Health and Safety Executive, Safety Assessment Principles for Nuclear Plants, HMSO, London, 1992

[36]. Guidance for Industry and FDA Staff , Guidance for the Use of Bayesian Statistics in Medical Device Clinical Trials. Food and Drug Administration 5630 Fishers Lane, Rm 1061, Rockville, MD 20852, 201;

[37]. Benefit-Risk Assessment for New Drug and Biological Products Guidance for Industry, U.S. Department of Health and Human Services Food and Drug Administration Center for Biologics Evaluation and Research (CBER) Center for Drug Evaluation and Research (CDER) October 2023.

[38]. [Schaller T, Hirschbühl K, Burkhardt K, et al. Postmortem examination of patients with COVID-19. JAMA 2020;323(24):2518–2520

[39]. Daniela Ghio at all, Demographics of COVID-19 hospitalisations and related fatality risk patterns, Health policy 126 (2022) 945–955]

[40]. C. Ghetti at all, Dosimetric and radiation cancer risk evaluation of high-resolution thorax CT during COVID-19 outbreak, Physica Medica 80 (2020) 119–124

[41]. Jon Shelton at all, 25 year trends in cancer incidence and mortality among adults aged 35-69 years in the UK, 1993-2018: retrospective secondary analysis, BMJ 2024;384:e076962 | doi: 10.1136/bmj-2023-076962;

[42]. Xiao-Wei Tang at all, Long-term trends in cancer incidence and mortality among U.S. children and adolescents: a SEER database analysis from 1975, Front Pediatr. 2024 Jul 5:12:1357093;

[43]. Yan Zhou at all, Long-term trends of lung cancer incidence and survival in southeastern China, 2011– 2020: a population-based study, BMC Pulmonary Medicine (2024) 24:25

[44]. L. Walsh et al, A Framework for Estimating Radiation-Related Cancer Risks in Japan from the 2011 Fukushima Nuclear Accident, Radiation research 182, 556–572 (2014)

[45]. Mossa-Basha M, Meltzer CC, Kim DC et al (2020) Radiology department preparedness for COVID-19: radiology scientific expert panel. Radiology. 16:200988

IMPACT OF GAMMA IRRRADIATION ON THE THERMODYNAMIC AND METAL BINDING PROPERTIES OF BOVIN SERUM ALBUMIN

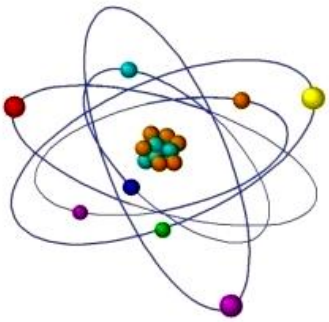

[1]Tinatin Dolidze[*]., [1]Maia Makharadze, [1]Sophio Uchaneishvili., [1]Nazi Ivanishvili., [1]Mikheil Gogebashvili.,[1,2] David Vashakidze., [1,2]Dimitri Khoshtariya.

[1] Ivane Beritashvili Canter of Experimental Biomedicine, Georgia,
[2]Ivane Javakhishvili Tbilisi State University, department of biophysics, Georgia

https://doi.org/10.63465/rrs520258978 *Corresponding author: tinatin.dolidze@gmail. com

ABSTRACT: *Effect of gamma(γ)- irradiation on the bovin serum albumin's (BSA) global thermodynamic stability and metal binding ability has been examined. ^{137}Cs was used as a source of γ-irradiation. It has been shown that irradiation of BSA solution with doses 50Gy and 100Gy causes drastic decrease of amount of proteins molecules capable to interact and form complexes with double charged copper ions while the global stability of BSA is in less extent effected under the same irradiation conditions.*

Keywords: irradiation, bovin serum albumin, double charged copper ions, differential scanning calorimetry

INTRODUCTION

Gamma (γ) irradiation is widely applied in various fields of our life such as industry, agriculture, medicine and etc. Use of irradiation in the medicine should be specially mentioned. Gamma irradiation can be helpful if properly used but at the same time, we must remember that ionizing radiation can severely alter and damage living systems, so its misuse (Incorrect dosage, duration of irradiation and etc.) can lead to irreversible and life-threatening consequences. Therefore, it is of great importance to study the impact of gamma irradiation on biological organisms and objects at both, the molecular and cellular levels in order to protect radiation safety [1-4].

In general, the subject of our interest is the study of the effect of gamma irradiation on blood serum albumin of mammals - Human serum albumin (HSA) and bovine serum albumin (BSA). HSA and BSA (molecular weight ca. 66500Da) are the most studied representatives of monomer globular proteins in serum plasma [5-9]. Human serum albumin is structurally, as well as functionally similar with bovin serum albumin [5,8,16,17] (see fig1). Due to this similarity often in laboratories during intensive experimental work relatively cheap and easily available BSA is used instead of expensive HBA [16,17]

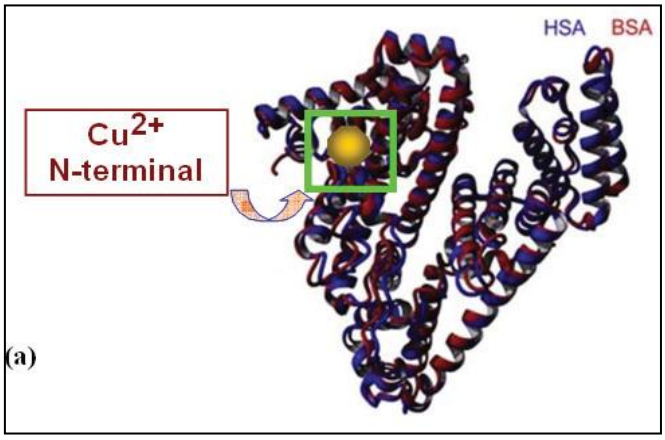

Fig.1. Structure of BSA (blue) and HAS (red) and N- terminal binding site for copper ions (yellow) sphere (according to Ref. [5,8,17])

Physiological function of serum albumins is maintenance of osmotic pressure in serum, transporting of fatty acids, amino acids, medicines, therapeutic agents, drugs, metal ions and etc [9-15]. BSA and HSA are an important transporter of the physiologically essential double charged copper (Cu^{2+}) and zinc (Zn^{2+}) ions as well as toxic nickel (Ni^{2+}) and Cd ($^{2+}$) ions in living organisms [9-18]. Electron paramagnetic resonance spectroscopy and fourier transform infrared spectroscopy was used to identify BSA/HSA specific metal binding sites and binding intensity [8,9,18]. In particular, albumins have partially selective metal binding sites with well-defined metal preferences and they can bind different amount of distinct metals. According to [9] one molecule BSA can bind up to 4 molecules of double charged copper ions. The N-terminal region of bovin serum albumin (sequence of Asp-Thr-His-Lys), provides a specific binding site for the first copper ion [5,8,9,17,18,]. As one can see from Fig.1, this chelating site is located at the peripheral area of protein. Binding sites of further Cu^{2+} ions has been marked as ``non-specific" [31]. Meanwhile, under different specific conditions metal ions binding to protein, can cause/induce proteins conformational and structural changes and eventually even aggregation [9,20-22]. Specifically, depending on the molar ratio of metal and protein ions in the solution, attachment of metal ions to protein, may impact protein's structure, induce proteins structural changes resulting in appearance of precipitate [19,20, 9]. According to authors [20] when adding double charged cobalt, nickel, ions (Co^{2+}, Ni^{2+}) to the HSA solution aggregation occurs if (Co^{2+}, Ni^{2+}) /HSA molar ratio exceeds 8, while BSA forms precipitate after binding approximately 6 or more copper ions and 8 or more zinc ions [19]. In [17] complex formation between BSA and divalent copper chloride ($CuCl_2$) in the solutions containing equal amounts (1.8×10^{-3} M) of albumin and divalent copper ions (so, [BSA]:[Cu^{2+}]= 1:1) has been studied using thermodynamic and voltammetric approach. According to the authors [17] complex formation was accompanied with a very dramatic shift in Cu^{2+} reduction process to much more negative potentials. Along with voltamperometric experiments complex formation was confirmed with combined microcalorimetric examinations [17].

The effect of gamma irradiation on the molecular structure of serum albumins is discussed in the literature [23-27], while specifically the influence of gamma irradiation on metal binding properties of serums albumins, to our knowledge, has not been studied yet. According [23] the results of distribution of specific length of Z-structures on the film surface as well as absorption and fluorescence spectroscopy and dynamic light scattering data, have shown that exposure of bovine serum albumin to gamma irradiation rays (source ^{60}Co) with doses between 1 and 200 Gy leads to minor changes in the structure of the protein. Changes happened when irradiation dose exceeds 200Gy [23,26,27]. However, according to Zarei [24] even absorbed dose 5 Gy (source ^{60}Co) causes structural changes in BSA, specifically primary structure is unaltered, while spectroscopic data revealed obvious changes in secondary and tertiary structure of protein. In the case, when source of irradiation is ^{137}Cs γ-rays, changes in the secondary structure and tertiary structure of BSA starts over irradiation doses 500 Gy, while, exposure up to the 500 Gy irradiation dose causes a minor change [25].

In present work we focused on the studies on effect of gamma irradiation on metal binding possibilities of bovin serum albumin with doubly charged copper ions (Cu^{2+}). Thermodynamic response of the BSA under irradiation conditions is also reviewed.

MATHERIALS AND METHODS

Bovin Serum Albumin (BSA), copper oxide ($CuCl_2 \cdot 2\ H_2O$), potassium Chloride (KCl) were purchased from Sigma and were used without further purification. Solution samples of bovin serum albumin (pH 6.1) were placed in plastic vials and irradiated at room temperature using ^{137}Cs as a gamma radiation source (Dose rate -1.1 Gy per minute).

The radiation doses were 50 Gy and 100 Gy, 200 Gy. Mikrocallorimetric measurements were performed with DSC instrument DASM-4A connecting to PC via the Interface unit PCI-DASM 4-A. All solutions were prepared using Milli Q water.

RESULTS AND DISCUSSIONS

Figure 2 and Figure 3 depict the zero-baseline-corrected calorimetric curves (partial heat capacity of protein versus temperature) for the temperature-induced melting of non irradiated and irradiated (with -50 Gy , 100 and 200 Gy) bovin serum albumin, correspondingly in 0.1 M phosphate buffer solution and in 0.1M phosphate buffer solutions containing 1 M NaCl. As one can see from figure 2 protein melting (endothermic) peak, as a whole, gradually shifts to lower temperatures and decreases in height when going from non irradiated to irradiated with dose 50 Gy sample and this trend continue when increasing the irradiation dose. Addition of NaCl (Figure 3) causes stabilization toward the transition temperature for non radiated [29] as well as irradiated BSA samples.

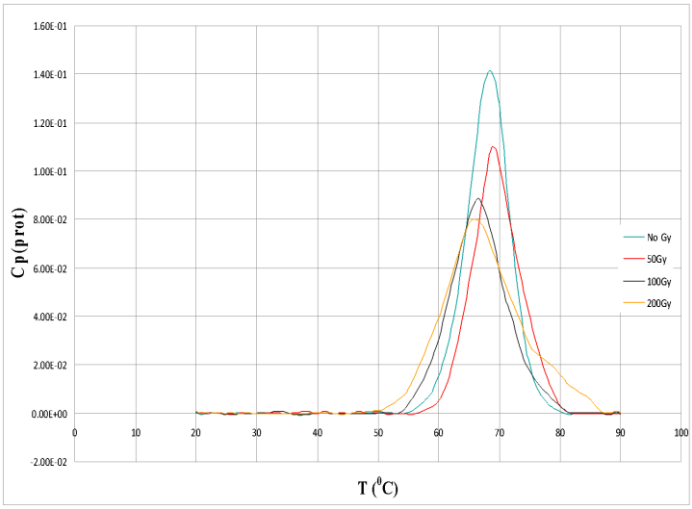

Fig. 2. The DSC melting curves of bovin serum albumin in 0.1 M PBS solution. From top to bottom: non- irradiated and irradiated with doses 50 Gy, 100 Gy and 200 Gy samples

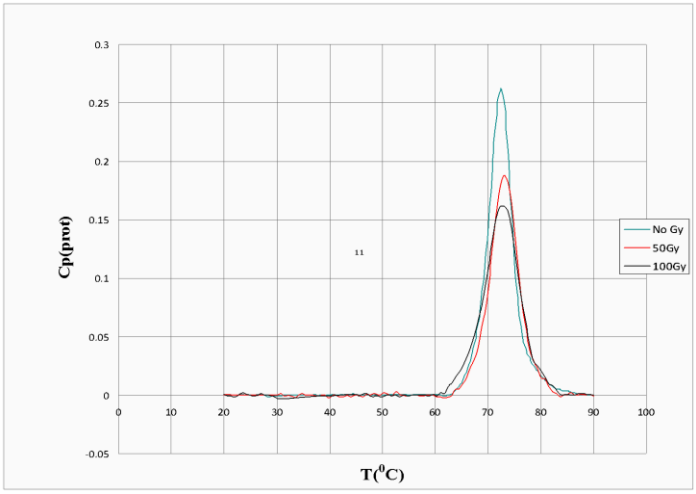

Fig.3. The DSC melting curves of bovin serum albumin in 0.1 M PBS +1 M NaCl. From top to bottom: non- irradiated and irradiated with doses 50 Gy, 100 Gy samples

Thermodynamic parameters of thermal melting for non irradiated and irradiated albumin, in pure phosphate buffer solution and phosphate buffer solution containing 1M NaCL, calculated from curves depicted in Fig. 2 and fig. 3 are gathered in Table 1.

Table 1. Thermodynamic parameters for thermal melting of non- irradiated and irradiated BSA in 0.1 M PBS and 0.1M PBS+ 1M NaCl solutions

solution	Irradiation dose [Gy]	Tm, [^{0}C]	ΔTm, [^{0}C]	ΔHcal, (arbitrary units)
0.1 M PBS	0	68.46	8.11	1.32
	50	67.9	8,72	1.05
	100	66.58	10.35	1.01
	200	65.89	13.02	1.19
0.1 M PBS + 1M NaCl	0	72.67	5.03	1.68
	50	73.4	6.09	1.39
	100	73.11	7.46	1.39

It is clearly visible from table1, that in 0.1 M PBS solutions there is small but distinct destabilization regarding the transition temperature, when going from non- irradiated to irradiated with dose 50 Gy sample , *Tm*, viz., 68, 46 ^{o}C for the non-irradiated BSA sample, versus 67.9 ^{o}C for the BSA sample irradiated with 50 Gy dose, and this tendency continuous with increasing irradiation doses.

The over-all melting enthalpy, Δ*Hcal* is decreasing gradually, while values of peak width at the half height (Δ*T*) are increasing, when going from non irradiated to radiated with doses 50 Gy, 100 Gy and 200 Gy samples.

It can be seen from the table 1, that adding 1 M NaCl to the 0.1M PBS solution of BSA causes some stabilization of transition temperature [29,30], in comparison with pure 0.1M PBS solution for non irradiated, as well as for irradiated samples. Meantime in 1 M NaCl + 0.1M PBS solutions, tendency for changes of Δ*Hcal* and Δ*T* remains the same (as in 0.1M PBS solution) when going from non irradiated to irradiated with doses 50 Gy, 100Gy samples. In overall, this kind of calorimetric behavior is characteristic for the "molten-globule" (MG) or "moltenglobule-like" states in which the protein's tertiary structure is still compact and native-like, but rather labialized [27].

So, based on calorimetric investigation results we can tell that gamma irradiation under above mentioned experimental conditions does not cause remarkable changes in BSA structure and stability this conclusion is in agreement with literature data [23-27].

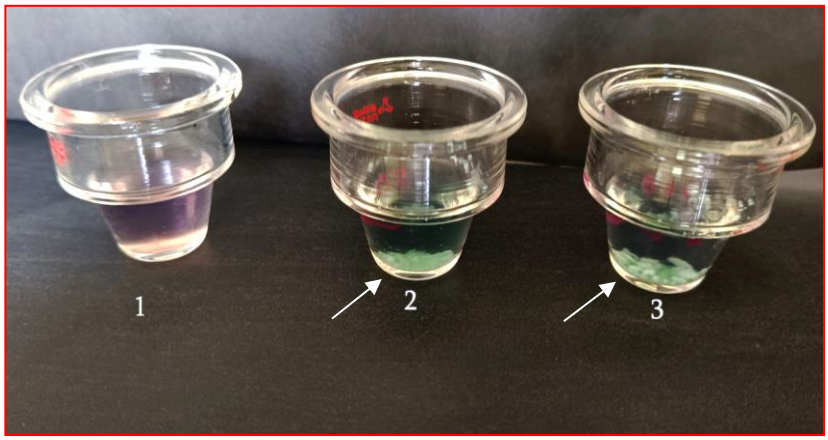

Picture 1. Glass cells containing mixture of BSA and $CuCl_2$ solutions. In cell 1- BSA solution was non irradiated; In cell 2 and cell 3 BSA solution was irradiated, correspondingly with dose 50Gy and 100 Gy (see text below)

Picture 1 shows three glass cells: all three glass cells contain mixture of (1.8×10^{-3} M) bovin serum albumin solution and (1.8×10^{-3} M) double charged copper chloride solution ([$CuCl_2$] / [BSA] = 1:1). Difference is that in the cell 1 BSA solution was not irradiated prior to mixing with $CuCl_2$ solution, while in other two cases (cells 2 and 3) BSA solution was irradiated correspondingly with dose 50 Gy and 100 Gy before mixing with double charged copper chloride. Meantime, solution in the cell 1 has pink colour and is without sediment, while in the cells 2 and 3 solution has green-blue colour and contains white precipitate (indicated by arrows). It should be noted, that water solution of bovin serum albumin (non irradiated as well as irradiated) has light yellow colour, while $CuCl_2$solution has greenish blue colour.

As it was shown in [17] and discussed in the introduction, complex formation between BSA and double charged copper ions is accompanied with colour changes: when blending equal concentrations (1.8×10^{-3} M) of non irradiated, light yellow BSA solution and bluish-green $CuCl_2$solution, mixture turns to pink (picture1, cell 1).

It can be seen from Picture 1 (cell2 and cell 3), that in contrast with case of non-irradiated BSA (cell 1), adding divalent copper chloride solution to the irradiated (dose 50 Gy and 100 Gy) BSA solution of the same concentration ([$CuCl_2$] / [BSA] = 1:1) results in forming a white precipitate, while the solution retains the characteristic greenish-blue color of divalent copper chloride.

For interpretation of above-mentioned results, we should bear in mind that, as it was shown in [19], one molecule of BSA can bind up to a maximum of 5 atoms of divalent copper ions. A further increase in copper to BSA ratio ([Cu^{2+}] : [BSA] ≥ 6) causes a changes in the protein's structure resulting in formation of proteins deposit[19]. Therefore, to explain appearance of precipitate in the mixture of equal concentrations (1.8×10^{-3}M) of $CuCl_2$ solution and the irradiated BSA solution (Picture 1, cell 2) we have to assume, that (after irradiation of 1.8×10^{-3}M BSA solution) the real ratio of divalent copper ions to BSA ions

([Cu 2+] : [BSA]) is not 1:1, but is at least 6 (or more). In other words, we have to assume, that irradiation of (1.8 x 10^{-3}) M BSA solution with a dose of 50 Gy effects BSA molecules metal binding sites and causes the decrease of the number of 'active' BSA molecules, which have the ability to bind copper ions, at least 6 times. So, the real concentration of "active" BSA molecules capable of binding metal ions, (as a result of irradiation of 1.8 x 10^{-3} M BSA solution with a dose of 50 Gy), is probably a maximum (3 10^{-4})M (1.8 10^{-3} M/ 6 = 3 10^{-4}M), i.e. approximately a maximum of 16,67% of the original concentration.

To check the assumption we take into account, that mixture of BSA and $CuCl_2$ has pink color and is without precipitate when ratio[$CuCl_2$] : [BSA] is equal to 1:1[17,19] and suppose that irradiated with a dose of 50 Gy (1.8 x 10^{-3})M BSA solution contains maximum 16, 67 % of the original concentration of BSA molecules with metal binding affinity (i.e. approximately 3 10^{-4}M**)**. So**,** we added (2 10^{-4} M) $CuCl_2$ solution to the irradiated with a dose of 50 Gy (1.8 x 10^{-3}) M BSA solution.

The mixture acquired a pink color (there was no precipitate) (not shown) as expected. When a similar experiment was performed on BSA solution irradiated with a dose of 100 Gy, abundant precipitation was observed, which indicates that much less than 16% of BSA molecules in the solution irradiated with a dose of 100 Gy have the ability to bind metal ions.

From the comparison of the impact of gamma rays on the general thermodynamic stability of protein with its impact on metal bindings possibility of BSA one can see that under γ-irradiation with doses 50 and 100 BSA molecules undergo relatively minor general structural changes (destabilization), while under same conditions about 84% of protein molecules loses their ability to bind copper ions. In other words, irradiation induces different effect on proteins global thermodynamic stability and on the local, protein- metal (N-terminal site - Cu^{2+}) interaction. It should be mentioned, that it is not mandatory that under different stabilizing/ destabilizing conditions, protein's local ligand- metal bond stability follow the path of global thermodynamic stability. For example, in the case of Cytochrome C in the presence of destabilizing agent [28] protein's local ligand- metal bond (Met 80- Fe^{3+}) stability was retained while global conformation was severely altered [28]. According to authors this probably was due the fact that porphyrin in Cytochrome C with triple charged iron ions was buried inside the protein and was not easily reachable for destabilizing agent urea [28].

Taking into account high penetrating ability of gamma rays [31,32] it is hardly believable that copper binding site (N-terminal, see fig.1) due to it's location at the periphery of protein, is easier damageable under influence of gamma rays than BSA molecules global thermodynamic stability in whole. More plausible explanation is that radicals generated under radiolysis of water molecules [32,33], in the course of gamma irradiation of BSA water solution, are responsible for drastic deterioration of chelating possibilities of protein molecules. This assumption will be the subject of our future investigations.

CONCLUSIONS.

Comparing the results of microcalorimetric investigations of biovin serum albumins thermodynamic stability before and after of irradiation of proteins solutions (source 137Cs, doses 50 Gy and 100Gy) on the one hand, and analyzing the BSA- metal binding possibility changes (under same irradiation conditions) on the other hand, we came to the conclusion that gamma irradiation affects both, the global stability of protein and protein – metal binding properties but in a in different extent. Specifically, gamma irradiation of BSA solutions with dose 50 Gy results in decrease of number of molecules capable to bind double charged copper ions down to approximately maximum 16 %; increase of radiation dose (up to 100 Gy) causes the further drastic decrease in number of 'complex formation capable' BSA molecules. Meanwhile, under the same conditions, γ-irradiation induces minor changes in the structure and global stability of BSA molecules.

REFERENCES

[1]. Carante M. P., Ramos R. L. and Ballarini F. (2023). Radiation Damage in Biomolecules and Cells 2.0 Int. J. Mol. Sci., 24, 3238. https://doi.org/10.3390/ijms24043238

[2]. Ballarini F., Carante M. P., Embriaco A. and Ramos R. L. (2022). Effects of ionizing radiation in biomolecules, cells and tissue/organs: basic mechanisms and applications for cancer therapy, medical imaging and radiation protection. AIMS Biophysics, Volume 9, Issue 2, 108–112.

[3]. Carante M. P. and Ballarini F. (2020). Radiation Damage in Biomolecules and Cells. Int. J. Mol. Sci. 21, 8188; doi:10.3390/ijms21218188

[4]. Kabudanian Ardestani S., Watabe H. (2021). Radioprotective effect of nanoceria and magnetic flower-like iron oxide microparticles on gamma radiation-induced damage in BSA protein AIMS Biophysics, Volume 8, Issue 2: 124-142. doi: 10.3934/biophy.2021010 (https://www.aimspress.com/article/doi/10.3934/biophy.2021010

[5]. Peters T. Jr. (1995). The Albumin Molecule: Its Structure and Chemical Properties. In: All About Albumin. San Diego: Academic Press. 9–II.

[6]. Penezić A. Z., Aćimović J. M., Pavićević I. D., Jovanović V. B., Takić M., Mandić L. M. (2018). The interplay between copper (II), human serum albumin, fatty acids, and carbonylating agent interferes with Cys 34 thiol reactivity and copper binding. Journal of Biological Inorganic Chemistry: JBIC: 24(1): 61-70.

[7]. Carter D.C., Ho J. X. (1994). Structure of serum albumin. Advances in Protein Chemistry. 45: 153–203.

[8]. Bal W., Sokołowska M., Kurowska E., Faller P. . (2013). Binding of transition metal ions to albumin: Sites, affinities and rates. Biochimica et Biophysica Acta (BBA) - General Subjects1830; Issue 12: 5444-5455.

[9]. Alhazmi H.A., (2019). FT-IR Spectroscopy for the Identification of Binding Sites and Measurements of the Binding Interactions of Important Metal Ions with Bovine Serum Albumin. Sci. Pharm *87*(1): 5.

[10]. Anraku M., Chuang VT., Maruyama T., Otagiri M. (2013). Redox properties of serum

albumin. Biochim Biophys Acta. 1830(12): 5465-72.
[11]. Singh N., Pagariya D., Jain S., Naik S., Kishore N. (2018). Interaction of copper (II) complexes by bovine serum albumin: spectroscopic and calorimetric insights. Journal of Biomolecular Structure and Dynamics. issue 9; 36: 2449-2462.
[12]. Kragh-Hansen U. (2016). Human Serum Albumin: A Multifunctional Protein. In: Otagiri M, Chuang VTG, editors. Albumin in medicine: pathological and clinical applications. Singapore: Springer Singapore. 1–24.
[13]. Matsura K., Sugumoto I. (2014). Absorption Spectral Analysis of Zn^{2+} or Cu^{2+} Coordination with Human Serum Albumin using Zircon. Journal of Analytical & Bioanalytical Techniques. 5(4).
[14]. Rezaei Behbehani G., Barzegar L., Mohebbian M., Saboury A. A. (2012). A Comparative Interaction between Copper Ions with Alzheimer's β Amyloid Peptide and Human Serum Albumin. Bioinorganic Chemistry and Applications. Article ID: 208641.
[15]. Rezaei Behbehani G., Barzegar L., Mohebbian M., Saboury A. A. (2012). A Comparative Interaction between Copper Ions with Alzheimer's β Amyloid Peptide and Human Serum Albumin. Bioinorganic Chemistry and Applications. Article ID: 208641.
[16]. Topala T., Bodoki A., Oprean L., Oprean R. (2014). Bovine Serum Albumin Interactions with Metal Complexes Clujul Med. 87(4): 215–219.
[17]. Dolidze T.D., Makharadze M., Uchaneishvili S., Nioradze N., Laliashvili L. (2021). New aspects of the interaction of copper (II) with serum albumin: voltammetric and microcalorimetric studies. Georgian Medical News v.318, No 9, p.139-142.
[18]. Quagraine E.K., Kraatz H. B., Reid R. S. (2001). Peptides mimicking the N-terminal Cu (II)-binding site of bovine serum albumin: synthesis, characterization and coordination with Cu (II) ions Journal of Inorganic Biochemistry 85, 23–32.
[19]. Lee V. E., Schulman J. M., Stiefel E. I., Lee C. C. (2007). Reversible precipitation of bovine serum albumin by metal ions and synthesis, structure and reactivity of new tetrathiometallate chelating agents Journal of Inorganic Biochemistry 101, 1707–1718.
[20]. Hedberg Y. S., Dobryden I., Chaudhary H., Wei Z., Per M Claesson P. M. (2019). Christofer Lendel Synergistic effects of metal-induced aggregation of human serum albumin Colloids Surf B Biointerfaces. Jan 1;173:751-758.
[21]. Jing P. P., Li Y. X., Su Y. H., Liang W. L., Leng Y. X. (2021). The role of metal ions in the behavior of bovine serum albumin molecules under physiological environment Spectrochim Acta A Mol Biomol Spectrosc. 2022 Feb 15;267(Pt 2):120604. doi: 10.1016/j.saa. 120604
[22]. Navarra G., Tinti A., Leone M., Militello V., Torreggiani A. (2009). Influence of metal ions on thermal aggregation of bovine serum albumin: aggregation kinetics and structural changes. J Inorg Biochem. Dec;103(12):1729-38. doi: 10.1016/j.jinorgbio.2009.09.023.
[23]. Glibitskiya D. M., Gorobchenkob O. A., Nikolovb O. T., Cheipeshc T. A., Roshald A. D., Zibarovd A. Z., Shestopalovaa A. V., Semenova M. A., Glibitskiya G. M. (2018). Effect of gamma-irradiation of bovine serum albumin solution on the formation of zigzag film textures Radiation Physics and Chemistry 144, 231–237.
[24]. Zarei H., Bahreinipour M. Eskandari K., MousaviZarandi S-A., Kaboudanian Ardestani S. (2017). Spectroscopic study of gamma irradiation effect on the molecular structure of bovine

serum albumin Vacuum 136, 91-96.
[25]. Gaber M. H. (2005). Effect of γ-irradiation on the molecular properties of bovine serum albumin. Journal of Bioscience and Bioengineering, 100(2), 203–206. doi:10.1263/jbb.100.203 (05,1,5 kGy)
[26]. Hu X., Song W., Li W., Guo C., Yu Z. and Liu R. (2016). Effects of γ -Irradiation on the Molecular Structures and Functions of Human Serum Albumin J Biochem Molecular Toxicology 30 (11):525-532.
[27]. Mishra K., Ojha H., Kallepalli S., Alok A., Kumar Chaudhury N. (2014). Protective effect of ferulic acid on ionizing radiation induced damage in bovine serum albumin. Int J Radiat Res 12 (2) :113-121. URL: http://ijrr.com/article-1-1221-en.html
[28]. Khoshtariya D. E., Dolidze T. D., Stefan Seifert S., Sarauli D., Lee G. and Eldik R. V. (2006). Kinetic, Thermodynamic, and Mechanistic Patterns for Free (Unbound) Cytochrome c at Au/SAM Junctions: Impact of Electronic Coupling, Hydrostatic Pressure, and Stabilizing/Denaturing Additives Chem. Eur. J12, 7041 – 7056.
[29]. Yamasaki M., Yano H., Aoki K. (1990). Differential scanning calorimetric studies on bovine serum albumin: I. Effects of pH and ionic strength. Int J Biol Macromol. Aug;12(4):263-8. doi: 10.1016/0141-8130(90)90007-w.
[30]. Yamasaki M., Yano H., Aoki K. (1991). Differential scanning calorimetric studies on bovine serum albumin: II. Effects of neutral salts and urea Int J Biol Macromol. vol 13. doi: 10.1016/0141-8130(90)90007-w.
[31]. Bal W., Christodoulou J., Sadler P. J., Tucker A. (1998). Multi-metal binding site of serum albumin Journal of Inorganic Biochemistry 70, 33-39.

[32]. Wang J., Chu L. (2016). Irradiation treatment of pharmaceutical and personal care products (PPCPs) in water and waste water: An overview Radiation PhysicsandChemistry125, 56–64.
[33]. Hina H., Nafees M., Ahmad T. (2021). Treatment of industrial wastewater with gamma irradiation for removal of organic load in terms of biological and chemical oxygen demand Heliyon 7 e05972 https://doi.org/10.1016/j.heliyon.2021.e05972

EFEECTS OF RADIATION ON THE OPTICAL PROPERTIES OF SPIRULINA PLATENSIS AFTER REPLACING POTASSIUM IONS WITH CESIUM IONS IN NUTRITION MEDIUM

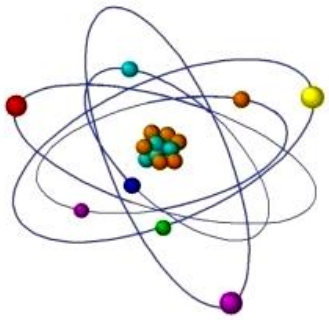

[1]Eteri Gelagutashvili*, [1,2]Mikheil Gogebashvili, [1]Eteri Ginturi, [1]Medea Janjalia, [1]Alex Gongadze, [1,2]Nazi Ivanishvili

[1]Iv. Javakhishvili Tbilisi State University, E. Andronikashvili Institute of Physics, Georgia
[2]Beritashvili Center of Experimental Biomedicine,
Laboratory of Radiation Safety Problems, Georgia

https://doi.org/10.63465/rrs520258979 *Corresponding author: eterige@gmail.com

ABSTRACT*: The optical properties of Spirulina platensis were studied under varying ratios of cesium and potassium ions, followed by gamma radiation exposure. The study highlights the critical role of potassium ions in the post-irradiation recovery process of irradiated cells, regardless of the presence of cesium ions. Analysis of the obtained spectra revealed a high level of stability in the optical properties of Spirulina platensis under ionizing radiation, when not observed difference in terms of the constituents of spirulina. These results indicate the low chemical toxicity of cesium ions. Additionally, the paper explores a possible mechanism for the inhibition of the post-irradiation recovery process, suggesting that it may be due to the replacement of potassium ions by cesium ions—an essential factor for the growth and development of Spirulina platensis cell cultures*.

Key words: *Spirulina platensis*, Cesium ions, Gamma irradiation

INTRODUCTION

Cyanobacteria, or blue-green algae, are among the oldest photosynthetic prokaryotes. Their broad range of physiological adaptations allows them to be utilized in various remediation methods for cleaning ecosystems affected by technogenic pollution, including radionuclides. Radioactive pollutants released during any accident or incident at a nuclear power facility include cesium-137. Radiocaesium is the most problematic element among radionuclides due to its high specific radioactivity, long half-life, and ability to accumulate in living organisms [1]. It is well known that algae exhibit high sensitivity to heavy metals. Heavy metals can interfere with photosynthesis and enzymatic metabolism in algae, leading to growth inhibition and further irreversible adverse effects. Therefore, algae can serve as a test model for assessing freshwater quality and pollutant toxicity.

Blue-green microalgae are rich in nutritional and bioactive compounds that promote various biological functions in the human body. One of the most practically significant properties of algae, particularly spirulina, is their potential efficiency in adsorption, which can be used as a cost-effective, effective, and non-toxic means for removing heavy metals from the body

[2]. The discovery of new technologies has drawn attention to algae-based adsorbents, which can remove radionuclides from the body. Spirulina has long been associated with detoxification, particularly the detoxification of heavy metals. It is highly effective in binding and removing toxic metals such as lead, cadmium, chromium, mercury, strontium, and thallium [3]. These properties have been the basis for numerous studies on pollution elimination through adsorption [4,5]. Most remediation methods are based on the interactions of various environmental elements with radionuclides, influencing their migration into living organisms. These interactions also involve cesium and potassium ions [6, 7]. This raises an important question: how significant is the presence of cesium and potassium ions in forming a radiobiological effect, as expressed by changes in the optical properties of *Spirulina platensis* culture?

MATERIALS AND METHODS

The research subject was a culture of blue-green algae, *Spirulina platensis*, cultivated on Zarrouk's medium. This medium is widely recognized as a standard growing medium for this organism [8]. Over time, many modified media have been developed to address various scientific and practical challenges [9,10]. The *Spirulina platensis* strain IPPAS B-256 was cultivated in Zarrouk's modified alkaline water-salt medium [8] under the following conditions: a temperature of 28°C, illumination of approximately 5000 lux, constant stirring, and periodic re-cultivation. Before the experiments, the cells were cultured for 7 days in standard Zarrouk' s medium. Subsequently, 175 mL of modified Zarrouk' s medium was added to the *Spirulina* culture grown in 25 mL of standard Zarrouk' s medium, and the culture was re-cultivated. However, under these conditions, *Spirulina* growth was not observed. To address this, 200 mL of the solution in cesium medium was retained, 200 mL of standard medium was added to it, and the mixture was set up for cultivation. Unlike the earlier setup, where the cesium concentration was 0.3 g/200 mL, the modified medium in this instance contained 0.15 g/200 mL cesium (a reduced composition). Control cultures were grown in Zarrouk's modified medium containing Cs(I) ions at a concentration of 0.15 g/200 mL. *Spirulina platensis* grown in a modified medium containing 0.15 g/200 mL of cesium was removed from cultivation after 2 week and subjected to prolonged gamma irradiation at a dose of 150 kGy. The irradiation was performed using a gamma installation with a ^{137}Cs radioisotope as the radiation source, operating at a dose rate of 1.1 Gy per minute. After irradiation spirulina was re-cultivated in standard Zarrouk's medium. The compositions of both standard Zarrouk's and modified Zarrouk's media are presented in Table 1.

Growth was measured by monitoring changes in absorbance at 560 nm using a Cintra 10e UV-Vis spectrometer. *Spirulina platensis* grows optimally within a pH range of 9÷11. This suspension of spirulina cells at pH 10.9 was used to record absorption spectra from 400 to 800 nm. The concentration of *Spirulina platensis* was determined based on instrumental data. Solutions of metal ions were prepared in deionized water using appropriate inorganic salts. The $CsCl_2$ reagent used was of analytical grade.

Table 1. Compositions of Zarrouk's media

Macronutrient	Standard Zarrouk's media (g/l)	Modified Zarrouk's media (g/l)
NaCl	1.0	1.0
CaCl2	0.04	0.08
NaNO3	2.5	2.5
FeEDTA	0.0131	0.0131
EDTA (Na)	0.08	0.08
K2SO4	1.0	-
MgSO4x7H2O	0.2	0.2
NaHCO3	16.8	16.8
K2HPO4	1	-
CsCl	-	2
A5 micronutrient H_3BO_3, $MnCl_2x4H_2O$, $ZnSO_4x7H_2O$, $CuSO_4x5H_2O$, MoO3.	1ml	1ml
The second solution NH_4VO_3, $K_2Cr_2(SO4)_4x24H_2O$ $NiSO_4x7H_2O$ $Na_2WO_4x2H_2O$, $Co(NO_3)_4x6H_2O$, TiO_2	1ml	1ml

RESULTS AND DISCUSSIONS

The main goal of the experiment was to study the optical properties of *Spirulina platensis* after replacing potassium ions with cesium ions in nutrition medium, followed by irradiation with gamma radiation. Figure 1 illustrates the absorption spectra of *Spirulina platensis* grown in a standard Zarrouk medium, where potassium (K^+) ions were substituted with cesium (Cs^+) ions. Two conditions were tested: in the first case, the Cs^+ concentration was 0.3 g/200 mL (1), and in the second case, the Cs^+ concentration was 0.15 g/200 mL (2). As observed in Figure 1, no growth or development of the culture was recorded at the higher Cs^+ concentration (0.3 g/200 mL). However, at the lower Cs^+ concentration (0.15 g/200 mL), the absorption spectra closely resembled those of the control cells.

The next stage of the study focused on examining the effect of radiation exposure on the culture grown in a modified Zarrouk medium containing Cs^+ ions at a concentration of 0.15

g/200 mL. These cells were exposed to gamma radiation at a total dose of 150 kGy, followed by the transfer of the irradiated culture to a standard Zarrouk medium. The results are presented in Figure 1. It can be observed that the absorption spectrum of *Spirulina platensis* after cultivation in the modified medium closely matches the spectrum of *Spirulina platensis* that was irradiated after cultivation in the modified medium (2) and subsequently re-cultured in the standard medium (3). The absorption spectra shown in the figure did not reveal any differences like the spectral composition; the only variation observed was in the concentration levels.

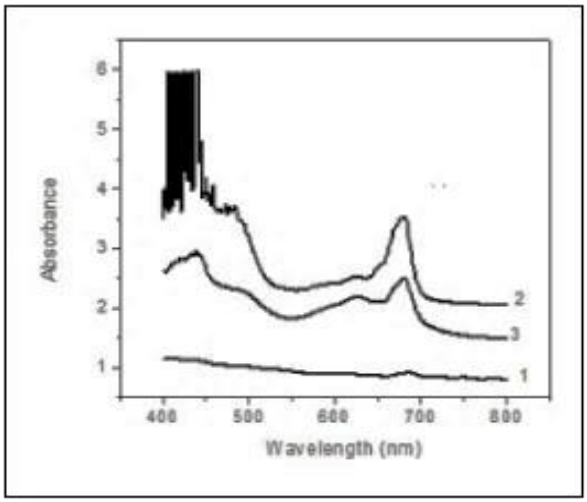

Figure 1. Effect of gamma radiation on the absorption spectra of *Spirulina platensis* at different K^+ and Cs^+ ion ratios

1 – Spirulina in the modified nutrient medium with a high concentration of Cs^+ ions (not irradiated). 2 – Spirulina in the modified nutrient medium with a balanced concentration of K^+ and Cs^+ ions before irradiation. 3 – Spirulina in standard Zarrouk nutrient medium used for post-irradiation cultivation of spirulina cells exposed to a gamma radiation after case 2.

Figure 2 presents the absorption spectrum characteristics of *Spirulina platensis*. The absorption peak at 681 nm corresponds to chlorophyll a (Chl a), while the peak at 621 nm is associated with phycocyanin (PC). Additionally, the peak at 440 nm is attributed to the Soret band of Chl a. The data presented in Figure 2 demonstrate that an increase in the metal concentration in the nutrient solution leads to a decrease in absorption intensity in both control (spirulina as control cultivated is in Zarrouk's modified medium containing Cs(I) ions at a concentration of 0.15 g/200 mL) and irradiated cells. Additionally, the effect of cesium ions on the same cellular components of *Spirulina platensis* was examined at the same gamma irradiation dose. Figure 3 illustrates the effect of cesium ions on the absorption intensity maxima on the constituents of spirulina at wavelengths of 440 nm, 621 nm, and 681 nm. Cases 1 and 2 in Figure 3 indicate that changes in the absorption intensity of *Spirulina platensis* components (chlorophyll a, phycocyanin, and carotenoids) follow a consistent pattern across all components. Specifically, as the cesium concentration increases, the absorption intensity decreases. This reduction occurs uniformly in both control cells and cells that were irradiated and subsequently recultivated.

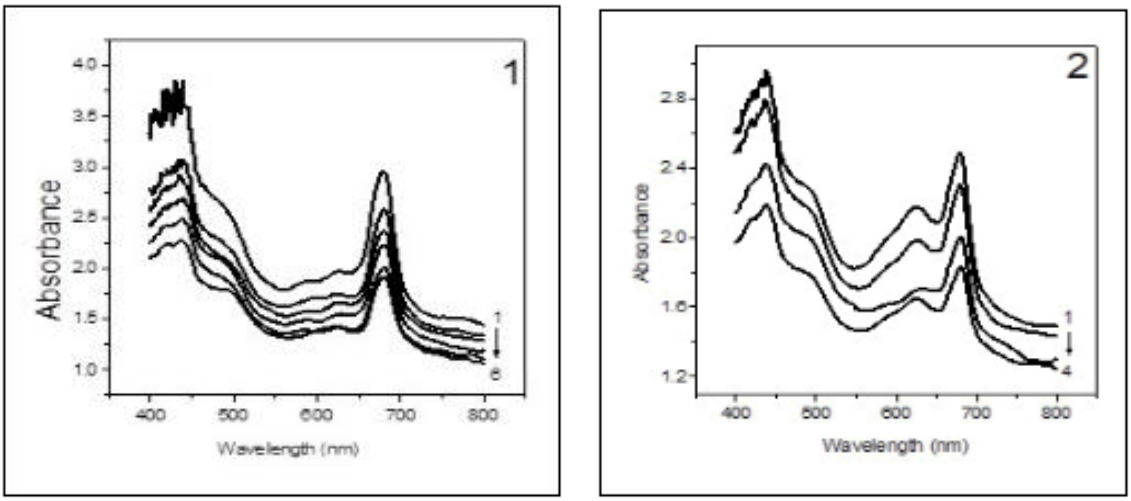

Figure 2. Effect of cesium ions ([Cs$^+$]1à6= (0; 4 ÷ 8 mM) on the absorption spectra of control (1) and irradiated and re-cultivated *Spirulina platensis* cells (2) [Cs$^+$]1à4= (0; 4 ÷ 6 mM).

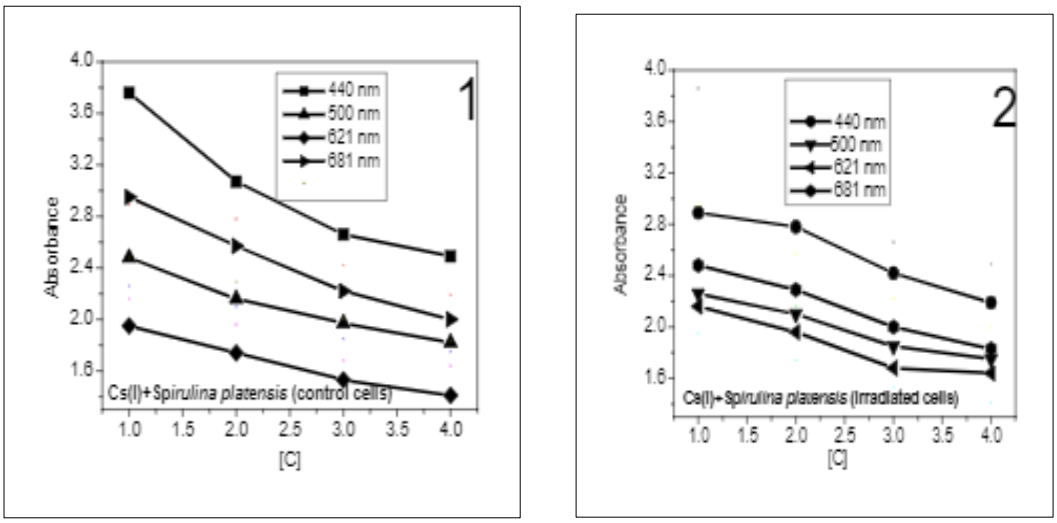

Figure 3. Effect of gamma radiation on changes in the spectral characteristics of *Spirulina platensis* components as control (1), as irradiated cells (2) after re-cultivation. (440 nm – Soret band of chlorophyll a.; 621 nm – Phycocyanin (basic protein); 681 nm – Chlorophyll a; 500 nm – Carotenoids).

By comparing the results in the figures, it is evident that the change between the maximum and minimum absorption values for the control culture at 440 nm is 33%, while for irradiated Spirulina platensis, it is 25%. At 500 nm, the changes are 27% for the control and 22% for the irradiated cells. At 621 nm, the changes are 28% and 24%, respectively, and at 681 nm, the values are 32% and 26%. The largest difference is observed at 440 nm, with an 8% variation. A similar effect has been reported in other publications [11-14]. In work [11], the analysis and identification of irradiated spirulina powder were conducted using three-stage infrared macro-fingerprint spectroscopy. The study demonstrated that the saccharides in the spirulina powder exhibited higher thermal stability than the proteins. However, the autopeaks of the irradiated

samples showed distinct differences compared to the non-irradiated sample. The extracted biomasses of four cyanobacteria (*Nostoc carneum, Nostoc insulare, Oscillatoria geminata, and Spirulina laxissima*) grown in axenic mass culture were tested for their ability to adsorb four radionuclides (^{134}Cs, ^{85}Sr, ^{226}Ra, and ^{241}Am) under various pH regimes. Additionally, two of the cyanobacterial biomasses *(N. carneum* and *O. geminata*) were phosphorylated before testing their capacity as radionuclide adsorbers. Non-phosphorylated cyanobacterial biomass showed very low adsorption of ^{134}Cs [9]. The accident at the Fukushima-1 nuclear power plant in March 2011 resulted in the release of exceptionally high levels of radionuclides into the environment, primarily ^{137}Cs, ^{90}Sr, and ^{131}I. Since these radionuclides are biophilic, they pose a significant risk due to their biological uptake and subsequent food chain contamination within the ecosystem. In a study [10], researchers selected microalgae and aquatic plants capable of effectively removing radionuclides from the environment. They demonstrated that these organisms have the highest ability to eliminate radioactive **^{137}Cs** through cellular accumulation. Recent studies have emphasized that adsorption is critical in removing **^{137}Cs** from wastewater for environmental remediation. Over the past decade, significant research has focused on new adsorbents, such as Prussian blue, graphene oxide, hydrogels, and Nano adsorbents, due to their remarkable cesium adsorption capacity [14]. However, microalgae remain one of the primary adsorbents.

Despite the practical importance of cesium uptake by cells, its physiological role has not been sufficiently studied. However, since ^{137}Cs is a close analog of potassium, cells tend to utilize it for similar functions. Nevertheless, cesium differs significantly from potassium. Experimental studies have shown that during passive transport, the permeability of cesium ions through cell membranes is approximately six times lower than that of potassium ions [15]. Additionally, cesium blocks potassium channels. Replacing potassium ions with cesium ions likely leads to inhibition, even when the proportion of cesium is no more than 2% of the total potassium content [16]. This may indicate the physiological distinctiveness of these elements. The arrangement of ions likely results from their specificity in passing through potassium channels. The sizes of the cations in question are such that potassium ions (**K^+**) exhibit the highest permeability. The other ions, due to their larger sizes and different capacities to lose hydration shells, face a slower rate of crossing cell membranes. Cesium ions, in particular, can block potassium channels, preventing the passage of potassium ions through them. These factors may explain the specificity of cesium ion action when exposed to the irradiated culture of *Spirulina platensis*.

Thus, the optical properties of *Spirulina platensis* grown in modified Zarrouk & apos;s medium with Cs^+ ions (0.15 g/00 mL), irradiated with ^{137}Cs gamma radiation (150 kGy), and subsequently re-grown in standard Zarrouk's medium do not show significant differences. Additionally, there are no observed differences in the content of Cs^+ ions in the same cellular components of *Spirulina platensis* between control cells and irradiated cells.

Based on the data obtained, we can conclude the following:

1. Cesium ions are not chemically toxic when affecting the optical properties of *Spirulina platensis*. Moreover, a high level of radioresistance can allow for the absorption of high concentrations of radioactive cesium (^{137}Cs) without significantly impacting the growth

and development of the culture, as well as the intensity of post-radiation recovery at high doses of ionizing radiation. It is possible, that the process of post-radiation recovery in *Spirulina platensis* culture completely halts in the absence of potassium ions in the nutrient medium.

2. The primary mechanism on post-radiation growth and development of irradiated cells is the partial replacement of potassium ions, which are essential for cellular life and in this case was not observed the negative effect of cesium ions.

REFERENCES

[1]. Iwamoto, Koji, and Yoshihiro Shiraiwa, 2017, Accumulation of cesium by aquatic plants and algae. Impact of cesium on plants and the environment, 171-185.
[2]. Yadav Mahendra, Kumar Vivek, Jain Shelly, Sandal, Nidhi Chauhan, Meenakshi, 2022/04/09, Assessment of Adsorption and Removal Efficacy of Spirulina Powder for Strontium and Thallium, Preprint, DOI:10.21203/rs.3.rs-1539864/v1.
[3]. Mahendra Yadav, Komal Rani, Nidhi Sandal, Meenakshi Kanwar Chauhan, 2022, An approach towards safe and sustainable use of the green alga Chlorella for removal of radionuclides and heavy metal ions, Journal of Applied Phycology, 24, 2117-2133.
[4]. Xindai Li, Guangming Xu, Meng Xia, Xinyao Liu, Fuqiang Fan, Junfeng Dou. Research on the remediation of cesium pollution by adsorption: Insights from bibliometric analysis Chemosphere, Volume 308, Part 2, 2022, 136445.
[5]. R. Jalali-Rad, H. Ghafourian, Y. Asef, S.T. Dalir, M.H. Sahafipour, B.M. Gharanjik Biosorption of cesium by native and chemically modified biomass of marine algae: introduce the new biosorbents for biotechnology applications. Journal of Hazardous Materials. Volume 116, Issues 1–2, 10, 2004, Pages 125-134.
[6]. Anna Burger, Irene Lichtscheidl. Stable and radioactive cesium: A review about distribution in the environment, uptake and translocation in plants, plant reactions and plants' potential for bioremediation. Science of The Total Environment. Volume 618, 15, 2018, Pages 1459-1485.
[7]. Shahjalal Khandaker, Megumu Fujibayashi, Takahiro Kuba. Innovative potassium hexacyanoferrate intercalated into layered double hydroxide adsorbent for efficient cesium removal from seawater. Separation and Purification Technology. Vol. 354, Part 5, 2025, 128984.
[8]. C Zarrouk. 1966, Contribution a l'etude d'une Cyanobacterie: Influence de Divers Facteurs Physiques et Chimiques sur la Croissanceet la Photosynthese de *Spirulina maxima* (Setchell et Gardner) Geitler. Ph. D. Thesis. University of Paris, France.
[9]. P Dalgaard and K Koutsoumanis.2001, Comparison of maximum specific growth rates and lag times estimated from absorbance and viable count data by different mathematical models. J. Microbiol. Meth., 43, 183-94.
[10]. PR Pai, A Manasa, T Kalaivani, CPM Ajeesh, C Rajasekaran and BN Prasad, 2008, Simplified Cost-Effective Media Variants for the Rapid Culture of *Spirulina platensis*. Recent Advances in Biotechnology, Excel India Publishers, New Delhi, 2008, 1-129.

[11]. Hai Jing Liu, Chang Hua Xu, Qun Zhou, Feng Wang, Wei Ming Li, Yi Ming Ha, Su Qin Sun, 2013, Analysis and identification of irradiated Spirulina powder by a Three - step infrared macro-fingerprint spectroscopy, Radiation Physics and Chemistry,85, 210-217.

[12]. Pohl, P., Schimmack, W., 2006, Adsorption of Radionuclides (^{134}Cs, ^{85}Sr, ^{226}Ra, ^{241}Am) by Extracted Biomasses of Cyanobacteria (Nostoc Carneum, N. Insulare, Oscillatoria Geminata and Spirulina Laxis-Sima) and Phaeophyceae (Laminaria Digitata and L. Japonica; Waste Products from Alginate Production) at Different pH. J Appl Phycol. 18, 135–143.

[13]. Fukuda, Sy., Iwamoto, K., Atsumi, M. et al.,2014, Global searches for microalgae and aquatic plants that can eliminate radioactive cesium, iodine and strontium from the radio-polluted aquatic environment: a bioremediation strategy. J Plant Res.127,79–89.

[14]. Muhammad Yaqub, Ladawan Mee-Ngern, Wontae Lee, 2024, Cesium adsorption from an aqueous medium for environmental remediation: A comprehensive analysis of adsorbents, sources, factors, models, challenges, and opportunities, Science of The Total Environment, 950, 175368.

[15]. Yurin V.M., Sokolik A.I., Kudryashov A.P. Regulation of Ion Transport Through Plant Cell Membranes. Minsk: Navuka i Tehnika, 1991. 272 pp. (in Russian).

[16]. Yudintseva E.V., Gulyakin I.V. Agrochemistry of Radioactive Isotopes of Strontium and Cesium. Moscow: Atomizdat, 1968. 472 pp. (in Russian).

A BRIEF OVERVIEW OF THE CAUSES OF LUNG CANCER AND MEASUREMENTS OF RADON CONCENTRATIONS

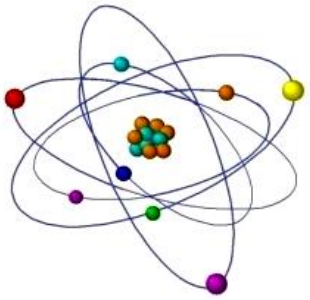

***Magda Metskhvarishvili[1], Samson Pagava[1], Kakha Gorgadze[1,2], Medea Burjanadze[1], Nikoloz Vachadze[3], Iamze Kalandadze[1,2], Natia Beriashvili[2]**

[1]"Talga" Institute of Georgian Technical University, Georgia
[2]Georgian Technical University, Faculty of Informatics and Control Systems
[3]Tbilisi State Medical University, Georgia

https://doi.org/10.63465/rrs520258980 *Corresponding author: m.metskhvarishvili@gtu.ge

ABSTRACT**:** *Ionizing radiation is a well-established carcinogen. A great number of epidemiologic and experimental studies demonstrated that radiation can cause most forms of cancer. Largest contribution to the exposure of general population by ionizing radiation comes from natural sources. Sources of ionizing radiation in a human's normal living environment are cosmic rays, terrestrial and internal radiation. In average, natural background radiation is responsible for annual effective dose of about 2-3 mSv although this value varies in wide range around the world and one can easily find the areas with up to 10 times greater exposures, mainly due to high levels of radioactive gas – radon. In general, inhalation of radon gas and its progeny is responsible for the greatest component of annual exposure of an average person (about 50%). In the article the causes of lung cancer are discussed. The most important cause of lung cancer is tobacco smoke. According to some estimates, about 90% of lung cancer cases are resulted from smoking. However, it is generally recognized that there are other risk factors, as well. The radon represents the second most important cause of lung cancer after tobacco. Indoor radon concentrations can vary greatly between different geographic regions and different types of building structures. In addition, they exhibit a large range of temporal variations. Since radon emanates from the soil beneath the building, the highest concentrations will be found in basements and first-floor rooms. However, more extensive and large-scale measurements and studies are needed. Assessment of radon concentration levels in different types of buildings throughout the country will allow to estimate the radiation doses due to radon exposure and associated risks for different population groups in Georgia.*

The results of the research obtained at some test objects in three districts of Tbilisi - Vake, Saburtalo, Nadzaladevi settlements, are also presented. Radon concentrations in apartments and soil gas has been measured, and gamma radiation background was determined also.

Key words*:* radon, cancer, radiation, exposure, soil

INTRODUCTION

Radon is a natural inert radioactive gas that is produced by the radioactive decay of uranium and thorium present in the Earth's crust. Radon migrates from the soil into the air and depending on a building's construction type and other geological and environmental factors, it may accumulate in practically all parts of the building – living, working, and other areas. Radon

enters the human body mainly through inhalation. Although radon, as an inert gas, mostly leaves the respiratory organs during exhalation, its radioactive decay products, especially polonium isotopes ^{218}Po and ^{214}Po, are deposited in the lungs and cause the irradiation of sensitive cells of the respiratory tract with high ionization potential alpha particles.

Although the main reason of elevated radon concentrations in indoor air usually is emanation of this gas from the subsoil, under some circumstances the building materials enriched by ^{222}Ra and radon dissolved in water may become the significant sources of exposure.

Radon decays into a series of short-lived radionuclides (fig. 1). Some of them – ^{218}Po, ^{214}Po, ^{214}Pb, and others – are also alpha-emitting. In general, under normal circumstances, the largest dose from radon and its decay products will be delivered to the lung. Doses to other organs and tissues are much smaller [1] and, therefore, when considering the radiological impact of radon and its progeny, the focus is usually placed on the risk of lung cancer.

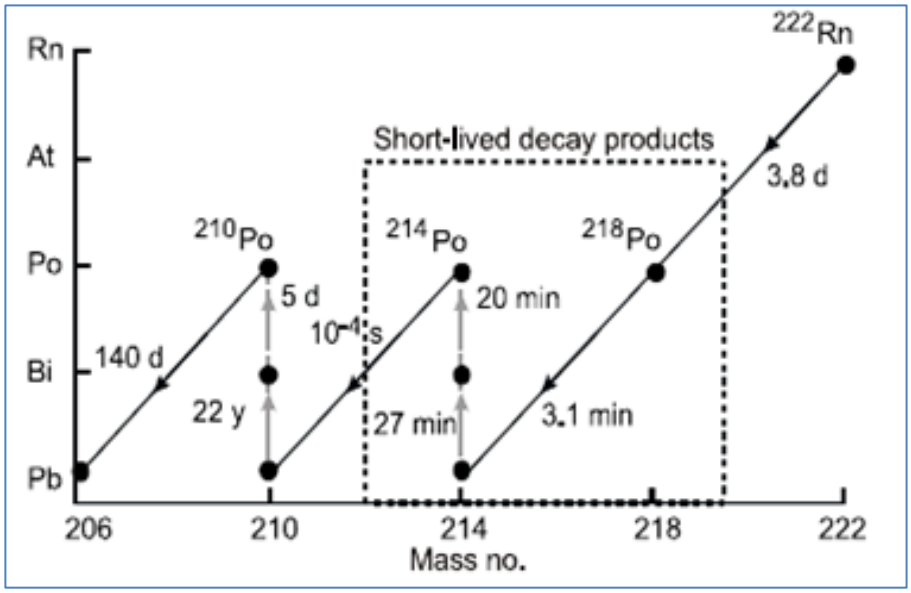

Fig. 1 Radon decay chain [1]

If radon gas is inhaled during normal respiration process, some fraction will be absorbed through the lung, but the majority will be exhaled. However, the short-lived radon progeny which are the isotopes of solid elements tend to be deposited on the bronchial epithelium and will decay there irradiating the cells lining the respiratory tract by high-LET alpha radiation.

Using sophisticated mathematical modeling methods, indicated that the doses resulted from inhaled radon progeny are non-uniformly distributed within the respiratory tract, with the highest values in the bronchial and bronchiolar airways [2].

The basal and secretory cells, located at the depth of 10-50 μm, are assumed to be the most probable target cells from which lung cancer originates [3]. Alpha particles emitted during the decay of ^{214}Po and ^{218}Po have the range of 48 to 71 μm in tissue and, therefore, are able to damage the DNA molecules of these cells, thus, giving rise to the potential malignant change, especially taking into account a bystander mutagenic effect which may amplify significantly the risk [4].

Radon Exposure

The first documentary evidence of carcinogenic effect of radon exposure comes as early as from the 16th century, in particular, from the German scholar Georgius Agricola (1495-1555) who described in his greatest work *De re metallica* the high mortality rates among the miners in the Carpathian Mountains of Eastern Europe. Autopsy studies of miners from that region carried out more than 300 years later, demonstrated that lung cancer should have been a common cause of death [5].

Discovery of high radon levels in underground mines in the early 20th century and epidemiologic studies of radon-exposed miners during the 1950s and 1960s confirmed the association between radon exposure and lung cancer (fig. 2) (The working level (WL) is defined as any combination of the short-lived radon progeny in one litre of air that results in the ultimate release of 1.3 x 105 MeV of potential α-particle energy. Exposure to this concentration for 170 h (or twice this concentration for half as long, etc.) is defined as a working level month (WLM). An individual living in a house with a radon concentration of 20 Bq m~3 will be exposed to around 0.08 WLM per year) [6, 7].

On the basis of these epidemiologic evidence, cellular mutagenesis studies and experimental research on animal species, World Health Organizati on (WHO)'s International Agency of Research on Cancer has classified radon as an A class human carcinogen [8, 9]

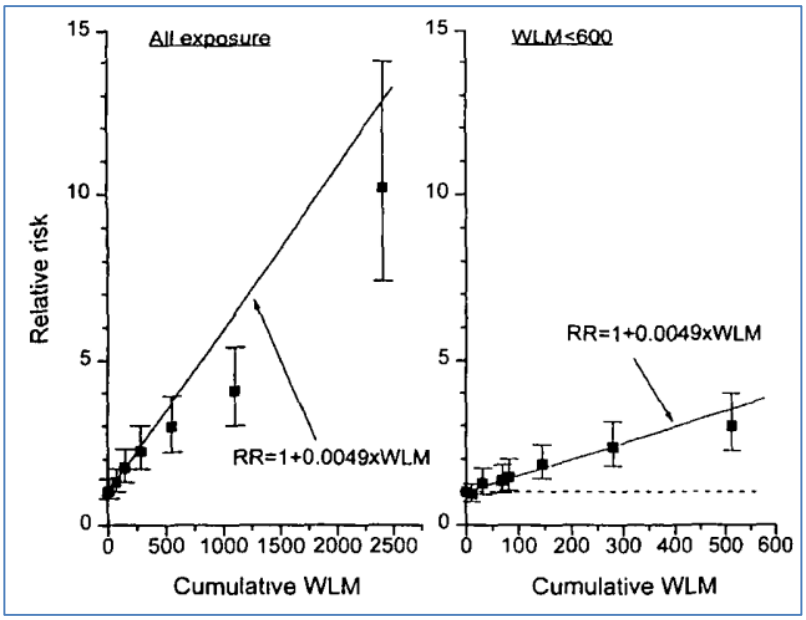

Fig. 2 Relative risk of lung cancer with cumulative radon exposure [6]

The established connection between radon and lung cancer in miners had raised concern for the possibility that exposure to radon in homes might also cause lung cancer in the general population, especially, taking into account that the risk of lung cancer from radon is related to both the radon level and the exposure duration [10]. Interest to this problem enhanced dramatically in the 1970s and 1980s when the residential buildings with significantly elevated indoor radon levels were discovered in a number of countries. One of the examples of such dwellings is the so-called Castleisland House in South-West Ireland where the radon

concentration of approximately 49,000 Bq/m^3 has been observed [11]. It is almost 250 times higher than the reference level of 200 Bq/m^3 for EU countries and 300 times higher than the action level of 4 pCi/l (148 Bq/m^3) established by US EPA [12].

Risk Estimates.

The US National Academy of Science BEIR VI committee published a comprehensive report on the health effects of radon in 1999. The committee used the results of 11 major studies of underground miners involving together about 68,000 men, of whom 2,700 have died from lung cancer. On the basis of these data, the committee derived two models for lung-cancer risk from radon exposure: "exposure-age-concentration model" and "exposure-age-duration" model. The calculations indicated that radon can be responsible for about 1 in 10 or 1 in 7 of all lung-cancer deaths, depending on which of these two models are used. The number of radon-related lung-cancer deaths resulting from that analysis could be between 3,000 and 33,000 each year [13].

However, extrapolation of the data derived from miner studies to the radon exposure of general population in homes is associated with some limitations and uncertainties due to differences in the age and sex composition of these two groups, environmental conditions in mines and residential buildings, dosimetric methods used, and the percentage of cigarette smokers within the considered populations [14]. The risk analyses conducted more recently usually take into account exposure-response relations derived both from cohorts of miners and from residential studies and consider the observed synergistic interaction between radon and smoking. Two examples of recent publications on this subject are the radon induced lung cancer risk analyses performed in Canada and France [15,16].

Within the Canadian study [Brand et al., 2005], the excess lifetime risk of lung cancer from radon in Canada is estimated on the order of 5/1,000 for the general population and as 40/1,000 for ever-smokers. Catelinois et al. concluded that "of the 25,134 lung cancer deaths in France during 1999, indoor radon probably caused 5-12%" [16].

In addition, to take into consideration the age dependence of radon induced lung cancer, published the practical tables of calculated lifetime relative risks for exposures between any two age intervals from 0 to 110, for various radon concentrations from 100 to 1,000 Bq/m^3 [10]. These data indicate that exposure in the first 33 years of life contributes to about half of the total excess risk and, consequently, the risk is higher for individuals in middle age (30-50 y), compared to the later years.

Experiment.

New research into radon-related lung cancer continues today. For example, according [17] researchers endeavor to ascertain the potential risk of lung cancer associated with measured radon concentrations. To this end, an extensive, long-term (2–3 months) radon monitoring campaign was executed by strategically positioning Columbia Resin-39 (CR-39) solid-state nuclear track detectors at 28 distinct locations. The overarching aim of this effort is to comprehensively assess the health hazards posed to both staff and students and subsequently institute any requisite mitigating measures. Also, the article [18] presents new research methods. In the publication [19] it is mentioned that public information materials about radon require revision. Specifically, they emphasize that radon causes lung cancer.

Measurements of radon concentrations at test facilities in different areas of Tbilisi [20], [21] showed how important it is to carry out these works in populated areas, take safety measures and transferring of information to the population. Radon concentrations and gamma radiation dose values was measured in individual apartments and soil gas located in Vake, Saburtalo and Nadzaladevi administrative districts of Tbilisi.

Relatively low (0.1 ÷ 5.0) kBq/m^3, medium (5.1 ÷ 10.0) kBq/m^3 and relatively high (10.1 ÷ 19) kBq/m^3 concentrations of radon were recorded in the soil gas. Gamma-dose distribution is not characterized by sharp features in the interval of 100-130 nSv h^{-1}. Relatively high concentrations of radon in soil gas were observed in three (northern, central, and southern) sub-latitudinal (east-west) bands characterized by strong and thick-bedded Paleogene rocks. All three bands represent a hypsometrically raised terrain, where fissured rocks directly protrude from the ground surface or are covered by a thin layer of soil. Average and relatively low concentrations of radon in soil gas were observed in the areas between the north, central and south sub-latitudinal direction bands, with hypsometrically depressed terrain, built with upper Paleogene-lower Neogene clays and sandstones, where dense rocks are overlain by typical, fluvial and slope rocks of Quaternary (anthropogenic) age. with alluvial (deluvian) clay-sand formations and a thick soil cover (Fig. 3).

Radon concentrations were measured in the air of basements and first floors of apartments and public buildings located in the study areas (Vake, Saburtalo and Nadzaladevi). Unlike the concentrations of radon observed in soil gas, their value does not exceed the legal concentration limit of the USA, EU and Georgia (Fig. 4). However, a large-scale study is necessary.

Risk associated with radon exposure is particularly relevant for Georgia, because the country's geological formations are characterized by a high content of uranium; in addition, many buildings are constructed with locally produced materials. Therefore, radon is a potentially serious problem in Georgia. Although the "National Environmental Hygiene Action Plan" and the "National Health Policy" recommend monitoring radon exposure, systematic assessment has not been conducted in Georgia to date, and there are practically no data on radon concentrations in buildings. According to the International Atomic Energy Agency, information on radon concentrations in Georgia cannot be found in international radiation information databases, as well as on global and regional radiological maps, unlike other European countries [22].

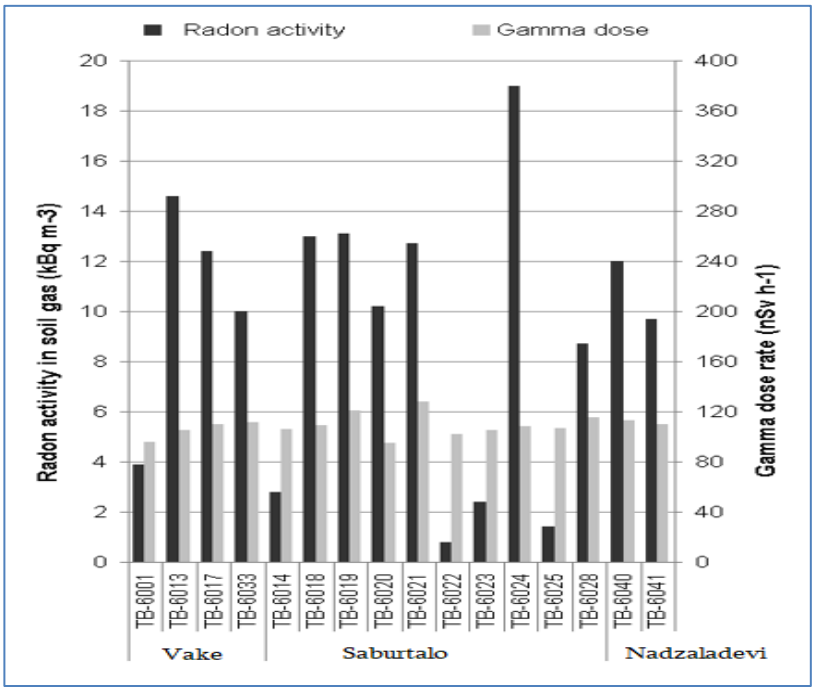

Fig. 3 Values of radon concentration and gamma radiation dose in soil gas

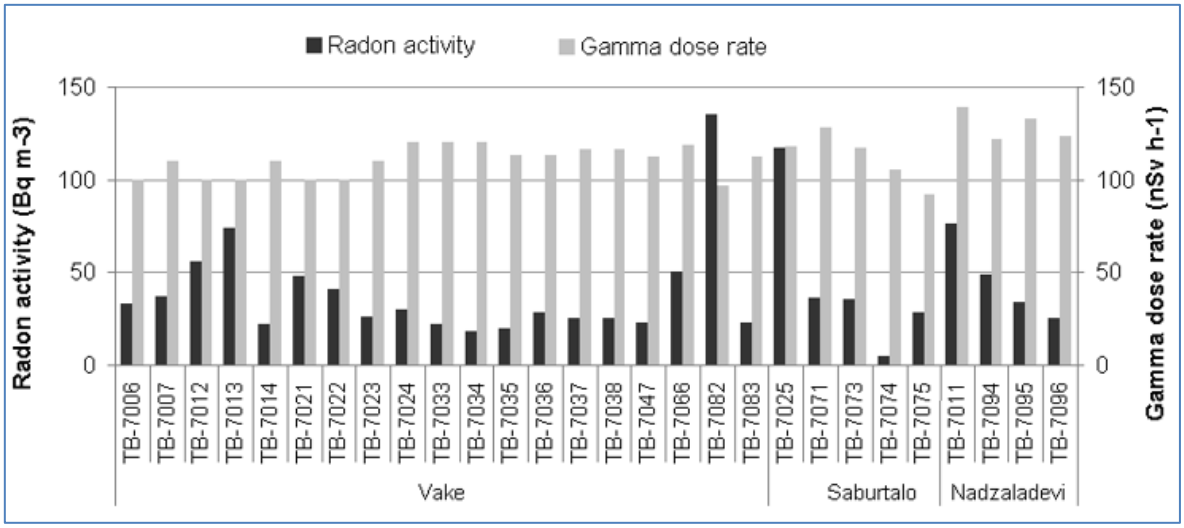

Fig. 4 Values of radon activity and gamma radiation dose in individual apartments

CONCLUSION

Because the risk of lung cancer is very high under conditions of constant radiation [23], it is very important to measure radon concentrations both in residential buildings and in spaces where people have to stay for a long time, such as offices, schools, gardens, etc.

REFERENCES

[1] Kendall G.M., Smith T.J. Doses to Organs and Tissues from Radon and its Decay Products. Journal of Radiological Protection, Vol. 22, pp. 389-406, 2002;

[2] Puskin J. S., James A.C. Radon Exposure Assessment and Dosimetry Applied to Epidemiology and Risk Estimation. Radiation Research, Vol. 166, pp. 193-208, 2006;

[3] Böhm R., Nikomedova D., Holy K. Use of Various Microdosimetric Models for the Prediction of Radon Induced Damage in Human Lungs. Radiation Protection Dosimetry, Vol. 104, No 2, pp. 127-137, 2003;

[4] Samet J.M. Residential Radon and Lung Cancer: End of the Story? J. Toxicology and Environmental Health A, Vol. 69, pp. 527-531, 2006;

[5] Frumkin H., Samet J.M. Radon. A Cancer Journal for Clinicians, Vol. 51, No 6, pp. 337-344, 2001;

[6] Darby S., Hill D., Doll R. Radon: A Likely Carcinogen at All Exposures. Annals of Oncology, Vol. 12, pp. 1341-1351, 2001;

[7] Darby S.C., Hill D.C. Health Effects of Residential Radon: A European Perspective at the End of 2002. Radiation Protection Dosimetry, Vol. 104, No 4, pp. 321-329, 2003;

[8] IARC. Man Made Mineral Fibers and Radon, 1988;

[9] IARC Working Group, Ionizing Radiation, Part2: Some Internally Deposited Radionuclides, 2001;

[10] Chen J. Estimated Risks of Radon-Induced Lung Cancer for Different Exposure Profiles Based on the New EPA Model. Health Physics, Vol. 88, No 4, pp. 323-333, 2005;

[11] Organo C. et al. High Radon Concentrations in a House near Castleisland, County Kerry (Ireland) – Identification, Remediation and Post-Remediation. Journal of Radiological Protection, Vol. 24, pp.107-120, 2004;
[12] WHO Info Sheet. Radon and Health. March, 2004;
[13] EPA Assessment of Risks from Radon in Homes, 2003;
[14] Neuberger J.S., Gesell F.G. Residential Radon Exposure and Lung Cancer: Risk in Non-Smokers. Health Physics, Vol. 83, No 1, pp. 1-18, 2002;
[15] Brand K.P., Zielinski J.M., Krewski D. Residential Radon in Canada: An Uncertainty Analysis of Population and Individual Lung Cancer Risk. Risk Analysis, Vol. 25, No 2, pp. 253-269, 2005;
[16] Catellinois O., Rogel A., Laurier D., Billon S., Hemon D., Verger P., Tirmarche M. Lung Cancer Attributable to Indoor Radon Exposure in France: Impact of the Risk Models and Uncertainty Analysis. Environmental Health Perspectives, Vol. 114, No 9, pp. 1361-1366, 2006;
[17] Yonca Yahsi Celen, Sule Oncul, Barıs Narin, Osman Gunay. Measuring radon concentration and investigation of it's effects on lung cancer. Journal of Radiation Research and Applied Sciences. V., Issue 4, December 2023, 100716. https://doi.org/10.1016/j.jrras.2023.100716
[18] Yangyang Feng**,** Xiongjie Zhang**,** Yan Zhang**,** Ye Zhang**,** Xingyu Tian**,** Rengui Huang**,** Jie Cao and Bin Tang. A new method for evaluating the stability of radon concentration in a radon chamber. IOP Publishing Ltd and Sissa Medialab. Journal of Instrumentation, V. 18, July 2023. DOI 10.1088/1748-0221/18/07/P07045
[19] Nancy Vogeltanz-Holm, Gary G. Schwartz. Radon and lung cancer: What do the public really know? Journal of Environmental Radioactivity. V. 192, December 2018, Pages 26-31
[20] M Metskhvarishvili, S. Pagava, K Gorgadze, Sh. Dekanosidze, I. Kalandadze, M Beridze, N. Beriashvili. Determination of Radon Concentrations In. Mtatsminda Districts of Tbilisi. Radiobiology and Radiation Safty. Vol. 2 No. 3 (2022). https://radiobiology.ge/index.php/rrs/article/view/4849
[21] Determination of radon concentrations in some districts of Tbilisi. International conference "Global practice of multidisciplinary scientific research" dedicated to the 100th anniversary of "Technical University of Georgia". June 24-26, 2022 S Georgia. Georgian Technical University. Georgian Science and Technology Association. IKSAD Institute. A collection of articles. pp. 1005-1009.
[22] Global Information System on Alcohol and Health (GISAH). Public health and environment. Radon database, National radon activities. Data by countries. World Help Organization 2021.
https://apps.who.int/gho/data/node.gisah.RADON01?lang=en
[23] Metskhvarishvili M., Pagava S., Gorgadze K., Dekanosidze Sh., Beriashvili N. Radon exposure and lung cancer. Georgian Scientist. V. 5, Issue 1, p. 219-227 (2023). https://doi.org/10.52340/gs.2023.05.01.18

3D VISUALIZATION OF NUCLEAR DAMAGES IN HISTONE H2B-GFP TAGGED HE-LA CELLS: POST-IRRADIATION IMAGING

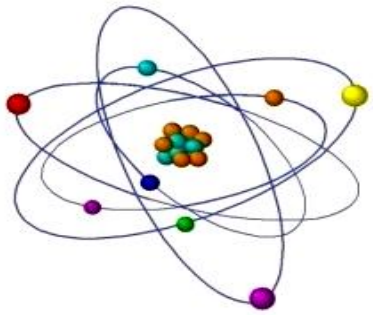

"[1,2]Lili Nadaraia*, [1]Veriko Okuneva,
[1,3,4] Mikheil Nanikashvili, [1]Pavel Tchelidze

[1] Scientific and Education Center by Carl Zeiss, New Vision University, Georgia
[2] Republic Center of Structure Research, Georgian Technical University, Georgia
[3] Georgian Scientific Industries LLC, [4] Georgian Science Innovation Organization, Georgia

https://doi.org/10.63465/rrs520258981 *Corresponding author: Email: nadaraia@gtu.ge

ABSTRACT: *Here we suggest visualization of the spatial nuclear changes using unique He-La cell line stably expressing histone H2B-GFP fused protein as a chromatin signature. To do this we offered Carl Zeiss LSM900 confocal microscope-based acquisition of Z-stacks, coupled with the 3D image reconstruction and rendering using ZEN and UCSF Chimera. Our recently displayed 2D images, showed that γ-irradiation leads to spatially very complex nuclear changes, so that one can easily defined that 2D approach is largely unable to yield precisely analyzed results. Meaning that in our experiments γ-irradiation in dose of 30 Gy leaded to the drastic nuclear deformations, followed by fragmentation and massive emergence of multi-nucleated cells, we resorted to only reliable analytical way, namely to 3D visualization and modeling approach. Our interest was spotlighted on the γ-irradiation induced nuclear and nucleolar changes due to: (i) the cell nucleus is the largest, highly ordered but dynamic cellular compartment, housing around 1.5 m DNA strand in common genome length. Although giant sizes complete genome is spatially precisely arranged being compacted inside confine of average 15-20 μm in diameter. Such a big sizes expose nuclear chromatin to natural but potentially damaging factors, particularly to γ-irradiation. Therefore, it is crucial to follow dynamics and degree of morphological damages, under permanent monitoring of nuclear viability; (ii) the common length of rDNA chromatin clustered as tandems of r-genes is also large enough to represent easily accessible target after being exposed to γ-irradiation. Because, the key function of the nucleolus, as a ribosome factory, plays central role in whole cellular metabolism, monitoring of related structural damages are particularly challenging.*

Using 3D imaging/modeling hardware combined with UCSF Chimera we managed to describe in details specific nuclear/nucleolar damages aroused as a consequence of γ-irradiation with dose of 30 Gy. In fact, present work represented first attempt to show modern digital 3D visualization facilities in order to motivate young Georgian bio-medical scientist to use available software and other microscopy-based digital techniques for the living and fixed cell/tissue 3D/4D imaging. Importantly, all these facilities are locally available at "Open Platform for Advanced Microscopy" established in New Vision University "Scientific and Education Center by Carl Zeiss".

Key word: He-La Cells, 3D-visualization, irradiation, nuclear damages, imaging

INTRODUCTION

Why Nucleolus? The nucleolus, a vital nuclear compartment, orchestrates ribosome biogenesis by producing polycistronic transcripts. It integrates gene-rich chromosomal domains, forming nucleolus-

associated DNA (naDNA). The common length of rDNA chromatin clustered as tandems of ribosomal genes (rRNA genes, rDNA chromatin, r-genes) is also large enough to represent prime target after being exposed to UV and γ-irradiation [15-27]. The nucleolus hosts molecular machinery that guides the transcription of ribosomal genes, pre-rRNA processing, and ribosome assembly. It is generally accepted that organized as nucleolus, sites of localization and transcription of r-genes, together with products of their activity, represent highly sensitive sensors of cellular stress. Therefore, various chemical stress factors (including anticancer drugs) that inhibit different steps of ribosome biogenesis have been used as the most suitable tools to study structure-functional aspects of the nucleolus in compliance with entire cell metabolism [28-38]. Thus, previous studies using the rRNA synthesis chemical inhibitor Actinomycin D (AMD) showcased drastic reorganization caused by intra-nucleolar movement of nucleolar constituents, namely fibrillary centers (FCs) and dense fibrillary component (DFC) due to concerted contraction of nucleolus-associated DNA chromatin (NAC) [14].

Because, the key function of the nucleolus, as a ribosome factory, plays central role in whole cellular metabolism, monitoring of related structural damages are particularly challenging. While chemical inhibition has been extensively investigated [28-38] the impact of physical DNA damage on nucleolar organization remains less understood. γ-Irradiation, a powerful inducer of DNA single- and double-strand breaks in plant and animal cells, causes large-scale nuclear deformation, chromatin condensation, and apoptosis [13, 27, 39-42]. However, its specific effects on nucleolar structure, particularly on NAC dynamics and FC and DFC complex (hereafter FC/DFC assembly), are poorly characterized. Given nucleolar high rDNA content and its involvement in metabolic stability, rDNA clusters are prime targets for γ-irradiation-induced damage. It is therefore critical to determine whether such physical damage induces nucleolar segregation pattern similar to those observed during chemical inhibition [14, 28-30, 34, 35] or if alternative structural adaptations occur. Furthermore, the role of nucleolar proteins in mediating these responses remains an open question, with particular interest in the behavior of Pol I associated architectural transcription factor UBTF and pre-rRNA early processing factor fibrillarin. It is well documented that UBTF has long been acknowledged as the most specific marker of FC, while fibrillarin became recognized as widely used marker of DFC [14, 50].

Why γ-Irradiation? Having broadly explored inactivation dynamics through chemical r-genes transcription inhibition, here we planned to delve into the nuclear and nucleolar molecule-structural reorganization under severe DNA damage by physical factor γ-irradiation that induces single- and/or double-strand breakages. Our idea posits on presumption that γ-irradiation-induced nucleolar inactivation dynamics can mirror changes observed with AMD induced rRNA synthesis inhibition. For example, focusing on nucleolar changes, we can investigate if physically damaged naDNA exhibits similar movement as those after induced chemically. Correspondingly, this report deals with the nuclear/nucleolar 3D reorganizations under severe DNA damage induced by γ-irradiation using 30 Gy dose. As the most reliable model justifying nuclear/chromatin damages as well as aiming to future radiobiological/bio-medical application we employed a cancer cell line, namely He-La cells stably expressing histone H2B-GFP fusion proteins [14]. Based on data obtained in previous study [51] we applied experimental model that involves 3D imaging of possible post-γ-irradiation nucleolar inactivation monitoring intra-nuclear/intra-nucleolar changes developed within 0 - 72 hours' period of post-irradiation imaging.

In summary, our study investigates the three-dimensional structure and dynamics of nuclear and nucleolar reorganization following DNA damage induced by γ-irradiation. Using post-radiation time-lapse imaging over 72 hours, we analyzed nuclear deformation, chromatin remodeling, and apoptotic events in He-La cells stably expressing histone H2B-GFP. Volume light microscopy in living and fixed cells revealed key changes, including chromatin clumping, nuclear cleavage, and multi-nuclear cell formation. To assess nucleolar reorganization, we visualized FCs, that represents transcriptionally active rDNA sites, through anti-UBTF immunolabeling in fixed H2B-GFP HeLa cells. For immunolabeling of pre-rRNA early processing nucleolar sites, structured as DFC we applied anti-fibrillarin immunostaining.

Undeniably, the most informative digitalized 3D/4D approaches are highly important for science and education as all they are properly aligned with modern bio-medical tasks [14, 36]. Notable, that currently, baccalaurean, postgraduates and PhD students in the majority of Georgian Universities are

unable to use corresponding computed 3D/4D microscopy analysis in any kind of scientific work. Obviously, that the major obstacle that conditioned extremely limited scientific application of 3D/4D microscopy in Georgia is very high price of corresponding hard and soft ware. Therefore, another important goal of presented study is to show the simple way how to overcome mentioned obstacles and to demonstrate where and how young scientists can learn and use our modern instrumentals for 3D/4D digital microscopy imaging. Here we demonstrated effectiveness of widely spread GFP-based in situ labeling method as well as modern imaging techniques including optical tomography approach. All these techniques gained high priority being combined with related free software like "ImageJ" and UCSF Chimera. Most importantly, guided by modern microscopy strategies, "Scientific and Education Center by Carl Zeiss" (SECCZ) at New Vision University (NVU) can play a teaching/developmental role for early career investigators looking for a home for their progressive ideas. So, we seek to create a mentoring and cutting-edge scientific environment, encompassing young specialists and helping elevate the impact of their research through now available modern digital 3D/4D light and electron microscopy approaches.

MATERIAL AND METHODS

We utilized histone H2B-GFP transfected He-La cells obtained from Prof. O. Piot (University of Reims Champagne-Ardenne, France). Importantly, that now this unique cell line is in open access at NVU SECCZ. As our main goal was study of changes in nuclear and nucleolar morphology the choice of this cell line was based on their distinct features. Among most important features were: (i) the nuclear fluorescence of these cells demonstrated high stability, crucial for obtaining brightly fluorescent, of post-irradiated cells; (ii) these cells exhibited prominent intra-nucleolar fluorescence, identified as nucleosomal domains with the ultrastructural appearance of intra-nucleolar condensed chromatin (ICC). This characteristic was vital for our study; (iii) He-La cells are known for their large FCs associated with prominent DFC zones, aiding in the immunocytochemical discrimination of nucleolar sub-territories involved in r-gene transcription and pre-rRNA processing.

All basic experimental conditions, such as cell culture maintenance, growing and seeding quantitative parameters of cells submitted for working culture irradiation, irradiation machinery and regime, as well as digital microscope 3D image acquisition and 3D reconstruction/ visualization parameters were performed in full accordance with early reported data [51]. Additionally, in order to record specific 3D nucleolar changes in two nucleolar components (NCs) i.e. FC and DFC we employed anti-UBTF and anti-Fibrillarin immunocytochemical staining according presented below protocols (see section 2.2.)

Short Description of Irradiation procedure and Post-Irradiation Imaging.

Before being submitted to γ-irradiation, cells were briefly rinsed with PBS (3 times during 5 min), immersed in fresh medium, and the dishes were delivered to "GUPOS" γ-installation. Irradiation of cells was conducted directly in Petri dishes at a temperature of 35+/- 20C. As a source of γ-irradiation, the Cs137 isotope with a dose of 1.1 Gy/min has been utilized. After irradiation, cells were washed in PBS (3x5 min), returned to the cultivation media, and then s γ-installation subjected to time-lapse imaging during 0-72 h using Carl Zeiss (Germany) LSM 900 microscopes equipped with Axio Observer Z1/7 inverted microscope and AiryScan 2 augmented resolution device as it was recently described [51].

Post-Fixation 2D/3D Visualization of UBTF and Fibrillarin

Imaging of UBTF labeled cells is widely used to identify under-condensed active, potentially active and inactive rDNA genes folded into the structure of interphase FC and metaphase NORs [14, 36]. Meanwhile, imaging of anti-Fibrillarin labeled cells was performed because it is present at high concentration within the DFC where its rRNA methyl transferase activity is required for rRNA processing [14, 50]. These characteristics allowed to follow FCs and DFC as well as to study of their 3D modifications induced by γ-irradiation. For post-fixation imaging of anti-UBTF and anti-fibrillarin

mono- and double-immunolabeled cells we used primary monoclonal antibody conjugated with AlexaFluor488 and AlexaFluor594, both purchased from Santa Cruz Biotechnology (USA). This type of antibodies allows by mono-immunolabeling to use only one block for nonspecific binding in normal goat serum (NGS, Novex, USA) as well as avoid incubation with biotinylated secondary antibody by mono- and double-immunolabeling, thus making duration of immunostaining procedure notably shorter. Testing primary monoclonal antibodies conjugated with AlexaFluor594 (anti-UBF/F9 fragment and anti-fibrillarin) and AlexaFluor488 (anti-fibrillarin), we elaborated two protocols that sufficiently differ from early used schemes [14, 34].

By mono-labeling both, anti-UBTF as well as anti-fibrillarin procedures included four similar steps, namely: (i) after brief rinsing in PBS γ-irradiated samples were fixed at room temperature (RT) during 10 min in 4% PAF diluted in PBS and adjusted to pH 7.2-7.4 by 0.1N NaOH and rinsed repeatedly in PBS (3x5 min); (ii) cells were permeabilized by incubation in 1% TritonX-100 diluted in PBS during 5 min, and extensively washed in PBS; (iii) to block nonspecific binding, cells were incubated in 10% NGS in PBS during 60 min at RT; (iv) after removing NGS the cells were covered either by mouse anti-UBF/F-9 fragment or by mouse anti-fibrillarin AlexaFluor594 conjugated primary antibodies diluted (1:20) in PBS containing 1% NGS overnight at 4oC. After cells were washed with PBS (3x5 min), selected samples were submitted to LCM imaging according procedure described in 2.4.

For simultaneous visualization of UBTF (in red) and fibrillarin (in green) we utilized double labelling according protocol that includes following 6 steps: (i) as it was described above, briefly rinsed γ-irradiated cells were fixed in 4% PAF and rinsed again (ii) cells were permeabilized in 1% TritonX-100 prepared in PBS during 5 min, and extensively washed in PBS; (iii) to block nonspecific binding, cells were incubated in 10% NGS in PBS during 60 min at RT; (iv) after removing NGS the cells were covered with anti-UBF AlexaFluor594 conjugated primary antibodies diluted (1:20) in PBS containing 1% NGS overnight at 4oC; (v) after rinsing in PBS (3x5 min) cells were secondly incubated in 10% NGS during 60 min at RT; (vi) NGS was removed and cells were covered with anti-fibrillarin AlexaFluor488 (1:20) dissolved in PBS containing 1% NGS over night at 4oC. Being washed in PBS cells were submitted to LCM imaging directly in culture boxes.

3D Reconstruction and Visualization

As we reported recently for preliminary time-lapse analysis and visualization behavior of living cells damaged by γ-irradiation, obtained time series were transformed into 2D movies using ZEN 3.0 software [51]. For control, we used high-magnification LSM imaging conducted before γ-irradiation treatment. Importantly, living cell imaging allowed us to identify significant for 3D imaging points so that worth for visualization, drastic changes were detected during 48 – 72 hours of post-irradiation image acquisition period. Next, points of interest were extracted from whole dataset in order to visualize the changes in nuclear/nucleolar structural parameters, as well as coalescence of ICC clumps during γ-irradiation in 3D. The Z-stacks have been collected using up to 70 virtual sections taken with 0.3 μm step between individual section. Cells were examined and imaged in 512x512 pxl format. 3D models were generated using ZEN 3.0, “ImageJ” and UCSF Chimera. For this, obtained LSM volumes were exported to mentioned software for 3D reconstruction, rendering, visualization and modelling. At the final stage rendered 3D models were analyzed using rotation/tilting options in order to select most appropriate foreshortenings of resulted models.

RESULTS

The 2D images and 3D model of the nuclear exterior in control cells, that includes global shape and outline are presented on Fig. 1, a-k. Cells are exclusively mononuclear, while nearly all nuclei revealed roundish or elongated shape, mostly with slightly wave-like contours (Fig. 1, a-c). Nuclei revealing more or less profound invagination were observed just occasionally. Notably, cultures examined entirely showed absence of multi-nuclear cells. Another credible criterion indicating the good “health” of cells in cultures was abundancy of dividing cells which were at different stages of mitosis (Fig. 1, a, c). Meanwhile, in control samples apoptotic cells were rarely seen (Fig 1, b).

Nucleoli were appeared against the brightly fluorescent chromatin as large dark, roundish or elongated territories (Fig. 1, a-c). The nucleoli were well detectable due to presence of prominently

fluorescent ring of peri-nucleolar condensed chromatin (PCC) delineating boundary of nucleolar territory. Nucleolar contours were predominantly roundish, while nucleoli with elongated or irregular outlines also could be registered. Nucleolar perimeter and interior regularly showed fluorescence of the NAC, presented in the form of intra-nucleolar inclusions i.e. condensed/nucleosomal chromatin cords (ICC cords) extending from PCC shell deep inside the nucleolar territory. PCC consistently exhibits higher fluorescence than ICC. Even at low magnification, it became obvious that nucleoli contain histone H2B-GFP positive structures of different sizes and appearances attributed to ICC. ICC inclusions have slightly less intense labeling than chromatin fluorescence (Fig. 1, a, c).

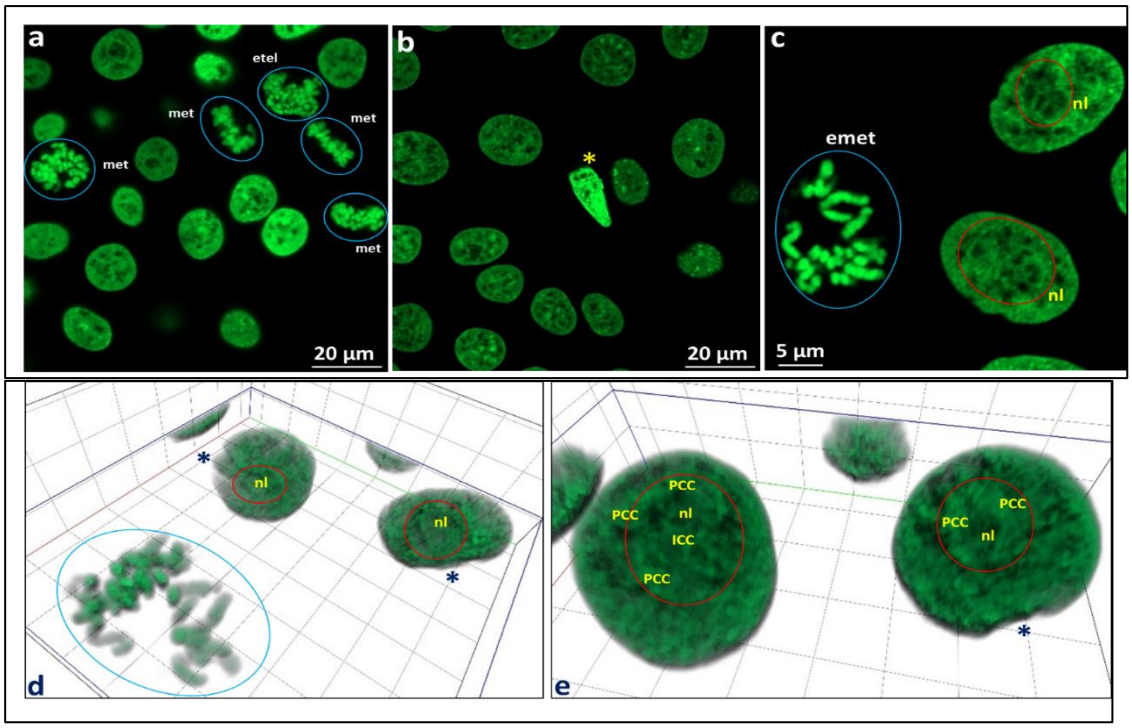

Fig.1 Structural features of nuclei in control He-La cells stably expressing histone H2B-GFP fusion protein

Fig. 1,a – c - note abundancy of mitotic cells (taken in blue circles on Fig. 1, a, c). Occasional apoptotic cells are also seen (marked by yellow star on Fig. 1, b). At low magnification nuclei mostly have roundish or elongated appearance and smooth contours (Fig. 1, a, b), while at higher magnification nuclei can reveal wave-like outlines due to small indentations (Fig. 1,c). Signs of more or less deep invagination or cleaved nuclei absent. Even at low magnification nucleolar territory is well recognizable by presence of profound ring of PCC that delineates nucleolar perimeter (see upper left nucleus on Fig. 1,a). At higher magnification intensively branched ICC network (outlined by red circles) became especially obvious (Fig. 1, c). Fig. 1, d, e - 3D models of nuclei generated by ZEN software, using aligned: (i) volume rendering; (ii) transparency mode by (iii) variable thresholds (correspond to mitotic cell and nuclei depicted. Nucleolar territories (nl) on both images are outlined by red circles. Nuclear periphery that shows small indentations are marked by stars on Fig. 1, d, e. Meanwhile, on Fig. 1, e PCC and ICC components of NAC are well recognizable. In spatial view 3D network formed by ICC is undeniable see left nucleus showed on Fig. 1, e). Note also thick PCC shell around nucleolus in right nucleus. Abbreviations: emet – early metaphase; etel – early telophase; met – metaphase; nl – nucleolus.

In 3D it became especially well recognizable that PCC forms around confines of the nucleolar territory prominent, solid, or locally disrupted shell (Fig. 1, d, e). Meanwhile, ICC forms intensively branching network connecting with PCC shell via many sites, both being integrated into unit NAC system. Indeed, 3D visualization and rotation of models reveal multiple cord-like structures emanating from the PCC shell. These "off springs" protrude inside the nucleolar territory, creating the impression of discrete ICC clumps on individual sections. Thus, after 3D modeling the existence of a unit ICC network that structurally communicates with the PCC shell became undoubted (1, d, e).

Regarding to 2D distribution and 3D organization of UBTF and fibrillarin positive NCs in fixed control cells we clearly visualized the relationships between the NAC and anti-UBTF immunolabeling. First of all, we detected UBTF fluorescence inside H2B-GFP positive intra-nucleolar network of NAC (Fig. 2, a-c). As a consequence, in 3D views the spatial interplay between GFP positive NAC and UBTF positive fluorescence became especially obvious, so that intensively branched ICC network appeared always intermingled with FCs (Fig. 2, d, e). Such a proximity of ICC and anti-UBTF tags shows the intimate link between nucleosomal, most probably non-ribosomal chromatin and relaxed r-chromatin folded into structure of FCs, i.e. interphase counterpart of mitotic NORs [14]. Moreover, we observed that ICC clumps, which were linked to UBTF positive FCs, were also attached to a PCC shell and created a bridge between these chromatin components. Hence, observing spatial integration of FCs into the whole network of NAC confirms early described tight link between nucleosomal and non-nucleosomal fractions of naDNA [14].

Secondly, histone H2B-GFP He-La culture allowed us to address also to 2D imaging of fibrillarin distribution and aligned imaging of 3D relationship of fibrillarin and UBTF complex with NAC (Fig. 3, a-g). In 2D fibrillarin positive labeling was always concentrated in cord-like structures that seemed were in tight association with NAC (Fig. 3, a-c). Corresponding 3D models are displayed on Fig. 3, d, e. Concomitant 3D visualization of the UBTF and fibrillarin couple as well as their relationship in control cells, produces clear evidence that these nucleolar proteins are closed together (Fig. 3, f, g). The close structural link between these nucleolar subdomains suggest the putative position of FC/DFC assembly inside ICC network. By this, fibrillarin positive DFC “covers” the chain-/necklace-like organized groups of FCs. Therefore, inside these units, discrete FCs (or their groups) are looking like embedded into a cord-like mass of DFC (Fig. 3, f, g).

As we described earlier, the post-irradiation time-lapse imaging showed that most profound nuclear/nucleolar alterations were detected within 48 – 72 hours’ period of post-irradiation image acquisition [51]. Correspondingly, here we exclusively focused on 2D images and 3D models of γ-irradiation-induced nuclear and nucleolar changes that develop during above mentioned post-irradiation time (Fig. 4, a-c and 5, a-f). It became clear that at this experimental point γ-irradiation in dose 30 Gy inflicts severe damage to nuclear chromatin structure displayed on Fig 4, a-c. Collected Z-stacks involving changes developed to the 72 hours revealed a three-stage process of nuclear evolution: (i) progressive nuclear invagination leading to a lobulated shape (Fig. 5, a, b); (ii) asymmetric nuclear fragmentation into unequal-sized micronucleoli (Fig. 4, a-c; 5, c-f); (iii) following asynchronous apoptotic nuclear degradation (Fig 4, a-c). Interestingly, that even after 72 post-irradiation hours a significant part of survived cells are mononuclear, while resting part can abundantly reveal deep invaginations and/or lobed nuclei. Nuclei slightly resembling control ones i.e. roundish with more or less smooth outlines, also existed, however we observed them just occasionally (Fig. 4, a, b).

Additionally, we interested whether γ-irradiation induced nucleolar inactivation pattern resembling NAC and FC/DFC assembly rearrangements observed with chemical inhibitors and called nucleolar segregation and capping [28-30, 34, 35]. As a rule, applied in our study dose of γ-irradiation leaded to the specific transformation of FCs and FC/DFC assembly. Unlike classical pattern of rRNA synthesis inhibition by chemical agent AMD, nucleolar segregation or capping was not observed. However, we registered asymmetric enlargement of one to three (rarely even more) FCs, acquiring giant but spherical form, which never been reshaped into crescent-like caps.

These peculiar entities always stud inside nucleolar territory, remaining spherical and being shifted to the interface between PCC shell and nucleolus [Fig. 4, b; 5, c-f). Interestingly, groups comprised several UBTF positive FCs which were of sharply smaller sizes could always be detected. Likewise, DFC never acquired cap-like structure always retaining its cord-like spatial arrangement (Fig. 5, b). Remarkably, that even after 72 hours, nucleoli remained large, irregularly shaped, and retained multiple FCs, suggesting a pre-segregated state rather than complete nucleolar segregation [14]. By this we conclude that even after 72 hours of post-γ-irradiation imaging period 30 Gy dose is unable to disassemble FC/DFC unity.

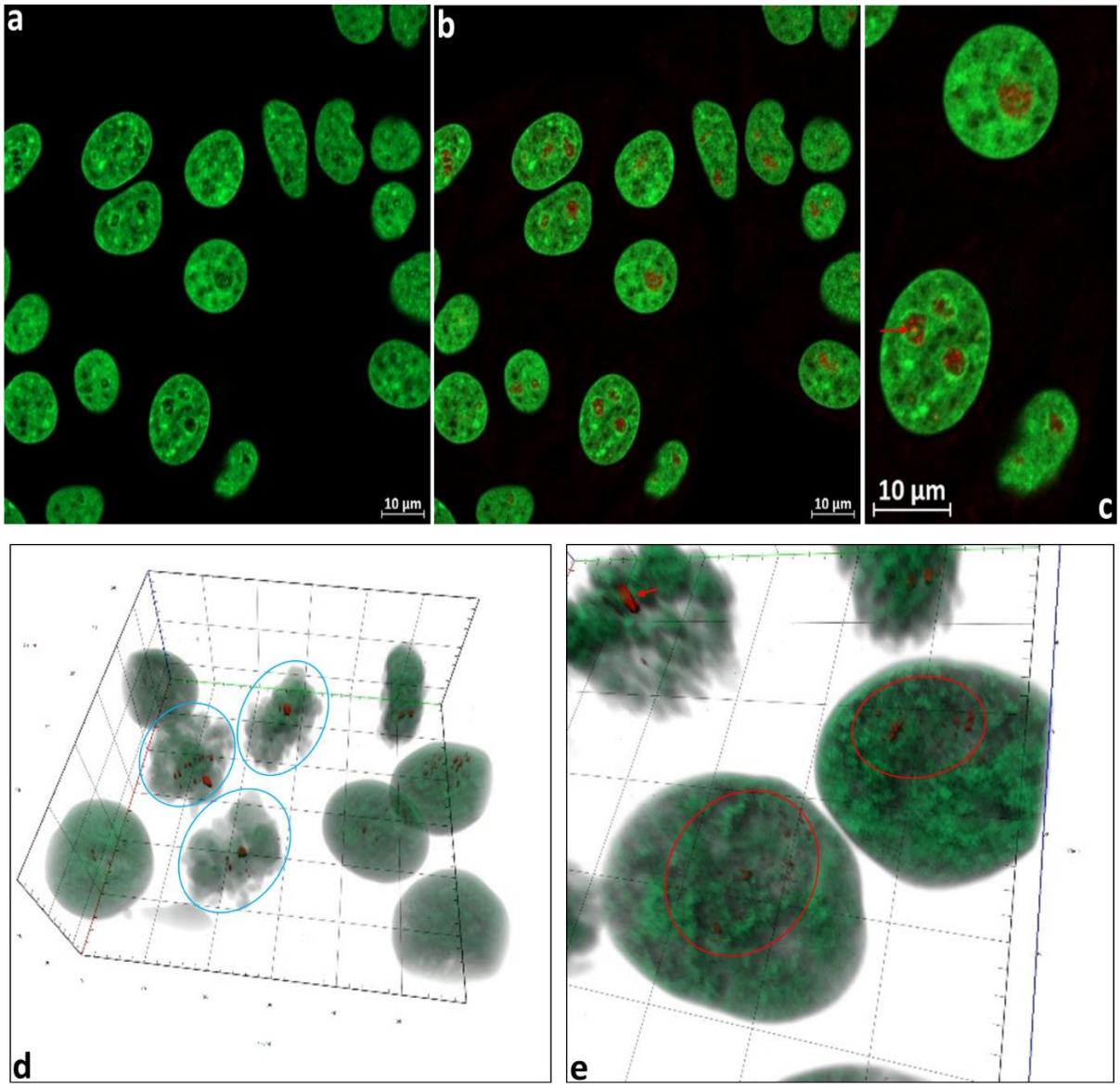

Figure 2. **Nuclear morphology in control histone H2B-GFP permanently transfected He-La cells submitted to anti-UBTF immunostaining**

Fig. 2, a – c - note prominent nuclear polymorphism, showing that beside roundish nuclei the elongated ones as well as nuclei with slightly curved contours were detected. Fig. 2, a – low magnification; histone H2B-GFP transfected He-La culture before immunolabeling. Even at low magnification nucleolar inclusions of ICC were regularly seen. Fig. 2, b – overlay of GFP and anti-UBTF labels; after immunostaining anti-UBTF label was exclusively concentrated inside nucleolar territory. Fig. 2, c – overlay of GFP and UBTF positive structures at higher magnification; integration of UBTF positive entities into unit NAC network became clear; note that red arrow indicates site of co-localization of green and red fluorescence, i.e. ICC and UBTF containing structures. Note also that PCC fluorescence was brighter than those of ICC. Fig. 2, d, e - ZEN generated 3D models reconstructed and rendered using same options as it was described on Fig. 1, d, e. 3D images clearly show integration of UBTF positive FCs into NAC network. Fig. 2, d – low magnification; UBTF positive signal was exclusively restricted by FC and NORs (mitotic cells were taken in blue circles). Fig. 2, e – high magnification; spatial visualization of link between FCs and NAC became better visible; red circles delineate nucleolar territory. Red star indicates large NOR.

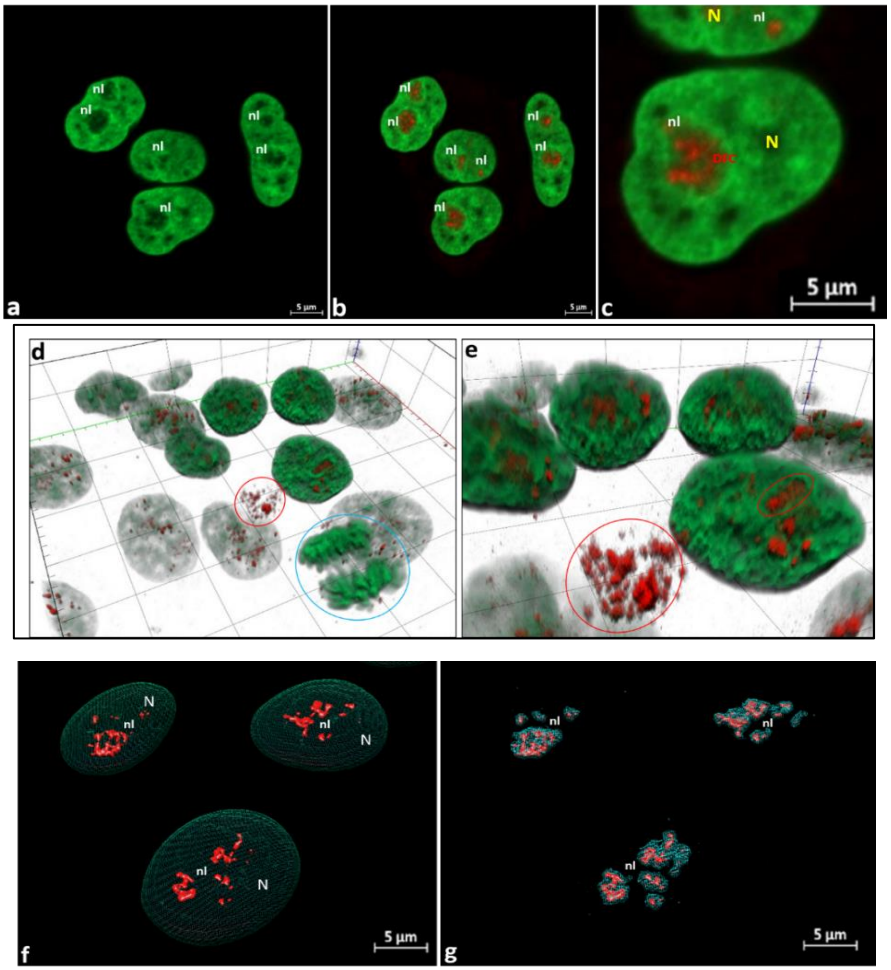

Figure 3. **Nuclear morphology in non-irradiated (control) histone H2B-GFP permanently transfected He-La cells submitted to anti-fibrillarin immunostaining. Note profound nuclear polymorphism, witnessing presence of cells with elongated/curved nucleolar outlines**

Fig. 3, a – low magnification; histone H2B-GFP transfected He-La culture before immunostaining. Both, ucleolar inclusions of ICC as well as well pronounced PCC ring were presented. 3, b – overlay of GFP and anti-fibrillarin positive structures; after immunostaining anti-fibrillarin label was concentrated within nucleolar territory. Fig. 3, c – overlay of GFP and fibrillarin positive structures at higher magnification, confirming integration of cord-like fibrillarin containing structure (DFC) into NAC network. Fig. 3, d, e - 3D models reconstructed and rendered using same options as it was described on Fig. 1, d, e. 3D models showing integration of fibrillarin positive DFC into NAC network. Fig. 3, d – low magnification; fibrillarin positive signal was gathered only inside DFC. Mitotic cells were taken in blue circle, while red circle outlines the region of anti-fibrillarin signal localization inside the nucleus that was not transfected, i.e. nucleus that don't emit green fluorescence of chromatin. Mitotic chromosomes were free from anti-fibrillarin label. Fig. 2, e – high magnification; left, large red circle delineates the anti-fibrillarin signal inside not transfected nucleus, while left, small red circle demonstrates cord-like organization of DFC. Fig. 3, f, g - 3D models, generated by "Chimera" software. Fig. 3, f - demonstrates spatial distribution of UBTF positive signal (red), showing necklace-lake organization of FCs inside nucleus (green) Fig. 3, g - 3D model, confirming intimate association of UBTF positive FCs and fibrillarin positive DFC (blue) in form of FC/DFC assembly. This igure shows only FC/DFC assembly which was extracted from nuclear interior. N – nucleus; DFC – dense fibrillar component; other abbreviations are same as on previous images.

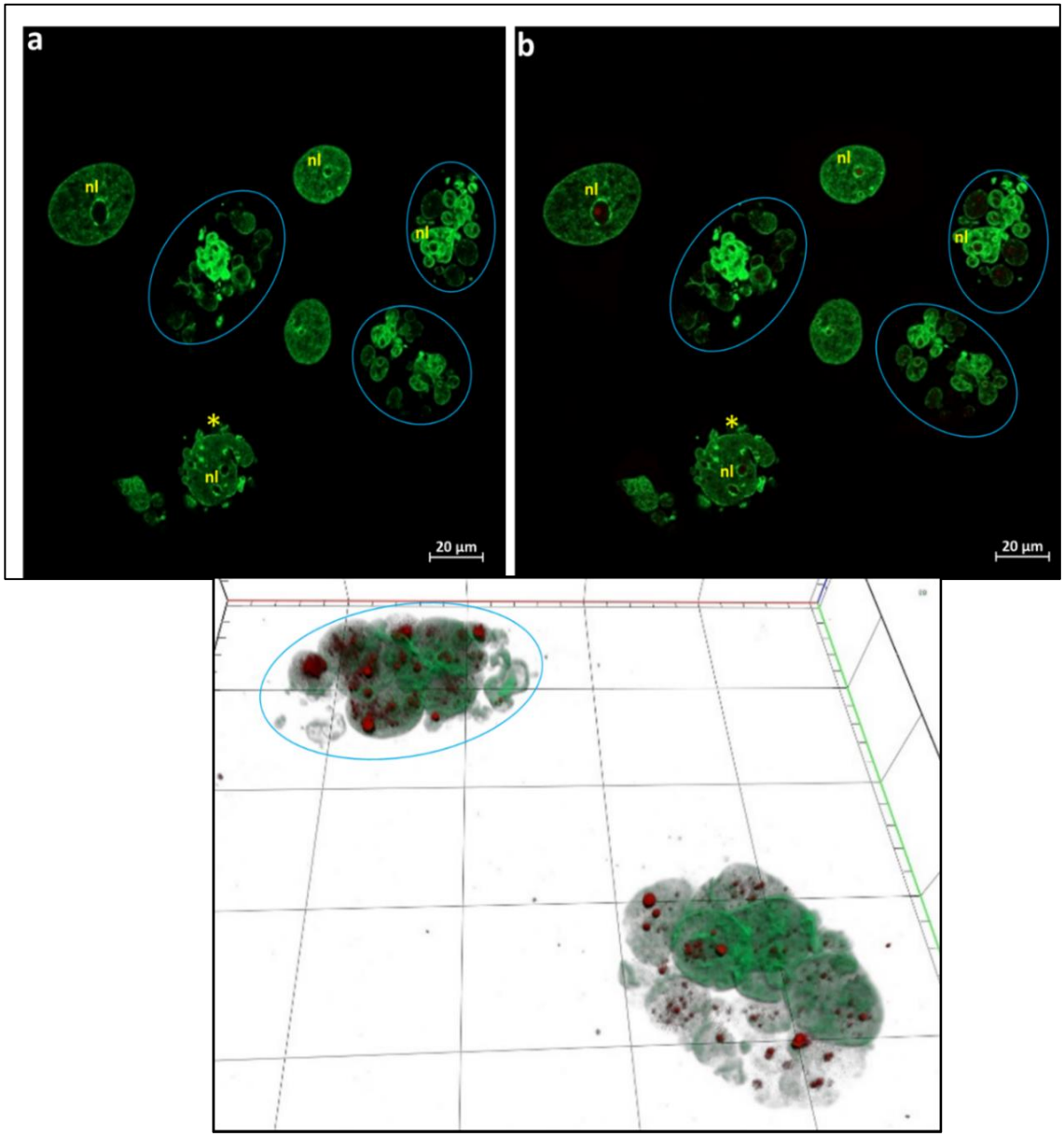

Figure 4. Effect of 30 Gy γ-irradiation upon nuclear structure of histone H2B-GFP transfected He-La culture

Images correspond to 72 hours of post-irradiation imaging period. Fig. 1, a – this image was taken before anti-UBTF immunostainig; 1, b – same nuclei after anti-UBTF immunostaining. Note, that beside severely damaged cells with cleaved nucleus (marked by yellow star) and multi-nuclear cells (taken in blue circles) we registered "survived" mononuclear cells which nuclei had close to control appearance. In all cases (including nucleolated fragments in multi-nuclear cells) nucleolar territory can be easily identified. Note also UBTF positive structure (FC) inside nucleolus of upper left cell. Fig. 4, c – ZEN generated 3D models reconstructed and rendered using same options as for cells showed on Fig. 1, d, e. These 3D models display severely damaged multi-nuclear cells (taken in blue circles) after anti-UBTF immunolabeling. Note spatial rearrangement of UBTF positive structures into nuclear fragments appeared at 72 hour of post-γ-irradiation image acquisition. Signs of disruption and chaotic redistribution of FCs inside nucleolated fragments were obvious.

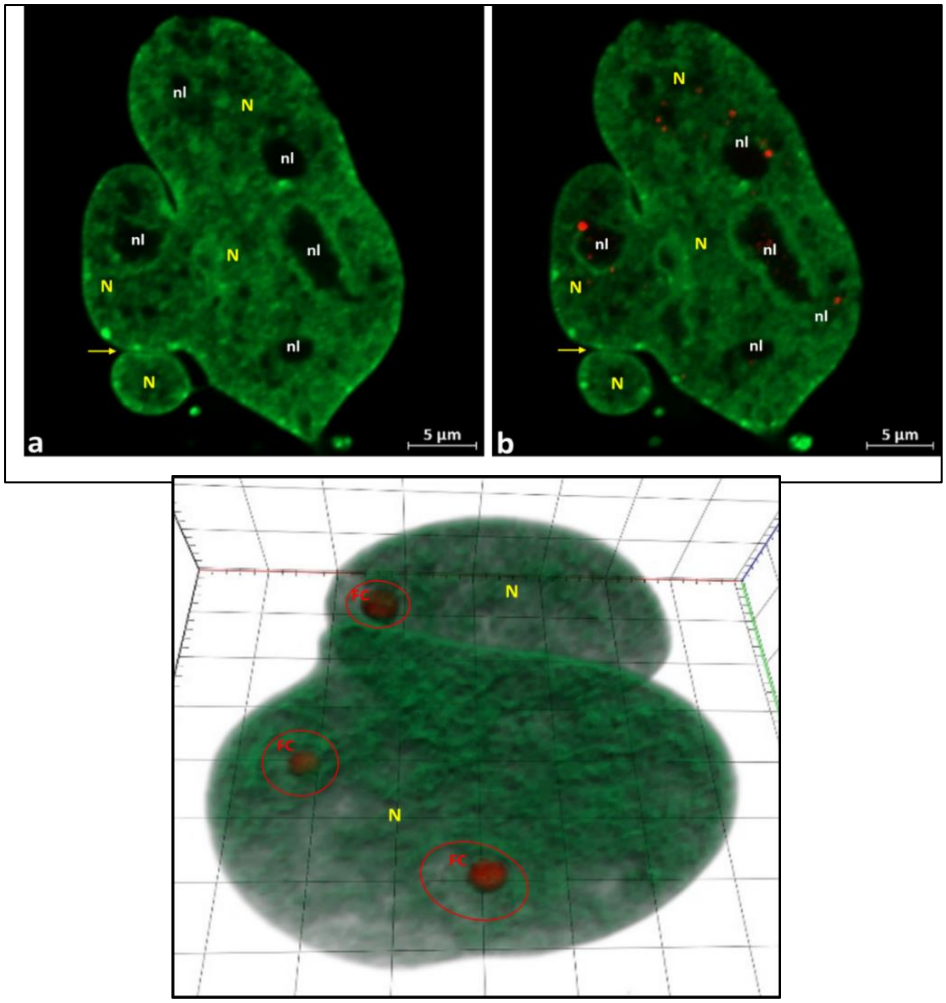

Figure 5. Severely damaged mononuclear histone H2B-GFP expressing He-La cell with lobbed/cleaved nucleus before (Fig. 5, a) and after (Fig. 5, b) anti-UBTF immunostaining.

Early stage of nuclear fragmentation (yellow arrows). Fig. 5, b – after anti-UBTF immunostaining picture of disruption/dispersion of FCs became undisputable. Fig. 5, c- e. Early step of nuclear fragmentation: formation of two closely located nuclear fragments appeared at 72 hours of post-irradiation imaging period. Images were taken before (Fig. 5, a) and after (Fig. 5, b, c) anti-UBTF immunostaining. Fig. 5, a – nucleolar territories surrounded by prominent PCC ring are well recognizable. Fig. 5, b, c - two not successive section planes extracted from Z-stack in order to demonstrate giant UBTF positive FCs in all nucleoli. Note exclusive intra-nucleolar localization of FCs that link to PCC. Note also direct structural contact between FC and protrusion of PCC into nucleolar territory. Importantly, we never observed classical picture of nucleolar segregation and capping. Fig. 5, f - the same nuclei as on Fig. 5, c – e, demonstrating early stage of nuclear fragmentation. This ZEN generated 3D model was reconstructed after anti-UBTF immunolabeling. Obviously, UBTF positive FCs increased to giant sizes, however still stud spherical and located inside nuclear territory (outlined by red circles). We never observed reshaping of spherical FC into crescent-lice caps. All abbreviations are same as on previous images.

DISCUSSION

Our major goal was to demonstrate the structural and functional interplay between γ-irradiation induced r-gene inactivation and large-scale modifications of intra-nucleolar structure with particular regard to possible territorial reorganization of NAC and related structures. Correspondingly, the present study focuses not only on profound nuclear and chromatin destruction but also on the re-organization of NAC, particularly ICC and PCC, in compliance with behavior of FC/DFC assembly, under severe DNA damage induced by γ-irradiation. Regarding nucleolar analysis, the key aspect to consider in this study was the impact of the less studied physical factor, particularly γ-irradiation upon nuclear/nucleolar chromatin structure and behavior of FC/DFC assembly.

As UBTF is specifically associated with active under-condensed rDNA genes it was extensively used as reliable marker of FCs in experiments applying either GFP tagging or immunostaining [14, 52, 53]. Meanwhile, fluorescent detection of fibrillarin, based on both GFP and immunolabeling approaches has widely been adopted by addressing to early pre-rRNA early processing nucleolar sites [14, 50]. Specifying the γ-irradiation induced UBTF and fibrillarin redistribution pattern resulting in particular behavior of FC/DFC assembly we concluded that the most peculiar changes we registered are: (i) never observed the picture when irregularly shaped nucleoli transform into small, sharply outlined and dense entities as it usual by nucleolar segregation. On the contrary, even passing through 72-hour post-irradiation image acquisition period in all survived cells nucleoli stud large enough and irregularly shaped; (ii) absence of typical segregation, expressed in transformation of FC/DFC assembly into crescent-like nucleolar caps, although γ-irradiation can induce transcription inhibition [46]. FCs along with tightly associated DFC "cover" stud always inside nucleolar territory; (iii) distinct demonstration using 3D models that despite asymmetrically enlarged one or two clearly spherical FCs, spatial organization of these r-chromatin containing NCs looked like drastically different as few extremely small UBTF positive entities stud permanently beside giant FCs; (iv) fibrillarin positive DFC undergoes minor changes still exhibiting cord-like fluorescence, even being collected through 72 hours acquisition period; (v) γ-irradiation unable to disassemble FC/DFC complex, so that giant as well as small FCs were always either fully or in part "wrapped up" by fibrillarin containing DFC.

While following the post-irradiation interplay of the NAC system with the FC/DFC assembly we emphasized that posing as an integral part of the nucleolus, the functional role of NAC still needs to be investigated. This largely increased the credibility of our data, indicating their particular significance as a novel insight in the intra-nucleolar dynamics of NCs. It is well established that, once formed, the nucleolus remains intimately associated with the physiological state of NAC. The structural remodeling of NAC can affect the spatial arrangement of active r-genes and the global organization of the nucleolar factories. As it was suggested, most likely, NAC constituents do not contain r-genes due to the absence of specific accessory factors necessary for the maintenance of the template in an under-condensed/open state [14, 34, 53]. Hence, the absence of UBTF facilitate the keeping of the nucleosomal structure of ICC and PCC. How NAC responds to the action of DNA-damaging factors, particularly radioactive exposure, remains largely unknown. It seems much more problematic to understand whether NAC still retains the ability to condense and drive the movement of NCs while naDNA undergoes γ-irradiation breakage and degradation.

Although the dynamics of γ-irradiation-induced NAC changes largely mirror inactivation pattern observed in AMD-induced rRNA synthesis inhibition, behavior of FC/DFC assembly completely differs from reorganization pattern observed by chemical inhibition of the nucleolus. In

cells exposed to γ-irradiation of 30 Gy dose, ICC structures gradually coalesce, being stepwise shifted towards PCC and forming coarser but increasingly fluorescent clumps. Most probably, despite severe naDNA damage ICC retains mobility and contraction, presumably driving tightly linked FCs to delocalize, as it was registered in AMD treated Histone H2B-GFP He-La cells [14].

Undoubtedly, massive and striking nuclear changes delay until 48 – 72 hours. Accordingly, we expected remarkable changes in NAC and FC/DFC assembly to these experimental points. Indeed, after treatment by 30 Gy dose drastic changes increasingly appear during 24-48 hours of post-irradiation image acquisition period. Here we revealed the bulk of highly deformed nuclei in both mononuclear and multi-nucleated cells, including apoptotic ones. In all survived mononuclear cells that reveal comparative resemblance with control morphology the integration of FC/DFC into NAC unit remains unchanged. Interestingly, that even highly damaged, multi-nucleated cells we could see nucleoli, but not in all nuclear fragments. Such nucleoli could exhibit deformed shape while UBTF and fibrillarin fluorescence remains quite bright.

Meanwhile, post-irradiation changes over 48 - 72 hours enabled the revealing of the nuclear/nucleolar evolution stages. For this, we resorted to key experimental points that were identified for detailed analysis. As a consequence, we convinced that 30 Gy dose of γ-radiation is unable to disassemble the FC/DFC and NAC unity despite deep and invertible destruction of the nucleus and nucleolus, that leads to nuclear fragmentation, cellular multi-nucleation with following apoptotic degeneration, nucleolar disruption and finally to cellular death. Importantly that NAC and FC/DFC unity is conditioned through nucleolar condensed chromatin, particularly ICC. Undoubtedly, one more intriguing issue worth further engagement is that even severe DNA damaging by 30 Gy regime indicated the maintenance of naDNA to contract thus drive nuclear and nucleolar dynamics. Therefore, trying to explain delayed nucleolar changes and relative stability of NAC and FC/DFC system during longer time, we could hypothesize that densest nucleolar composition can serve somehow as kind of “shield”. In turn, due to intra-nucleolar localization, hence being possibly better protected, r-chromatin can remain viable longer than some, “less protected” nuclear functional compartments as well as cytoplasmic organelles. At least this suggestion is worth to be included in our planed next experiments aiming detection of single and double DNA strand breakages.

Moreover, our study specifically focuses on the mechanisms of multi-nuclear cell formation and nucleolar changes accompanying asynchronous apoptotic destruction. Although emergence of the multi-nuclear cell and asynchronous apoptosis in nuclear cells was frequently registered after UV and γ-irradiation [6, 8, 54], up to date, there is no comprehensive explanation of underlying sub-cellular and molecular mechanisms. Importantly, our results enabled to hypothesize at least one of the possible sub-cellular mechanisms of multi-nuclear cell emergence. We think that described processes unfold in distinct stages, hence presenting possible underlying cellular mechanisms. The consequential steps of post-irradiation dynamics of this process may develop in two steps. Initially, the formation of deep invaginations of the nucleus takes place that imparts a cleaved and/or lobbed shape to nuclei. During the second step, trough the increasingly deepened invagination nuclei “disrupt” into separate fragments or so that each lobe gives rise to individual micronucleus. Understanding how these nuclear transformations interact with nucleolar components is essential for characterizing the cellular response to severe DNA damage. We anticipate that nucleolar structural alterations induced by γ-irradiation will correlate with the progressive fragmentation of nuclear material, offering novel insights into the interplay between chromatin integrity and

nucleolar stability. In this context we observed two kinds of nuclear cleavage process. If the resulting lobe "engulfs" the nucleolus, nuclear disruption forms the nucleolated micronucleus. In opposite cases, micronuclei became anucleolated. Interestingly, apoptosis-associated changes develop asynchronously in both nucleolated and anucleolated micropnuclei. Disruption of the nucleus into individually functioning micronuclei as well as following apoptosis were frequently registered in multi-nucleated cells emerged as a result of UV and γ-irradiation [for example see: 8, 54]. However, according our best knowledge there was no comprehensive explanation of underlying sub-cellular and molecular mechanisms, while our observations can be considered as new and original.

In summary, the study contributes valuable insights into the structural changes in nuclear and nucleolar structure under severe DNA damage, highlighting the significance of NAC in nucleolar organization. The observed similarities between chemical inhibition and γ-irradiation effects emphasize the role of NAC in cellular responses to different stressors. Additionally, nucleolar behavior under γ-irradiation may provide a comparative framework for understanding cellular responses to other forms of genotoxic stress, including oxidative damage and radiation-induced senescence. Given the pivotal role of the nucleolus in cellular stress responses, its alterations may serve as biomarkers for assessing DNA damage severity and predicting cellular fate. The findings of this study have broader implications for cancer biology, as nucleolar disorganization is frequently observed in malignancies characterized by genomic instability.

CONCLUSION

The methodology employed in this study allows for detailed real-time observation of chromatin and nucleolar behavior in response to DNA damage, providing new insights into nuclear and nucleolar resilience and adaptation. Furthermore, the presence of large-scale chromatin rearrangements following irradiation raises important questions regarding the mechanistic links between nuclear deformation, chromatin dynamics, and nucleolar integrity. Notably, organisms are permanently exposed to physical stressors such as UV-radiation and γ-irradiation, yet the structural consequences of such damage on nucleolar architecture remain underexplored. By characterizing nucleolar responses to γ-irradiation at the molecular and structural levels, this study provides new insights into how nuclear and nucleolar components adapt to DNA damage and contribute to cellular stress responses. Amazingly, the structural consequences of such damage on nucleolar architecture remain underexplored. By characterizing nucleolar responses to γ-irradiation at the molecular and structural levels, this study offers new technical approaches that could facilitate elucidation how nuclear and nucleolar components adapt to DNA damage and contribute to cellular stress responses.

As we have seen our research generated a number of issues, challenging to be explored in first line. For example, among the most appealing topics could be: what is damages degree and what type of breaks undergoing both, relaxed and condensed intra-nucleolar fractions of chromatin, being concealed/“protected” by extremely compact composition of the nucleolus? Obviously, the suitable experimental strategies may deal not only with whole cell nucleoli, but may be amenable to purified nucleoli. In this regard, another interesting question is: whether or not applied 30 Gy γ-irradiation irradiation affect critically template and/or linked transcription machinery, so that isolated nucleoli became transcriptionally unable. Importantly, this issue as well as other related topics are in progress now at SECCZ.

REFERENCES

[1]. Akbari, E., Eui-Jin Park, E-J., Ajit Kumar Singh, A. K., Vinazyak, V., Virk, R. K. A., Wereszczynski, J., Musselman, C. A. (2023) Multiscale genome organization symposium—annual biophysical society meeting. Biophysical Reviews 15(3), DOI: 10.1007/s12551-023-01063-8;
[2]. Frederick, J., Virk, R. K. A., Ye, I. C., Almassalha, L. M., Wodarcyk, G., Van Derway, D., Gonzalez, P. C., Nap, R. J., Agrawal V., Anthony, N. M., Carinato, J., Li, W. S., Dunton, C. L., Medina, K. I., Kakkaramadam, R., Jain, S., Shahabi, S., Ameer, G., Szlafer, I. G., Backman, V. (2024). Leveraging chromatin packing domains to target chemoevasion in vivo. bioRxiv Preprint, DOI: 10.1101/2024.11.14.623612;
[3]. Eid, A., Eshein, A., Li, Y., Virk, R., Van Derway, D., Zhang, D., Taflove, A., Backman, V. (2020) Characterizing chromatin packing scaling in whole nuclei using interferometric microscopy. Optics Letters, 45(17): 2-5;
[4]. Yue Li, Y., Eshein, A., Virk, R., Eid, A., Van Derway, D., Frederick, J., Bleher, R., Szlafer, I. G., Dravid, V., Vadim Backman (2020) Nanoscale Chromatin Imaging and Analysis (nano-ChIA) Platform Bridges 4-D Chromatin Organization with Molecular Function. Microscopy and Microanalysis, 26(S2): 1-5;
[5]. Nishimaki, N., Tsukimoto, M., Kitami, A., Kojima, S. (2012) Autocrine regulation of γ-irradiation-induced DNA damage response via extracellular nucleotides-mediated activation of P2Y6 and P2Y12 receptors. DNA Repair: 11: 657-665;
[6]. Lee, C. H., Wu, S. B., Hong, C. H., Yu, H. S., Wei, Y. H. (2013) Molecular mechanisms of UV-indiced apoptosis and its effects on skin residential cells: The Implication in UV based Phototherapy. Int. J. Mol. Sci., 14(3): 6414-6435;
[7]. Ghorai, A., Bhattacharyya, N. P., Sarma, A., Ghosh, U. (2014) Radiosensitivity and induction of apoptosis by high LET carbon ion beam and low LET gamma radiation: A comparative study. Scientifica, 2014: 1-10;
[8]. Salucci, S., Burattini, S., Batistelli, M., Baldassarri, V., Maltarlo, M. C., Falcieri, E. (2013) Ultraviolet B (UVB) Irradiation-Induced Apoptosis in Various Cell Lineages in Vitro. Int. J. Mol. Sci., 14: 532-546;
[9]. Juliana, H., Osaki, Espinha, Y. T., Magalhaes, Forti, F. L. (2015) Modulation of RhoA GTPase activity sensitizes human cervix carcinoma cells to γ-radiation by attenuating DNA repair pathways. Oxidative Medicine and Cellular Longevity, 2016: 1-11;
[10].Zhoo, H., Zhuang, Y., Li, R., Liu, Y., Mei, Z., He, Z., Zhou, F., Zhou, Y. (2018) Effect of different doses of X-ray irradiation on cell apoptosis, cell cycle, DNA damage repair and glycolysis in He-La cells. Oncology Letters, 11: 42-54;
[11].Azzouz, P., Khan, M. A., Sweerey, N., Palaniar, N. (2018) Two-in one: UV radiation simultaneously induces apoptosis and NETosis. Cell Death Discovery, 4: 51-78;
[12].Brunner, S., Varga, D., Bozó, R., R. Polanek, R., Tőkés, T., Szabó, E. R., Molnár, R., Gémes, N., Szebeni, G. J., Puskás, J. L., Erdélyi, M., Hideghéty, K. (2021) Analysis of ionizing radiation induced DNA damage by superresolution dSTORM microscopy. Pathology and Oncology Research, 27: 160-173;
[13].Vickers, E. R. (2022) Human Adipose Stem Cells Exposed to Gamma radiation and inactivity (stasis) show increased cancer markers and DNA damage. A preliminary assessment of a pharmaceutical formulation to reverse these effects and its applications for medical radiotherapy and the space industry. Journal of Cancer Therapy, 13: 7-19;
[14].Tchelidze, P., Benassarou, A., Kaplan, H., O'Donohue, M. F., Lucas, L., Terryn, C., Rusishvili, L., Mosidze, G., Lalun, N., Ploton, D. (2017) Nucleolar sub-compartments in motion during rRNA synthesis inhibition: contraction of nucleolar condensed chromatin and gathering of fibrillary centers are concomitant. PLOS one: 30: 2-37;
[15].Busch, H., Smetana, K. (1970) The Nucleolus. New York, Academic Press: 1-282;
[16].Smetana, K., Busch, H. (1974) The nucleolus and nucleolar DNA. In: Busch H, editor. The Cell Nucleus. New York, Academic Press: 73-147;

[17].Hadjiolov, A. (1985) The Nucleolus and ribosome biogenesis. In: Alfert, M, Beerman W, Goldstein, L, Porter, KR, Site P, editors. Cell Biology Monographs Wien, New York, Springer Verlag: 1-263;
[18].Thiry, M., Lafontaine D. (2005) Birth of a nucleolus: the evolution of nucleolar compartments. Trends in Cell Biology, 15:194-199;
[19].Boisvert, F. M., van Koningsbruggen, S. N., Navascues, J., Lamond, A. I. (2007) The multifunctional nucleolus. Nat Rev Mol Cell Boil, 8:574-585;
[20].Stults, D. M., Killen, M. W., Pierce, H. H., Pierce, A. J. (2008) Genomic architecture and inheritance of human ribosomal RNA gene clusters. Genome Res, 18:13-18;
[21].Hernandez-Verdun, D., Roussel, P., Thiry, M., Sirri, V., Lafontaine, D. (2010) The Nucleolus: structure/function relationship in RNA metabolism. WIREs RNA, 1:415-431;
[22].Pederson, T. (2010) The nucleus introduced. Cold Spring Harb Perspect Biol, 10:1-16;
[23].Olson, M. O. J. (2011) The nucleolus: A nuclear body full of surprises. In: Olson M. O. J. editor. The Nucleolus. Protein Reviews, New-York, Dordrecht, Heidelberg, London: Springer, 15:5-17;
[24].Baserga, S. J., DiMario, P. J., Duncan, F. E. (2019) Emerging roles for nucleolus 2019. JBC, 295(16): 5535-5537;
[25].Berus, T., Markieicz, A., Biecek, P., Orlowska-Heitzman, J., Aalon, A., Romnowska-Dixon, B., Donizi, P. (2020). Clinical significance of nucleoli cytomorphology assessment in patients with uveal melanoma. Anticancer Research, 40 (6): 3505-3512;
[26].Lafita-Navarro, M. C. Conacci-Sorrell, M. (2022) Nucleolar stress: From development to cancer. Seminars in Cell and Developmental Biology, 136(4): 11- 23;
[27].Korsholm, L.M., Gál, Z., Bernáldez, B. N., Quevedo, O., Boukoura, S., Lund, CC., Larsen, D. (2020) Recent advances in the nucleolar responses to DNA double-strand breaks. Nucleic Acids Research, 48 (17): 2-12;
[28].Reynolds, R. C., Montgomery P. 3O., Hughes, B. (1964) Nucleolar “caps” produced by actinomycin D. Cancer Res, 24: 1269-1277;
[29].Simard, R., Langelier, Y., Mandeville, R., Maestracci, N., Royal, A. (1974) Inhibitors as tools in elucidating the structure and function of the nucleus. In: Busch H, editor. The Cell Nucleus. New York: Academic Press: 447-487;
[30].Puvion-Dutilleul, F., Mazan, S., Nicoloso, M., Pichard, E., Bachellerie, J. P, Puvion, E. (1992) Alterations of nucleolar ultrastructure and ribosome biogenesis by actinomycin D. Implication for U3 snRNP function. Europ J Cell Biol, 58:149-16;
[31].Olson, M. (2004) Sensing cellular stress: another new function for the nucleolus? Sci STKE, 10;
[32].Mayer, C, Grummt, I. (2005) Cellular stress and nucleolar function. Cell Cycle, 4:1036-1038
[33].Shav-Tal, Y., Blechman, J., Darzacq, X., Montagna, C., Dye, B. T., Patton, J. G. (2005) Dynamic sorting of nuclear components into distinct nucleolar caps during transcriptional inhibition. Mol Biol Cell, 16:2395-2413;
[34].Tchelidze, P., Kaplan, H., Terryn, C., Lalun, N., Ploton, D., Thiry, M. (2019) Electron Tomography Reveals Changes in Spatial Distribution of UBTF1 and UBTF2 Isoforms within Nucleolar Components during rRNA Synthesis Inhibition. Journal Structural Biology, 208(2): 191-204;
[35].Michel, J., Nolin, F., Wortham, L., Lalun, N., Tchelidze, P., Banchet, V., Terryn, C., Ploton, D. (2019) Various Nucleolar Stress Inducers Result in Highly Distinct Changes in Water, Dry Mass and Elemental Content in Cancerous Cell Components: Investigation Using Nano-Analytical Approach. Nanoteranostics, 3:179-195;
[36].Corman, A., Sirozh, O., Lafarga, V., Fernandez-Capetillo, O. (2023) Targeting nucleolus as a therapeutic strategy in human disease. Trends in Biochemical Science, 48(3): 274-287;
[37].Potapova, T. A., Jay R Unruh, J. R., Conkright-Fincham, J., Banks, C. A. S., Florens, L., David Alan Schneider, D. A., Gerton, J. L. (2023) Distinct states of nucleolar stress induced by anticancer drugs. eLife, 12:1-30;
[38].Pigg, H. C., Alley K. R., Griffin, C. R., H. Moon, C. H., J. Kraske, S. H., J. DeRose, V. J. (2024) The unique Pt(II)-induced nucleolar stress response and its deviation from DNA damage response pathways. JBC, 300(11): 8567-8581;

[39].Sellins, K. Cohen, J. (1987) Gene induction by gamma-irradiation leads to DNA fragmentation in lymphocytes. J. Immunol., 139(10): 3199-3206;
[40].Sudprasert, W., Navasumrit, P., Ruchiravat, M. (2006) Effects of low-dose gamma radiation on DNA damage, chromosomal aberration and expression of repair genes in human blood cells. Int J Hygiene Env Health, 209(6): 503-511;
[41].Dona, M., Ventura, L., Macovei, A., Confalonieri, M., Savio, M., Giovannini, A., Carbonera, D., Balestrazzi, A. (2013) Gamma irradiation with different dose rates induces different DNA damage responses in Petunia x hybrida cells, J Plant Physiol., 170(8): 780-787;
[42].Uttayarat, P., Tangtong, T., Sukapirom, K., Boonsirichai, K. (2015) Gamma irradiation induces DNA double-strand breaks in fibroblasts: a model study for the development of biodosimeter, J. Phys.: Conf. Ser., 611: 012-030;
[43].Tankovskaia, S. A., Kotb, O. M., Dommes, O. A., Pasten, S. V. (2018) DNA damage induced by gamma-radiation revealed from UV absorption spectroscopy. J. Phys.: Conf. Ser., 1038: 24-26;
[44].Georkilas, A. (2021) Role of DNA Damage and Repair in Detrimental Effects of Ionizing Radiation. Radiation, 1(1): 1-4;
[45].Afify, A., Ali, H. M., Sayed, R. M. (2024) Estimating the impact of gamma radiation on biochemical aspects and DNA damage by comet assay in Galleria mellonella male. Entomological News, 131(1): 30-42;
[46].Mikhalkevich, N., Russ, E., Iordansky, S. (2023) Cellular RNA and DNA sensing pathways are essential for the dose-dependent response of human monocytes to ionizing radiation. Front. Immunol., 14: 123-136;
[47].Lisowska, H., Deperas-Kaminska, M., Haghdoost, S., Parmryd, I., Wojcik, A. (2010) Radiation-induced DNA damage and repair in human γδ and αβ T-lymphocytes analysed by the alkaline comet assay. Genome Integrity, 1: 8-9;
[48].Ghorbani, Z., Fardid, R. (2021) Effects of low-dose gamma radiation on expression of apoptotic genes in rat peripheral blood lymphocyte. Journal of Biomedical Physics and Engineering, 11(6): 693-700;
[49].Alghoul, E., Basbous, J., Constantinou, A. (2023) Compartmentalization of the DNA damage response: Mechanisms and functions. DNA Repair, 128: 2-12;
[50].Zhang, X., Wenxin Li, W., Sun, S., Liu, Y. (2024) Advances in the structure and function of the nucleolar protein fibrillarin. Front. Cell Dev. Biol., 12: 14-24;
[51].Nadaraia, L., Okuneva, O., Gogebashvili, M., Ivanishvili, N., Tchelidze, P. (2023) Nucleolar dynamics: reorganization of nucleolus-associated condensed chromatin under DNA damage induced by different doses of γ-irradiation. Journal of Radiology and Radiation Safety, 4(5): 18-36;
[52].Zatsepina OV, Voit R, Grummt I, Spring H, Semenov MV, Trendelenburg M. The RNA polymerase Ispecific transcription factor UBF is associated with transcriptionally active and inactive ribosomal genes. Chromosoma 1993, 102:599-611;
[53].Mais C, Wright JE, Prieto JL, Raggett SL, McStay B. UBF-binding site arrays form pseudo-NORs and sequester the RNA polymerase I transcription machinery. Genes Dev 2005, 19:1-15;
[54].Braten, M., Banreed, H., Berg, K., Moan, J. (2000) Induction of multinucleated cells caused by UVA exposure in different stages of the cell cycle. J Photochem Photobiol B: Biology, 71(5): 620-626;

CAN CHRONIC RADIATION BE RADIOPROTECTIVE FOR PLANT SUBJECTS EXPOSED TO THE INHIBITING ACTION OF ACUTE GAMMA RADIATION?

(low-dose radiotherapy, "reverse radioadaptation")

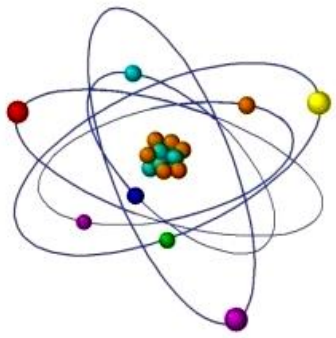

[1]Oleksandr Mikhyeyev*, [2]Oksana Lapan

[1]Institute of Cell Biology and Genetic Engineering, National Academy of Science of Ukraine

[2]National Aviation University, Ukraine

https://doi.org/10.63465/rrs520258986 *Corresponding author: Email: mikhalex7@yahoo.com

ABSTRACT*: A new classification of types of radio-modifying effects is proposed, both in terms of the sequence of action of the main (inhibitory and hormesis doses) and modifying factors and in terms of the sign (direction) of the radio-modifying influence. The division of adaptive reactions into ordinary, hypo-, and hyper adaptive reactions is substantiated. Special attention in the work is given to the effects of positive post-radiation modification, essentially having, in the case of using ionizing radiation, the nature of radiotherapy (non-oncological), that can be conditionally called 'reverse radio adaptation'. Experimental evidence of its existence is presented, which can be the basis for the method of 'low-dose radiotherapy' of radiation damage.*

Key words: radiation hormesis, modification of radiation, hyper radio adaptation, reverse adaptation

INTRODUCTION

The scientific metric analysis of publications in radiobiology and radioecology shows that about a third of these works are dedicated to studying pre- and post-radiation modification of radiobiological effects. This focus makes sense as the ultimate aim of radiobiology and radioecology, predominantly serving human interests, is to develop a unique "set of tools" or levers for managing radiobiological reactions to minimize or maximize their consequences. If radiation modification is understood as the processes and results of influencing the outcome of radiobiological reactions, and limited to considering only the inhibitory effects of acute ionizing radiation exposure, then a general classification of radio-modifying factors (methods, influences, etc.) can be proposed, which can be any agent in nature – from physical to biological (see Tables 1 and 2). As seen from the content of the tables we do not use the concept of 'radioprotection' widely applied when describing radio modifying effects (Grodzinsky, Gudkov, 1973; Rozhdestvensky, 1985) due to its overly broad (ambiguous) content. On the other hand, we allow a broader interpretation of 'radiotherapy' understanding it not only as a the method of treating oncological diseases but also as the result of positive use of ionizing radiation in the post-radiation period, i.e., after the object receives the 'main' (inhibitory) dose, the radiotherapeutic (according to our classification) action of a factor of any nature in the corresponding dose/power/concentration/activity, etc.

Table 1. Classification of the types of radio modifying effects in terms of the sequence of action of the main radiation (testing in inhibitory dose/power/concentration, etc.) and the modifying factor of any nature.

Radio modification			
Preradiation		Postradiation	
Positive (radio prophylaxis, ‘radio adaptation’, ‘adaptive response’, hyper-radio adaptation)	Negative (preradiation sensitization, hyporadio adaptation)	Positive (non-oncological radiotherapy, reverse radio adaptation')	Negative (postradiation radiosensitization)

Table 2. Classification of the types of radio-modifying effects of factors of any nature based on the sign (direction) of the radio-modifying influence during the inhibitory action of ionizing radiation.

Radio modification			
Positive		Negative	
Preradiation (radio prophylaxis, ‘radio adaptation’, ‘radioadaptive response’, hyper-radio adaptation)	Postradiation (non-oncological radiotherapy, ‘reverse radio adaptation’)	Preradiation (preradiation radiosensitization, hyporadio adaptation)	Postradiation (postradiation radiosensitization)

Why do we put ‘radio adaptation’ and ‘radio adaptive response’ in quotes? Traditionally, ‘radio adaptation’/’radio adaptive response’ refers to a new state of a biological object in which it demonstrates increased radio resistance compared to the original to the action of a radiation stressor. However, it is clear that any biological object, if it can maintain its qualitative specificity and/or individuality, is thus already accommodated (adapted) to a complex of external and internal factors. In other words, a biological object in a state of adaptability (adaptedness) maintains the values of its structural-functional indicators (parameters, properties) at the previous (original, constitutive, endogenous, background, control) level. This state can be called ‘ordinary adaptation’ or ‘ordinary adaptedness’. It is also clear that the original state of the object can be changed under the influence of any exogenous or endogenous factor, and it, ultimately, or at some stage of the post-factor period will have either an unchanged level of resistance (‘ordinary adaptedness’) or changed. Thus, after the impact of any modifying factor at a specific point in time, the object can be in one of the following states:

original adaptation (adaptedness, adaptability) in terms of resistance (the biological object has a constitutive, ‘ordinary’ current, ‘control’ level of adaptedness); original adaptedness (like all other types of adaptedness) can also be cross, i.e., manifest in relation to other factors;

hyper adaptation (super adaptability) in terms of resistance (corresponds to the state of eustress according to H. Selye (1982)), in which the original resistance of the object to subsequent effects of the same or different (cross hyper adaptation in terms of resistance) factor is increased to some extent;

hypo adaptation (decreased resistance, ‘under adaptability’) in terms of resistance (the state of distress according to H. Selye (1982)), associated with a decrease in its original (current) resistance (similarly - cross hypo adaptation in terms of resistance). In this regard, depending on the type of acting factor and the type of ‘acquired’ adaptability, it is necessary, for example, to talk about hyper-radio adaptability, hypothermia adaptability, etc.

In the biological literature devoted to the problem of adaptation, practically no attention is paid to the fact that changing the degree of adaptability of an object is incorrectly described using only the concept of ‘adaptedness’, since, as we have already said, the object is always in a state of adaptedness of a certain level. We, talking about hyper- or hypo adaptedness, emphasize the need to characterize the direction of change of the original level of adaptedness with the corresponding terms.

It is especially important to emphasize this issue when considering radiobiological phenomena, which allows avoiding the ambiguity of the often used concept of ‘radioadaptive response’, which inadequately reflects the observed phenomenon (increase in the level of original radio adaptability) since, in fact, any reaction of an object to the impact is adaptive. Another matter is in which direction (decrease or increase) the level of original adaptability of the object will change.

As for the modification of positive (hormetic, hyperbiotic, etc.) effects of ionizing radiation (Kuzin, 1995), attempts to classify its possible types, as far as we know, were not made. As a working version of the classification of radio hormesis effects, the following is proposed (see Tables 3 and 4).

Tables 3 and 4 classify the types of modification of the radio hormesis effect of ionizing radiation by factors of any nature. It is noted that this classification is somewhat cumbersome in terminological terms, as it does not use established terminology, which simply does not exist. This is not surprising, since the phenomenon of radiation hormesis and the based-on-it phenomenon of hyper-radio adaptation (Mikheev, 2015) have not yet gained ‘recognition in the wider radiobiological community’. It is also clear that the time has not come yet for the realization of the need to study the modification of such an ‘elusive’ effect as radiation hormesis.

Table 3. Classification of types of modification of radio hormesis effects from the point of view of the order of action of the main (in radio hormesis dose/power) and modifying factors

Radio modification			
Preradiation		Postradiation	
Positive (increase in resistance before radiation)	Negative (decrease in resistance before radiation)	Positive (increase in resistance after radiation)	Negative (post-radiation decreases in resistance)

Table 4. Classification of types of modifications of radioprotective effects in terms of the sign (direction) of the radio modifying influence on resistance

Radio modification			
Positive		**Negative**	
Preradiation (enhancement of resistance before radiation)	Postradiation (enhancement of resistance after radiation)	Preradiation (reduction of resistance before radiation)	Postradiation (reduction of resistance after radiation)

In the study we focus in detail on one type of post-radiation positive modification of the effect of the radiation factor in inhibiting doses (in italics in Tables 1 and 2). Radiobiology is well aware of the positive post-radiation effects of incubation conditions (lowered temperature, 'starvation medium', etc.) (Korogodin, 1966). In this case, post-radiation factors create conditions for more effective/resultant work of intracellular and supracellular recovery systems. Our approach is unique in attempting to use ionizing radiation itself as a positively acting post-radiation factor. In other words, we tried to test the possibility of "treating" (providing a 'radiotherapy' effect) acutely irradiated objects with additional irradiation in the post-radiation period. In fact, we have 'turned' into a standard scheme (algorithm) for studying a radio-adaptive (more precisely, hyper-adaptive) response, when an adapting dose of ionizing radiation is applied after the so-called test dose, which has an inhibitory effect on a biological object.

In studying the effect of radio adaptation (positive pre-radiation modification), a traditional interaction scheme is employed between modifying (adapting or de-adapting) factors and test factors, where the action of the first precedes the action of the second in time. This approach covers almost all cases of prophylactic (protective) and sensitizing actions of the first impact in relation to the second, which acts as inhibitory (Myheev, Gushcha, Shilyna, 2002). Our study is based on the assumption that if the applied adapting and test factors are of similar nature (e.g., ionizing radiation in the first and second cases), they primarily act at the same level of system-object integration, implying that the effect of their joint action is independent of the order of their application.

As an adaptive effect, hormesis doses are usually used and, if it, when applied after a test effect, reduces the degree of negative influence of the test effect, then this will obviously indicate a therapeutic type of modifying influence of the adapting effect. In the biology of plant and animal resistance to stressors, this possibility (in fact, radiation 'homeopathy') has not been sufficiently studied. We studied this modification, termed 'reverse adaptation', where various impacts, including chronic ionizing radiation, served as therapeutic influences on plant subjects.

MATERIALS AND METHODS.

In experiments investigating the 'homeopathic' effect of chronic ionizing radiation, 4-day-old pea sprouts of the Kharkiv-317 variety were used. The sprouts were initially irradiated at the 'RESEARCHER' gamma installation with a dose of 6 Gy at a power of 4.2 Gy/s. The dose was chosen based on data from preliminary experiments in which it temporarily inhibited the growth activity of seedlings with subsequent recovery. Irradiated seedlings were divided into two groups, one of which served as a relative control (absolute - non-irradiated seedlings), and the second was experimental. The latter sprouts were placed under chronic gamma radiation from a water solution of cesium-137 chloride in a glass ampoule. At a 5 cm distance from the source, the gamma background power was about 500 μGy/h (0.5 mGy/h, 50 mrad/h). This power 'provided' irradiation of the object at a dose of about 1.0 cGy per day. Plants were grown

in a thermostat at a temperature of 24°C, illumination intensity of 2.2 kLx and light-dark mode: 14 hours of light + 10 hours of darkness.

RESULTS AND DISCUSSION

The therapeutic (‘homeopathic’) effect of post-radiation irradiation was observed in experiments with bean, evening primrose and pea seedlings (see Fig. 1 and 2). Noteworthy (Fig. 2) is the coincidence of the dynamics of radio adaptation proper (‘adaptive response’) and ‘reverse adaptation’ obtained according to the scheme when test irradiation precedes the adapting dose.

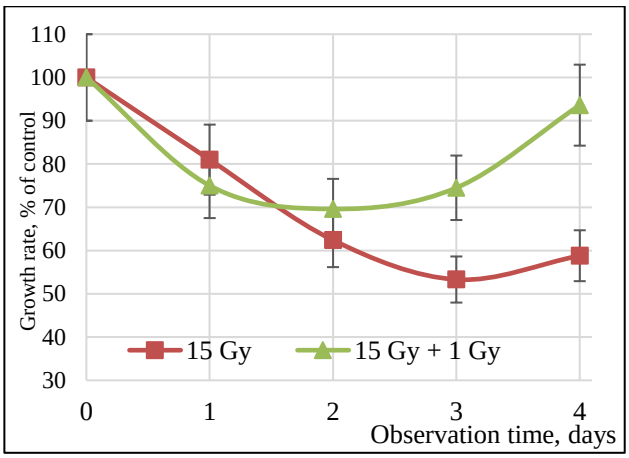

Fig. 1. Effect of acute gamma irradiation on the growth rate of the main root of bean sprouts

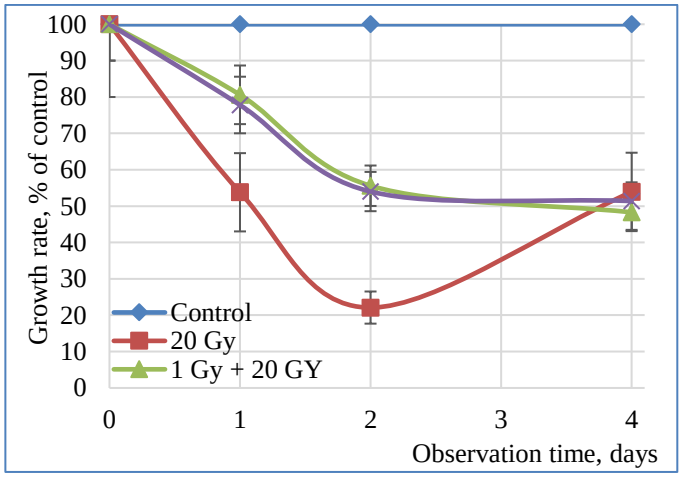

Fig. 2. The dynamics of effects from different schemes of applying acute gamma irradiation to evening primrose sprouts

Similar to direct (ordinary) adaptation, reverse adaptation was observed to have a transitive character, meaning over time, the parameters of the experimental variant approached those of the control variant. It is hypothesized that post-radiation ‘radiotherapeutic’ procedures modify the work of recovery systems in irradiated plants, creating additional opportunities for more complete recovery at the intracellular (molecular) or cell-population levels. The

completion of recovery processes at a specific level, for example, at the cellular level, means the emergence of conditions for its modification even before the completion of corresponding processes at higher levels. This circumstance allows for the application, after inhibiting or even lethal exposure to the object, of impacts that would have been adapting if applied before the inhibiting test exposure. The effect of such influence is identical to the effect of the traditional prophylactic scheme, where the first dose acts as adapting (‘training’).

Particularly of interest, given the need to assess the impact of increased radiation background caused by the Chernobyl accident, was the study of ‘reverse adaptation’ when chronic ionizing radiation is used as a radiotherapeutic means. Figure 3 presents summarized data from ten independent experiments studying the ‘radiotherapeutic’ action of chronic gamma radiation. It is observed that the effect does not manifest immediately, partly explained by the gradual accumulation of absorbed dose from the source of chronic radiation. Nonetheless, the effect is clearly registered and possesses cumulative property, meaning a gradual dose accumulation, leading to the return of growth parameters to the control level (in this case, to the growth parameters of plants acutely irradiated with a dose of 6 Gy). It's evident that if observations continued under these conditions, due to further accumulation of absorbed dose under chronic irradiation, the growth activity of the experimental plants would likely be inhibited. However, it is possible that the applied power of chronic irradiation would not significantly affect subsequent growth phases of the plants. Chronic radiation exposure (see Fig. 4) has a hormetic (positively stimulating) effect on growth characteristics. This supports the similarity, and possibly the identity, of mechanisms between ‘direct’ and ‘reverse’ adaptation discussed earlier.

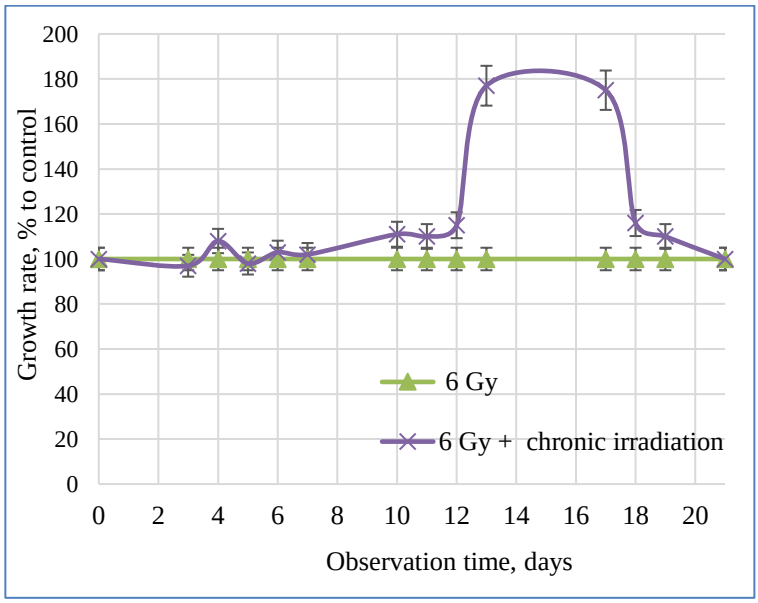

Fig 3. The impact of post-radiation conditions on the growth response of pea sprouts of the Kharkiv-317 variety. It shows plants acutely irradiated with a dose of 6 Gy compared to plants acutely irradiated with 6 Gy and then placed under the influence of a gamma radiation source with a power of 500 μGy/h.

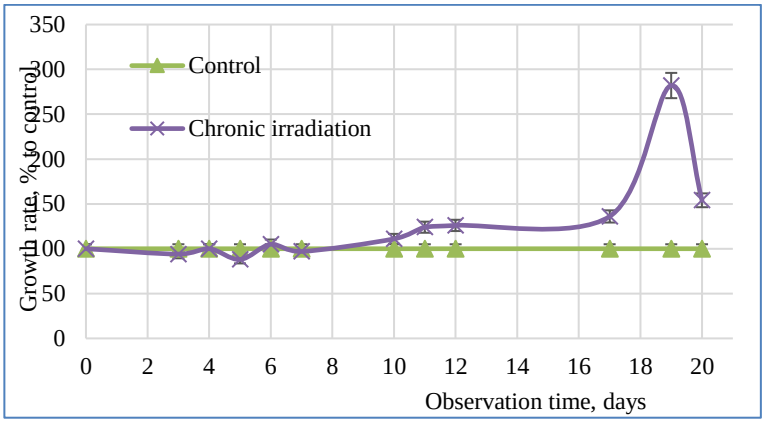

Fig. 4. The effect of chronic irradiation (500 μGy/h) on the growth response of the roots of pea seedlings of the Kharkovsky-317 variety (Control - non-irradiated plants, Chronicle - plants located in the field of action of a gamma irradiation source with a power of 500 μGy/h)

It should also be noted that the onset of the 'therapeutic' effect of chronic irradiation (8-10 days after the start of the experiment) almost coincides with the onset of the hormetic effect of chronic irradiation.

Due to technical reasons preventing long-term incubation of plants, the further fate of irradiated sprouts under chronic gamma radiation remained unclear. However, it is evident that the ultimate effect of 'chronic exposure' as a factor modifying the inhibitory effect of acute gamma irradiation would depend on its power and accumulated absorbed dose. Regardless, considering the potential nonspecific action of chronic radiation as a therapeutic means, it wouldn't be difficult to develop a methodology for its use to reduce negative effects not only of ionizing radiation but also of other chemical and biological factors. While factors of any nature can be used for therapeutic impact, as previously mentioned, we emphasize the somewhat paradoxical statement that radiation damage can be minimized using radiation effects, of course, in appropriate doses or powers of ionizing radiation.

Thus, the presented results suggest an experimental basis for a 'low-dose radiotherapy' method which may find its application in treating acute radiation sickness.

REFERENCES

[1] Grodzinsky D. M., Gudkov I. N. (1973). Protection of plants from radiation damage. M.: Atomizdat, p.232 (in Russian).

[2] Korogodin V. I. (1966). Problems of post-radiation recovery. M.: Atomizdat, 312 (in Russian).

[3] Kuzin A. M. (1977). Ideas of radiation hormesis in the atomic age. M.: Nauka, 137 (in Russian).

[4] Mikheev A. N. (2015). Hyper-adaptation. Stimulated ontogenetic adaptation of plants. K.: Phytosociocenter, p.423 (in Russian).

[5] Mikheev O. M., Gusha M. I., Shilina Yu. V. (2002). Endogenous and exogenous factors in the implementation of the phenotypic adaptation potential of plants (theoretical and experimental aspects). On Sat. Physiology of growing plants in Ukraine for thousands of years. Vol. 2, 82 – 87 (in Ukrainian).

[6] Rozhdestvensky L. M. (1985). Mechanisms of the radioprotective effect and indication of the effectiveness of radioprotectors. M.: Energoatomizdat, 125 (in Russian).

[7] Selye G. (1982). Stress without distress. M.: Progress, 1982. 128 (in Russian).

STUDIES OF NATURAL RADIOACTIVITY IN ROCKS OF SOUTH CAUCASUS
(Kazbegi region, Georgia)

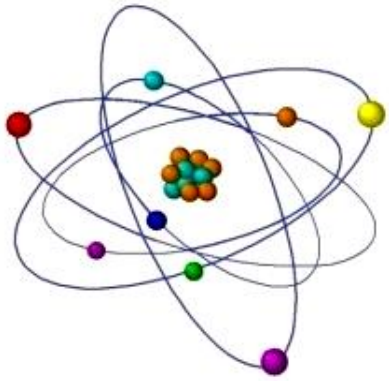

Eremia Tulashvili*., Bela Kvirkvelia., Lela Mtsariashvili., Manana Chkhaidze., Irina Ambokadze

Academician N.Kekelidze Materials Research Scientific-Research Institute, Ivane Javakhishvili Tbilisi State University, Georgia

https://doi.org/10.63465/rrs520258987 *Corresponding author: Email: eremia.tulashvili@tsu.ge

ABSTRACT: *There are given results of radioactivity research in the rock samples within the territory of Kazbegi municipality, Georgia. Twenty-three samples have been collected from 22 locations. Up to 22 radionuclides were identified. Activity concentration of radionuclides of Th-232 family was in the limits from 19.2 to 57.9 Bq/kg (mean, 42.4 Bq/kg), U-238 family – from 16.5 to 38.5 Bq/kg (mean, 31.1 Bq/kg), U-235 family - from 1.03 to 2.40 Bq/kg (mean, 1.91 Bq/kg). Also, individual radionuclides have been identified: K-40 – from 204 to 1069 Bq/kg (mean, 632 Bq/kg), Cs-137 – from 0.18 to 2.69 Bq/kg. Radium equivalent activity varied from 58.2 to 192 Bq/kg (mean, 136 Bq/kg).*

Key words: radionuclides, rocks, activity concentration, South Caucasus

INTRODUCTION

Radioactivity is a part of the natural environment: the earth's surface, rocks, atmosphere, human body, food. The main part of the Earth’s radioactive elements is contained in the rocks that make up the Earth's crust. From here, radioactive elements pass into the soil, then into plants, and finally, together with plants, they enter animal and human organisms.

The radioactivity of rocks and ores is determined by the content of radioactive rock-forming minerals. Depending on the qualitative and quantitative composition of these minerals (in particular, uranium-containing rocks), the conditions of formation, age and degree of metamorphism, their radioactivity varies very widely. The radioactivity of rocks and ores is higher when the concentration of minerals containing naturally occurring radioactive elements (mainly the families of uranium, thorium, and potassium-40) is higher.

The radioactive elements of various radionuclides in rocks may affect the health. Thus, numerous studies have been performed in many regions of the world, and the obtained data can be used to establish if the local controls are needed.

For example, previous work [1] has focused on samples of igneous rocks (dolerite, granite, and granitic gneisses), sedimentary rocks (shales, limestones, sandstones) and metamorphic rocks (black shale, slate, graphite, marble, quartz mica, calcareous schist, and quartz), selected in the state of Kashmir (Pakistan). As a result of this work it was determined that activity

concentration of Ra-226 varied in the range from 4.63 to 108.54 Bq/kg (mean activity concentration was 37.32 Bq/kg), the concentration of Th-232 in the range of ≤1.80 – 110.73 Bq/kg (mean activity - 38.57 Bq/kg), and the concentration of K–40 - in the range of 9.55 – 1135.55 Bq/kg (mean activity – 465.62 Bq/kg). The authors noted that the concentrations of Cs-137 activity in all samples were below the detection limit. The radium equivalent activity of the samples was estimated, which varied in the range of 20.6 - 294 Bq/kg (the average activity value was 126 Bq/kg), which is significantly lower than the maximum recommended value of 370 Bq/kg [2, 3].

In a different work [4], samples of Tufa deposits from four separate occurrences in the Dinaric Region of Croatia were studied. It was found that the activity concentration of Th-232 varied in the range of 1.0 - 12.9 Bq/kg with an mean value of 4.5 Bq/kg; the mean average concentration of U-238 was noticeably higher and amounted to 7.5 Bq/kg (range 1.3 - 14.6 Bq/kg); results comparable to U-238 were obtained for Ra-226 – the mean value was 7.3 Bq/kg, the range is from 2.9 to 13.0 Bq/kg. The technogenic radionuclide Cs-137 was also found in the studied samples, which activity concentration varied in the range of 3.9 - 77.8 Bq/kg with mean value of 24.6 Bq/kg; the authors explain this as contamination of Cs-137 originating from rainwater; obsolete calcareous tuff is not a closed system, and sampling was performed after an accident in 1986, which was accompanied by heavy rains in this area. The ratios of radionuclide activities were also calculated, the values of which for U-238/Th-232 varied in the range of 0.81 - 5.30 with the mean value of 2.41, and for Ra-226/U-238 in the range of 0.59– 2.22 with the mean value of 1.10.

Studies of various rocks used as building materials have been conducted in Romania [5]. The activity concentrations of the radionuclides Th-232, Ra-226, K-40, and Cs-137 in tufa were 9.8, 10.5, 180, and 9.6 Bq/kg, respectively.

Authors of the work [6] examined several dozen limestones samples, selected throughout Turkey. The activity concentration of Ra-226 varied in the range of 0.7 - 55.1 Bq/kg with the mean value of 19 Bq/kg, Th-232 – in the range of 1.2 - 20.9 Bq/kg with the mean value of 4.3 Bqkg, and K-40 – in the range of 10.1 - 258.4 Bqkg with the mean value of 55 Bq/kg. Based on the measurement results, the equivalent activity values were calculated, which varied in the range of 3.2 - 81.6 Bq/kg with the mean value of 29.4 Bq/kg.

Studies of the radioactivity of various environmental objects in Georgia have been conducted in the past and were mainly stimulated by the accident at the Chernobyl nuclear power plant in 1986.

The authors of this work participated in a number of studies of radioactivity on the territory of Georgia, including the radioactivity of rocks [7, 8, 9, 10, 11].

In this work, a study of natural and technogenic radioactivity was conducted in the part of the territory of the Kazbegi municipality. The aim of the work was to establish the radionuclide content and background concentrations of radionuclides in various geological structures in the study area, to study the level of gamma-ray radioactivity, as well as to assess the corresponding radiological risk to the local population and tourists.

MATERIALS AND METHODS

Study area:

Kazbegi municipality is part of the Mtskheta-Mtianeti region. The municipality is located entirely in the mountainous part of Georgia. The height above sea level varies from 1,700 m to 5,000 m. The area of the municipality is 1081.7 km^2. The municipality borders the Russian Federation in the northern part.

The main orographic unit of the territory is the Main Caucasian Ridge. The relief of the municipality is mountainous in nature – mostly rocky and difficult to access. Erosive, volcanic and glacial landforms are developed. Karst rocks are found sporadically. The basis of the Kazbegi mountain range consists of sandstones that formed in the Jurassic period, as well as basalt formations such as quartzite, clay shales and clay deposits. Lava pillows are a part of the geology of the region. Cliffs have formed on the slopes of the Daryal Gorge, on the walls of which basalt sections and layers of frozen lava are visible.

Twenty-three rock samples were selected at twenty-two control points in the study area (two samples of different rocks were selected at the control point Kz-33). Table 1 contains a list of control points, their brief description, geographical coordinates, as well as a list of selected samples and their types.

Sampling and analysis:

Sampling and sample preparation

Samples were selected from the outcropped rocks and put in plastic containers (volume up to 2.0 L). After drying in the laboratory, samples were broken into pieces < 40 mm and then were crushed using a special crusher (jaw crusher Retsch) to a size of approximately 1 mm. Then samples were dried at 105 - 110°C to constant weight and their bulk density was then determined. These values were used for the description of sample geometry. The samples were sealed in Marinelli beaker and stored for more than four weeks to achieve secular equilibrium between Ra-226 and Rn-222.

Measurement of gamma-radiation activity

Measurements of the radionuclide content of the studied samples and the activity concentration of radionuclides were carried out using a Canberra GC2020 gamma-spectrometer with a semiconductor germanium detector with a relative efficiency of 24%. The acquisition time for gamma spectra was 48 hours. The Genie-2000 S500 software with additional modules was used for the analysis, in particular, S506, an Interactive Fit Program. This program was used to “decompose” the interference peak in the 186 keV region in all spectra (in this region, the program identifies one peak resulting from the interference of two closely spaced peaks U-235 (185.715 keV) and Ra-226 (186.211 keV)). Using the S506C program, the spectral curve is mathematically processed, as a result of which two Gaussian peaks with energies corresponding to U-235 and Ra-226 are created in this region. When programmatically identifying peaks and calculating the concentration of activity, the tolerance value was set in such a way that only U-235 was compared to the low–energy peak, and only Ra-226 to the high-energy peak. As the results showed, in particular for Ra-226, the error in determining its activity concentration was mainly in the range of 8.8 - 24%. His activity

was compared with the activity of his daughters Pb–214 and Bi-214, the error in determining which lay in the range from 2.4 to 3.0%. The obtained activity values of Ra-226, Pb-214 and Bi-214 differed little from each other. Thus, it can be considered that the error in determining the concentration of Ra-226 in this way is quite satisfactory, and this method was also used to determine the activity concentration of U-235 along the 185.715 keV line. The obtained values of U-235 activity were compared with the values of U-238 activity (which was determined by the Th-234 - 63.3 keV line with an error in the range of 6.3 - 14%). The value of the ratio of their activities (U-238/U-235 = 21.7 [12]) was used as a criterion. With large deviations from this value (more than 10%), the 185.715 keV line (as well as the 63.3 keV line) was reanalyzed using the S506 program. (In some cases, in low-activity samples, the activity of Ra-226 was refined by the average activity of Pb-214 and Bi-214 and the resulting value was taken into account in the final assessment activity values U-235). To determine the activity of Th-232, the average values for Ac-228, Ra-224, Pb-212, Bi-212 were used, the errors of which ranged from 3.2 to 7.2%. The activity ratios U-238/Th-232 (which for closed systems is assumed to be 0.81 [13, 14]), Ra-226/U-238 and Pb-210/Ra-226 (equilibrium value 1.00) was also determined, which are used to evaluate the mechanism of various geochemical processes.

Table 1
List of control points (CP), types (ST) of investigated samples

#	CP	Lt(N); Ln(E)	Description of CP	SN	ST
1	Kz-1	42.7332; 44.6319	Mtavarangelozi Monastery complex	416-R	St
2	Kz-4	42.7351; 44.6353	“-“	401-R	Dt
3	Kz-5	42.6670; 44.6299	Stepantsminda-Larsi road, Chkhere River gorge	398-R	An
4	Kz-10	42.6937; 44.6410	Terek River valley	415-R	St
5	Kz-20	42.6420; 44.6364	Tbilisi-Stepantsminda road, near the entrance to Stepantsminda	414-R	St
6	Kz-21	42.6381; 44.6352	Near the confluence of the rivers Terek and Snostskali	399-R	Cl-Sl
7	Kz-28	42.5595; 44.7022	Villagrs Karkucha-Juta road	409-R	Sl
8	Kz-31	42.5948; 44.6697	Village Akhaltsikhe	413-R	Al
9	Kz-33	42.6035; 44.5682	Village Goristsikhe	418-R	An-Bs
10	“-“	“-“	“-“	420-R	An
11	Kz-37	42.5719; 44.5240	Village Kobi	417-R	An
12	Kz-39	42.5604; 44.5121	Village Kobi	402-R	An
13	Kz-42	42.5849; 44.5535	Village Kanobi	403-R	Tf
14	Kz-50	42.5516; 44.4944	Surroundings of Kobi village	406-R	Ss
15	Kz-54	42.5380; 44.4763	Cross Pass Travertine	411-R	Dc
16	Kz-55	42.6236; 44.6097	Near the entrance to the village Arsha	397-R	Cl-Sl
17	Kz-59	42. 6230; 44.5983	Village Arsha, Gaiboteni	405-R	An
18	Kz-61	42.6237; 44.6098	Surroundings of Arsha village	404-R	Cl-Sl
19	Kz-64	42.6099; 44.5740	Village Tkarsheti	400-R	An
20	Kz-66	42.6582; 44.6229	Gergeti Trinity Church	412-R	Cl-Sl
21	Kz-69	42.6575; 44.6376	Village Gergeti	410-R	Cl-Sl
22	Kz-75	42.5000; 44.4836	Panorama Gudauri	407-R	Tf
23	Kz-76	42.4766; 44.4777	Village Gudauri	408-R	Tf

Notes: **1**. Lt(N) – latitude (north); Ln(E) – longitude (east). **2**. SN – sample number. **3.** *Rock types*: An - Andesite; Dc - Dacite; Dt - Diorite An-Bs - Andesite-basalt; Tf – Tuff; Ss - Sandstone; Al - Aleuropelite St – siltstone; Cl-Sl - Clay-slate; Sl – Slate.

To account for the effect of the matrix content, based on the literature data, the chemical content of rocks [15] was established, which were then used in special software (LabSOCS) for efficiency calibration in calculating the activity concentration. The LabSOCS system allows

you to create calibrations based on the effectiveness of laboratory quality without the use of radioactive calibration sources. A special library containing lines of 41 radionuclides and other specific sources (351 lines in total) was used to identify radionuclides. The NuDat database was used to compile the library [16].

To assess the potential radiation risk of terrestrial radioactivity for the population living in the studied region, various indicators were calculated.

To assess the radiological hazard, the radium equivalent activity of Ra_{eq} (Bq/kg) and the annual effective dose of AEDE (mSv/y) were calculated; the calculation was carried out according to the formulas [17]:

$$Ra_{eq} = A_U + 1.43A_{Th} + 0.07A_K \quad (1)$$

where A_U, A_{Th}, and A_K are the activity concentration (Bq/kg) of U-238, Th-232, and K-40, respectively;

$$AEDE = D \times N_h \times k_1 \times k_2 \quad (2)$$

where N_h is the number of hours per year (=8760 h), k_1 is the conversion factor of the effective dose rate into the absorbed dose rate in the air for adults, 0.7 Sv/Gy, k_2 is the outdoor coefficient (the proportion of time spent outdoors) which is 0.2, D is the absorbed dose rate (nGy/h):

$$D = k_U A_U + k_{Th} A_{Th} + k_K A_K \quad (3)$$

where k_U, k_{Th}, k_K are the so–called dose coefficients equal to 0.462, 0.604 and 0.0417, respectively.

To characterize the samples according to the degree of radioactivity, taking into account the accepted limit value of Ra_{eq} - 370 Bq/kg (equivalent to a dose of gamma radiation of 1.5 μSv/y) [18] several groups of samples were identified in terms of equivalent activity, in particular:

- group 1 – non-radioactive samples with an activity of no more than 30 Bq/kg;
- group 2 – with low radioactivity in the range from 30 to 100 Bq/kg;
- group 3 – with average radioactivity in the range from 100 to 300 Bq/kg;
- group 4 – samples with increased radioactivity in the range from 300 to 1000 Bq/kg.

Calculations of other indicators were also carried out to assess the radiation hazard, in particular:

- External hazard index (H_{ex}) is a widely used hazard index which represents the external exposure, and который рассчитывался по формуле:
$$H_{ex} = (A_U/370) + (A_{Th}/259) + (A_K/4810) \quad (4)$$
- Internal hazard index (H_{in}): in addition to external hazard index, radon and its short-lived products are also hazardous to the respiratory organs; the internal exposure to radon and its daughter progenies is quantified by the internal hazard index H_{in}, which is given by the equation:
$$H_{in} = (A_U/185) + (A_{Th}/259) + (A_K/4810) \quad (5)$$

The values of the indices (H_{ex}, H_{in}) must be less than unity for the radiation hazard to be negligible [19].

RESULTS AND DISCUSSION

According to the results of the analysis of gamma spectra up to 22 radionuclides are identified in rock samples - family Th–232 (Ac-228, Th-228, Ra-224, Pb-212, Bi-212, Tl-208), family U-238 (Th-234, Pa-234, Th-230, Ra-226, Pb-214, Bi-214, Pb-210), family U-235 (U-235, Th-231, Th-227, Ra-223, Rn-219, Pb-211), separate radionuclides Be-7, K-40, Cs-137 (also some specific lines are identified that arise as a result of the interaction of cosmic rays with the material of detector or sample).

Table 2 and Table 3 show the results of measuring the activity concentration (A, Bq/kg) of the main radionuclides for the studied samples, radium equivalent activity (Ra_{eq}, Bq/kg), activity ratios, their average (av), minimum (mn) and maximum (mx) values, as well as other data.

Table 2
Activity concentration (A, Bq/kg) of radionuclides of the families Th-232, U-238 (Th-234), U-235, Ra-226, Pb-214, Bi-214, Pb-210), radionuclides Be-7, K-40 and Cs-137, as well as their average (av), minimum (mn) and maximum (mx) values in rocks of various types

#	FN	CP	ST	A, Bq/kg									
				Th-232	U-238	Ra-226	Pb-214	Bi-214	Pb-210	U-235	Be-7	K-40	Cs-137
				Magmatic									
1	398-R	Kz-5	An	31.3	26.8	20.5	25.9	24.3	<M	2.01	-	450	<M
2	400-R	Kz-64	An	41.0	34.5	35.0	32.5	29.6	34.2	2.15	-	610	<M
3	401-R	Kz-4	Dt	45.0	31.8	31.2	31.7	29.5	-	1.51	-	788	<M
4	402-R	Kz-39	An	38.2	29.3	21.7	30.3	28.3	<M	1.98	-	530	-
5	405-R	Kz-59	An	40.0	30.0	21.8	30.7	28.3	28.9	2.17	<M	522	0.54
6	411-R	Kz-54	Dc	37.6	25.8	18.5	26.7	25.7	<M	1.60	4.70	534	-
7	417-R	Kz-37	An	37.5	33.5	35.4	29.6	27.7	<M	2.30	5.58	526	<M
8	418-R	Kz-33	An-Bs	39.5	32.0	29.1	32.0	29.4	41.5	2.40	3.00	593	0.82
9	420-R	Kz-36	An	39.9	33.6	31.7	31.1	29.2	32.5	2.27	6.26	588	<M
			av	38.9	30.8	27.2	30.1	28.0	34.3	2.04	4.88	571	0.68
			mn	31.3	25.8	18.5	25.9	24.3	28.9	1.51	3.00	450	0.54
			mx	45.0	34.5	35.4	32.5	29.6	41.5	2.40	6.26	788	0.82
				Sedimentary									
10	403-R	Kz-42	Tf	42.5	31.5	25.5	33.6	31.2	24.0	2.23	<M	573	<M
11	406-R	Kz-50	Ss	42.4	31.1	27.8	30.3	28.2	30.9	1.91	4.17	632	0.49
12	407-R	Kz-75	Tf	28.1	21.6	24.7	21.1	19.5	24.4	1.21	4.23	441	1.46
13	408-R	Kz-76	Tf	31.7	24.4	20.1	25.5	23.3	20.4	1.49	<M	414	-
14	413-R	Kz-31	Al	57.9	34.5	34.1	33.4	31.4	34.4	2.20	6.63	911	<M
15	414-R	Kz-20	St	41.9	31.7	31.2	30.3	28.7	40.6	2.04	6.22	579	2.69
16	415-R	Kz-10	St	55.0	38.5	34.4	37.4	34.8	50.1	2.15	-	1069	<M
17	416-R	Kz-1	St	19.2	16.5	11.8	17.4	16.1	32.6	1.03	<M	204	-
			av	39.8	28.7	26.2	28.6	26.7	32.2	1.78	5.31	603	1.54
			mn	19.2	16.5	11.8	17.4	16.1	20.4	1.03	4.17	204	0.49
			mx	57.9	38.5	34.4	37.4	34.8	50.1	2.23	6.63	1069	2.69
				Metamorphic									
18	397-R	Kz-55	Cl-Sl	51.7	34.3	-	31.9	29.3	34.9	1.16	<M	844	1.03
19	399-R	Kz-21	Cl-Sl	43.5	36.5	33.2	33.8	31.4	29.1	1.83	1.82	605	<M
20	404-R	Kz-61	Cl-Sl	55.5	32.3	23.3	32.2	30.1	<M	1.96	3.48	910	0.18
21	409-R	Kz-28	Sl	52.4	35.9	39.6	33.1	31.0	21.1	2.12	10.7	703	0.40
22	410-R	Kz-69	Cl-Sl	50.7	35.0	26.7	34.1	31.8	39.0	2.04	<M	711	<M
23	412-R	Kz-66	Cl-Sl	52.0	34.7	34.7	32.5	30.6	-	2.10	7.13	800	0.86
			av	51.0	34.8	31.5	32.9	30.7	31.0	1.87	5.79	762	0.62
			mn	43.5	32.3	23.3	31.9	29.3	21.1	1.16	1.82	605	0.18
			mx	55.5	36.5	39.6	34.1	31.8	39.0	2.12	10.7	910	1.03

The activity of radionuclides of the families varies significantly in different samples (Table 2), in particular, Th-232 – in the range of 19.2-57.9 Bq/kg (on average 42.4 Bq/kg), U-238 – 16.5-38.5 Bq/kg (31.1 Bq/kg), Ra-226 - 11.8-39.6 Bq/kg (27.8 Bq/kg), U-235 - 1.03-2.40 Bq/kg (1.91 Bq/kg). K-40 activity varies in the range of 204-1069 Bq/kg (632 Bq/kg). Be-7 was recorded in 12 samples in the range from 1.82 to 10.7 Bq/kg (in some samples - in trace amounts) Technogenic radionuclide Cs-137 was recorded in 9 samples in small quantities (0.18-2.69 Bq/kg), and in some samples it was recorded in trace amounts. The activity ratios of U-238/U-235 vary in the range from 14.1 to 36.1 with an average value of 20.8, and generally correspond to the value of 21.7 (accepted for natural objects).

The ratio U-238/Th-232 in most samples (14 out of 23) is within ± 10% of the average value of 0.81 (for closed systems), and in the remaining samples deviate from the average value in a smaller direction (from 0.58 to 0.71).

Table 3

Radium equivalent activity (Ra_{eq}, Bq/kg), activity ratios U-238/U-235; U-238/U-235, Ra-226/U-238 and Pb-210/Ra-226, dose rate (D, nGy/h) and annual effective dose (AEDE, mSv/y) as well as their average (av), minimum (mn) and maximum (mx) values in rocks of various types

#	FN	CP	ST	Ra_{eq}, Bq/kg	D, nGy/h	AEDE, mSv/y	H_{ex}	H_{in}	U-238/ U-235	U-238/ Th-232	Ra-226 /U-238	Pb-210 /Ra-226
						Magmatic						
1	398-R	Kz-5	An	103	50.0	0.061	0.29	0.36	21.2	0.86	0.77	-
2	400-R	Kz-64	An	136	66.1	0.081	0.38	0.47	17.4	0.84	1.01	0.98
3	401-R	Kz-4	Dt	151	74.7	0.092	0.42	0.51	22.7	0.71	0.98	-
4	402-R	Kz-39	An	121	58.8	0.072	0.34	0.42	21.6	0.77	0.74	-
5	405-R	Kz-59	An	124	59.8	0.073	0.34	0.43	14.1	0.75	0.73	1.32
6	411-R	Kz-54	Dc	117	56.9	0.070	0.33	0.40	18.7	0.68	0.72	-
7	417-R	Kz-37	An	124	60.1	0.074	0.34	0.44	28.5	0.89	1.06	-
8	418-R	Kz-33	An-Bs	130	63.3	0.078	0.36	0.45	15.1	0.81	0.91	1.42
9	420-R	Kz-36	An	132	64.2	0.079	0.37	0.46	23.1	0.84	0.94	1.02
			av	***126***	**61.5**	**0.075**	**0.35**	**0.44**	***20.3***	***0.80***	***0.87***	***1.19***
			mn	***103***	**50.0**	**0.061**	**0.29**	**0.36**	***14.1***	***0.68***	***0.72***	***0.98***
			mx	***151***	**74.7**	**0.092**	**0.42**	**0.51**	***28.5***	***0.89***	***1.06***	***1.42***
						Sedimentary						
10	403-R	Kz-42	Tf	132	64.1	0.079	0.37	0.45	20.9	0.74	0.81	0.94
11	406-R	Kz-50	Ss	136	66.3	0.081	0.38	0.46	20.8	0.73	0.89	1.11
12	407-R	Kz-75	Tf	92.6	45.3	0.056	0.26	0.32	17.6	0.77	1.14	0.99
13	408-R	Kz-76	Tf	99	47.6	0.058	0.27	0.34	17.5	0.77	0.82	1.02
14	413-R	Kz-31	Al	181	88.9	0.109	0.51	0.60	18.1	0.60	0.99	1.01
15	414-R	Kz-20	St	132	64.0	0.079	0.37	0.45	18.8	0.76	0.99	1.30
16	415-R	Kz-10	St	192	95.6	0.117	0.54	0.64	23.8	0.70	0.89	1.46
17	416-R	Kz-1	St	58.2	27.7	0.034	0.16	0.21	14.8	0.86	0.72	2.77
			av	***128***	**62.5**	**0.077**	**0.36**	**0.43**	***19.0***	***0.74***	***0.91***	***1.32***
			mn	***58.2***	**27.7**	**0.034**	**0.16**	**0.21**	***14.8***	***0.60***	***0.72***	***0.94***
			mx	***192***	**95.6**	**0.117**	**0.54**	**0.64**	***23.8***	***0.86***	***1.14***	***2.77***
						Metamorphic						
18	397-R	Kz-55	Cl-Sl	167	82.2	0.101	0.47	0.56	36.1	0.66	-	-
19	399-R	Kz-21	Cl-Sl	141	68.4	0.084	0.39	0.49	23.6	0.84	0.91	0.88
20	404-R	Kz-61	Cl-Sl	175	86.4	0.106	0.49	0.58	27.6	0.58	0.72	-
21	409-R	Kz-28	Sl	160	77.5	0.095	0.45	0.54	18.4	0.69	1.10	0.53
22	410-R	Kz-69	Cl-Sl	157	76.4	0.094	0.44	0.53	17.7	0.69	0.76	1.46
23	412-R	Kz-66	Cl-Sl	165	80.8	0.099	0.46	0.55	20.3	0.67	1.00	-
			av	***161***	**78.6**	**0.096**	**0.45**	**0.54**	***23.9***	***0.69***	***0.90***	***0.96***
			mn	***141***	**68.4**	**0.084**	**0.39**	**0.49**	***17.7***	***0.58***	***0.72***	***0.53***
			mx	***175***	**86.4**	**0.106**	**0.49**	**0.58**	***36.1***	***0.84***	***1.10***	***1.46***

The Ra-226/U-238 ratios for 10 samples are within ± 10% of the equilibrium value, for 11 samples less than the equilibrium value (0.72-0.89), and in one sample more than the equilibrium value (1.14). The Pb-210/Ra-226 ratio for 8 out of 15 samples was within ± 20% of the equilibrium value, in some samples they differed from the equilibrium value by more than ± 20% - in 6 samples more, and in 1 sample less (Note: the ratios of radionuclide activity were not determined in all samples, so as in a number of samples, the activity of the corresponding radionuclides was less than MDA or was not recorded). The values of radium equivalent activity varied in the range of 58-192 Bq/kg (average value of 136 Bq/kg), while the lowest activity was observed for sedimentary rock samples with an average value of 58.2 Bq/kg, and for samples of magmatic and metamorphic rocks, the average Ra_{eq} values were 103 and 141 Bq/kg, respectively. Similarly, lower absorbed dose rates were observed for sedimentary rock samples (27.7 nGy/h) compared with samples of magmatic (50.0 nGy/h) and metamorphic (68.4 nGy/h) rocks, and, accordingly, the values of the annual effective dose varied from the lowest values for sedimentary rocks (with an average value of 0.034 mSv/y) to high values for magmatic (0.061 mSv/y) and metamorphic (0.084 mSv/y) rocks. It should be noted that the main number of samples (87.0%) in terms of activity in radium equivalent belongs to groups with average radioactivity, and a small number of samples (13.0%) belongs to the group with low radioactivity (Table 3).

As noted above, rock samples were taken in a geological area characterized by a sufficiently complex geotectonic structure. The types of samples collected corresponded to all three main groups of rocks – magmatic, sedimentary and metamorphic. Each of these groups has a specific mineralogical and chemical composition, as well as a mechanism of rock formation, which is mainly associated with a large range of radioactivity concentrations occurring for almost all identified radionuclides, as well as the activity ratios of some radionuclides.

The values of the U-238/U-235 ratio obtained for all samples correspond to the natural value within the margin of error, which, in addition to the methodological aspect, allows us to conclude that there is no pollution by anthropogenic U-235. The ratios of U-238/Th-232 and Ra-226/U-238, which are close to the average and equilibrium values for magmatic samples, allow us to conclude that these primary rocks apparently represent closed systems. To a certain extent, this is confirmed by a slight deviation of the Pb-210/Ra-226 ratio from the equilibrium value (which can be explained by the compacted texture of these rocks).

However, the features of the activity ratio observed in sedimentary and metamorphic samples (which are secondary rocks), in particular, deviations from the average value of the U-238/Th-232 ratio and the equilibrium value of Ra-226/U-238 indicate that these systems were not closed, and in the past, there were various geochemical processes.

For example, in works [20, 21] it is noted that Th isotopes, which in natural environments occur only in a tetravalent form, form compounds practically insoluble in water and are transferred mechanically in the form of stable minerals, while U isotopes occur in both 4- and 6-valence forms - in the 4-valence form, they are close to Th in chemical properties, and in the 6-valence form they are characterized by high chemical activity, and migrate over long distances in the form of solutions with waters. These processes can lead to a decrease in the U-238/Th-232 ratio relative to the average value, especially in metamorphic rocks, where an increased porous structure could contribute to their greater intensification (which was observed, for example, in samples 397-R, 404-R, 409-R, 410-R, and 412-R).

These same factors, as well as the influence of hypergenesis (weathering), can lead to an imbalance in the radioactive series of the family, in particular, between U and Ra. Here, in addition to the above reasons, the influence of differences in the chemical properties of the elements is significant. In particular, the isotope Ra is easily leached and washed away by

waters: in natural formations, Ra-226 often accumulates in quantities exceeding equilibrium with uranium. In the studied samples, deviations from the equilibrium values are relatively small, from which it can be concluded that the above factors played an insignificant role in this region.

The more noticeable deviations of the U-238/Th-232 activity ratios from the average values observed in the work for sedimentary and metamorphic rocks are apparently determined to a greater extent by the processes of hypergenesis. As is known, the Cretaceous period (when most sedimentary rocks were formed) was characterized by the dominance of land on Earth, the climate was hot and dry, deposits of chalk, carbonates, clay shales and others were formed. Mountain systems were formed, and before that, inland seas and vast swamps. All this contributed to the intensification of the process of hypergenesis, intensive leaching of radioactive elements in the process of rock formation or metamorphism. As a result, there was a noticeable decrease in the content of radioactive elements in these rocks. After the Cretaceous period, the climate changed, the temperature dropped, and this factor contributed to a change in the conditions of hypergenesis, which could contribute to an increase in the content of radionuclides during rock formation (which we observe for samples of the Neogene and Quaternary periods).

There is no significant deviation from the equilibrium value in the Pb-210/Ra-226 ratio, which is also noted in [21] for rocks. It can be assumed that the absence of superequilibrium (allochthonous) Pb-210 in rocks (compared to soils, where its noticeable presence is often recorded) is due to their compacted structure, as a result of which, as noted above, radionuclides are in a “sealed” state in them, and radon migration does not take place in them. The slight excess observed in several samples may be associated with the deposition of Pb-210 from atmospheric air.

The insignificant concentrations of the natural radionuclide Be-7 observed in some samples appear in the samples as a result of precipitation, and in some cases can be identified in gamma spectra. Technogenic radionuclide Cs-137 also gets onto samples as a result of atmospheric precipitation. Usually, the presence of Cs-137 in natural objects (for example, in soil) is associated, as mentioned above, with the Chernobyl disaster. Over the past period, its number has decreased as a result of both disintegration and migration. In the conducted studies, it was observed in several samples in insignificant concentrations (compared with soils where its concentration is noticeably higher), which is apparently due to the intensive process of leaching from the surface of the samples.

The obtained activity values in radium equivalent are noticeably lower than the recommended value of 370 Bq/kg [2, 3].

CONCLUSION

In this work, the radionuclide content and activity concentration of gamma-emitting radionuclides were studied in various rock samples collected on the territory of the Kazbegi municipality.

As a result of the conducted studies, it was found that up to 22 radionuclides are mainly detected in the selected rock samples, in particular: family Th-232 - Ac-228, Th-228, Ra-224, Pb-212, Bi-212, Tl-208 (a total of 6 radionuclides); family U-238 – Th-234, Pa-234, Th-230, Ra-226, Pb-214, Bi-214, Pb-210 (7 radionuclides in total); family U-235 - U-235, Th-231, Th-227, Ra-223, Rn-219, Pb-211 (6 radionuclides in total); other natural radionuclides Be-7, K-40, technogenic radionuclide Cs-137. For the studied samples, the average activity values of the radionuclides of the Th-232 and U-238 families are approximately the same (42.4 Bq/kg and 31.1 Bq/kg, respectively) and significantly exceed the average activity of the radionuclides of

the U-235 family (1.91 Bq/kg). The activity of radionuclide K-40 varies in the range of 204-1069 Bq/kg (the average value was 632 Bq/kg); in some samples, a small amount of natural radionuclide Be-7 and technogenic radionuclide Cs-137 was recorded. The main number of samples (87.0%) in terms of activity level in radium equivalent belongs to the groups with medium radioactivity, and a small number of samples (13.0%) belongs to the group with low radioactivity. The obtained activity values in radium equivalent are noticeably lower than the recommended value of 370 Bq/kg.

Thus, the radioecological situation of the territory of the Kazbegi municipality in terms of radioactivity of rocks can be assessed as normal, not posing a danger to the resident population.

ACKNOWLEDGMENT

The project was supported by Shota Rustaveli National Science Foundation of Georgia (SRNSFG) [grant number BRG-I-23-363].

REFERENCES

[1] M. Rafique, A.R. Khan, A. Jabbar, S.U. Rahman, S.J.A. Kazmi, T. Nasir, W. Arshed, Matiullah. Evaluation of radiation dose due to naturally occurring radionuclides in rock samples of different origins collected from Azad Kashmir. Russian Geology and Geophysics, 2014, 55, pp. 1103–1112.

[2] Report of the United Nations Scientific Committee on the Effect of Atomic Radiation to the General Assembly (UNSCEAR 1988), "Sources, effects and risks of ionizing radiation", United Nations, New York, 1988.

[3] International Commission on Radiological Protection. The 2007 Recommendations of the International Commission on Radiological Protection. ICRP Publication 103. Ann. ICRP 37, Oxford: Pergamon, 2007.

[4] S. Frančišković-Bilinski, D. Barišić, A. Vertaćnik, H. Bilinski, E. Prohić. Characterization of tufa from the Dinaric Karst of Croatia: mineralogy, geochemistry and discussion of climate conditions. Facies, 2004, 50, pp. 183–193. doi 10.1007/s10347-004-0015-8.

[5] A. Pantelica, I.I. Georgescu, M.D. Murariu-Magureanu, I. Margaritescu, E. Cincu. Thorium determination in intercomparison samples and in some Romanian building materials by gamma ray spectrometry. Radiation Protection Dosimetry, 2001, 97 (2), pp. 187–191.

[6] Ş. Turhan. Radioactivity levels of limestone and gypsum used as building raw materials in turkey and estimation of exposure doses. Radiation Protection Dosimetry, 2010, 140 (4), pp. 402–407.

[7] N. Kekelidze, T. Jakhutashvili, B. Tutberidze, E. Tulashvili, M. Akhalkatsishvili, L. Mtsariashvili. Radionuclides in rocks of southern part of Mtskheta-Mtianeti region (Georgia). Journal of Geochemical Exploration, 2018, 190, pp. 1-9, 2018 https://doi.org/10.1016/j.gexplo.2018.02.010.

[8] N. Kekelidze, T. Jakhutashvili, B. Tutberidze, E. Tulashvili, M, Akhalkatsishvili, L. Mtsariashvili. Radioactivity of rock samples of different origin (the central region of the Main Caucasian Range, Georgia). Science and Engineering Applications, 2017, 2, pp. 181-192, http://www.jfips.com/saea/articles/2/14/.

[9] N. Kekelidze, T. Jakhutashvili, B. Tutberidze, E. Tulashvili, M. Akhalkatsishvili, L. Mtsariashvili. Radioactivity of rock samples in the Shida Kartli Region (Georgia). International Journal of Agriculture, Environment and Bioresearch, 2018, 3 (3), pp. 98-118. http://ijaeb.org/view2.php?issue=3.

[10] N. Kekelidze, T. Jakhutashvili, B. Tutberidze, E. Tulashvili, M. Akhalkatsishvili, L. Mtsariashvili, M. Chkhaidze, I. Ambokadze. Radioactivity of Rocks in Several Regions of East Georgia. *In book* "Radionuclides: Properties, Behavior and Potential Health Effects"; Chapter 3. Editors Nataša Todorović and Jovana Nikolov. Series: Environmental Science, Engineering and Technology. Nova Science Publishers, Inc., Hauppauge, NY, USA; 2020.

[11] E.V. Tulashvili, B.D. Tutberidze, M.R. Akhalkatsishvili, L.A. Mtsariashvili, M.A. Chkhaidze. Evaluation of radioactivity of the rocks in the foothills of the Main Caucasian range in the territory

of Kakheti region (East Georgia). Journal of Radiobiology and Radiation Safety, 2021, 1 (2), pp. 75-86. https://doi.org/10.48614/rrs120213306.
[12] M.J. Anagnostakis, E.P. Hinis, D.J. Karangelos, N.P. Petropoulos, P.K. Rouni, S.E. Simopoulos, Z.S. Žinić. Determination of depleted uranium in environmental samples by gamma-spectroscopic techniques. Archive of Oncology, 2001, 9 (4), pp. 231-236.
[13] A. Navas, L. Gaspar, M. López-Vicente, J. Machín. Spatial distribution of natural and artificial radionuclides at the catchment scale (South Central Pyrenees). Radiation Measurements, 2011, 46, pp. 261-269.
[14] M. Ivanovich. Uranium series disequilibrium: concepts and applications. Radiochim. Acta, 1994, 64, pp. 81-94.
[15] R. Jubelt, P. Schreiter. Rocks identification guide. Mir, Moscow, 1977 [in Russian].
[16] National Nuclear Data Center, Brookhaven National Laboratory, USA. http://www.nndc.bnl.gov/nudat2/
[17] United Nations Scientific Committee on the Effect of Atomic Radiation (UNSCEAR). Exposure from natural radiation sources. New York: United Nations, 2000.
[18] OECD. Exposure to radiation from the natural radioactivity in building materials. Report by a group of experts of the OECD, Nuclear Energy Agency, Paris, France, 1979.
[19] H.M. Diab, S.A. Nouh, A. Hamdy, S.A. El-Fiki. Evaluation of natural radioactivity in a cultivated area around a fertilizer factory. Journal of Nuclear and Radiation Physics, 2008, 3(1), pp. 53-62.
[20] R.M. Kogan, I.M. Nazarov, Sh.D Fridman. Basics of environmental gamma-spectrometry. Atomizdat, Moscow, 1976 [in Russian].
[21] N.A. Titaeva. Nuclear geochemistry. MGU, Moscow, 2000 [in Russian].

THE SIGNIFICANCE OF RADIOLOGICAL PARAMETERS OF MULTI-LAYERED ARCHAEOLOGICAL SITES IN DATING BIOGENIC ARTIFACTS

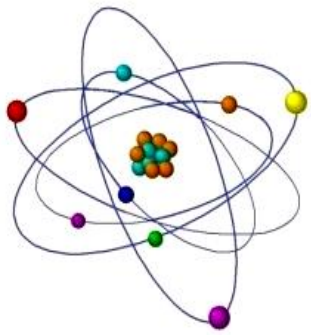

[1]Vakhtang Licheli, [2,3]Mikheil Gogebashvili*,
[2,3]Nazi Ivanishvili, [4]Eremia Tulashvili, [2]Saba Suladze,
[3]Sopho Kalmakhelidze, [2]Grigol Mamniashvili

[1]Iv.Javakhishvili Tbilisi State University, Georgia
[2]Iv.Javakhishvili Tbilisi State University, E. Andronikashvili Institute of Physics, Georgia
[3] Iv.Beritashvili Canter of Experimental Biomedicine, Georgia,
[4] Iv.Javakhishvili Tbilisi State University, Academician N.Kekelidze Materials Research Scientific-Research Institute, Georgia

https://doi.org/10.63465/rrs520258988 *Corresponding author: Email: gogebashvili@gmail.com

ABSTRACT: *The methodological scope of archaeology as a scientific discipline continues to expand in parallel with advancements in modern technology. In recent years, multidisciplinary analytical approaches have gained particular attention, especially in the dating of biogenic artifacts. This study investigates the radioisotopic parameters of a cultural layer dated to the 11th–10th centuries BCE, using the multi-layered archaeological site of Grakliani (Georgia) as a case study. The research highlights the significance of radiological indicators in surrounding soil zones for dating tooth enamel artifacts based on Electron Paramagnetic Resonance (EPR) signals. The analyzed radioisotopic spectrum offers an effective method for assessing layer stability and identifying potential mixing in multi-layered archaeological sites. By examining isotopes from the uranium-thorium series and the specific radioactivity of radioactive potassium, the study proposes an analytical approach that serves two key purposes: first, to determine the integrity or disturbance of cultural layers, and second, to calculate the actual integral dose affecting biogenic artifacts. The latter aspect is particularly crucial for improving the accuracy of dose estimations in EPR signal dating, ultimately leading to more precise chronological assessments of archaeological materials.*

Key words: radiological parameters, multi-layered archaeological sites, ating artifacts

INTRODUCTION

Dating artifacts from archaeological sites remains one of the most significant challenges in the field [1,2]. Various dating approaches exist, relying on physicochemical and biological methodologies [3,4,5]. Among these, the Electron Paramagnetic Resonance (EPR) dosimetry method stands out, as it measures the concentration of radiation-induced radicals in irradiated tooth enamel tissues [6,7,8]. This method offers a relatively low detection threshold for absorbed radiation doses. The intensity of the EPR signal provides crucial information about the cumulative radiation exposure an artifact has experienced over time. Radiation monitoring and dosimetric analysis, including the dating of biogenic artifacts, are based precisely on the

examination of signals in the spectra of tooth enamel tissues [9,10]. Notably, the EPR dating method has an extensive overlapping range, spanning several centuries and often exceeding the capabilities of radiocarbon analysis. In EPR dosimetry-based dating, a key issue is the detection of radiation doses accumulated by the studied object from natural radiation sources over centuries. This factor is crucial for determining the artifact's age, as it allows for the experimental assessment of an equivalent radiation exposure level in comparison with radiologically treated materials. Additionally, it helps address significant radiological challenges, such as the continuity of the artifact's location, the uniformity of the soil matrix surrounding the artifact in terms of radiological parameters, and the identification of dose contributions resulting from anthropogenic radionuclide exposure over a specific period.

In Electron Paramagnetic Resonance (EPR) dosimetry-based dating, a major challenge is accurately measuring the radiation doses that an artifact has accumulated from natural radiation sources over centuries. This measurement is essential for determining the artifact's age, as it enables researchers to experimentally assess its equivalent radiation exposure in comparison to materials that have undergone radiological treatment. Furthermore, this method tackles significant radiological challenges, such as ensuring the artifact's spatial stability over time, evaluating the uniformity of the surrounding soil matrix in terms of its radiological properties, and identifying contributions from anthropogenic radionuclides over a specific period.

MATERIALS AND METHODS

The research object was the archaeological excavation site of "Grakliani" (Eastern Georgia). The chronological range of the research layers at Grakliani Hill encompasses 1.5–2 million years of human settlement history in this area. In this regard, it is noteworthy that the site comprises 11 cultural layers, which, in turn, form several methodological challenges [11].

Grakliani Hill is a multi-layered archaeological monument that confirms 300,000 years of uninterrupted social development, spanning from the Stone Age to the Roman period. This, in turn, can be used as an adequate model for studying the radiological parameters of various archaeological zones.

Soil samples were taken from functionally different locations of one of the cultural layers. After mechanical processing to achieve powder condition, the samples were dried in a thermostat at a temperature of 105–110°C

The content of radionuclides was determined by gamma-spectrometry (Gamma-Beta Spectrometer, Atomtex-MKC-AT-1315 and Gamma-Spectrometer CANBERRA with liquid nitrogen cooled germanium detector).

RESULTS AND DISCUSSION

The radiological study of layers in multi-century archaeological sites, particularly those in open areas, has several specific characteristics shaped by the nuances of their formation. A cultural layer refers to the soil deposits at a site of human habitation that preserves material

evidence of human activity. The scientific methodology for studying these cultural layers often emphasizes the concept of the "in situ preserved cultural layer." In practical archaeology, the primary goal is to establish a comprehensive list of objective criteria necessary for dating the artifacts discovered. For dating purposes, when tooth enamel is exposed to radiation, it produces a complex, asymmetric Electron Paramagnetic Resonance (EPR) signal. This signal serves as a source of information for determining the structure of the analyzed biogenic artifact and the duration of its presence at a specific location [12]. However, a key issue in this process is assessing the integral dose received by the particular artifact during its prolonged burial and preserved state.

To conduct radiological analysis, we selected a specific layer from the archaeological site of "Grakliani" (Georgia), which is dated to the 11th-10th centuries BCE. Soil samples for radioisotopic analysis were taken from the natural profile of the given area and various locations within the identified cultural layer. Naturally, when using EPR spectrometry for dating, there is a possibility of error due to the influence of anthropogenic radionuclides (technogenic) on the results.

As is well known, since the second half of the 20th century, due to nuclear weapon testing, the presence of technogenic radionuclides has been detected in the atmosphere, the environment, and especially in the soil. Radioactive decay and migration processes have led to the contamination of landscapes with artificial radionuclides. In this regard, the territories of Georgia are no exception [13]. The deposition and distribution of such radionuclides on the Earth's surface are uneven, influenced both by nuclear weapon testing (global dispersal) and during emergencies (such as the Chornobyl and Fukushima nuclear plants). This circumstance, in turn, creates specific methodological challenges in studying the accumulation of artificial radionuclides.

During the radiological study of an archaeological excavation site, it is essential to exclude the factor of technogenic radionuclides. To eliminate the possibility of anthropogenic radioisotope contamination in the excavation areas, surface monitoring of the surrounding soils was conducted. The criterion for anthropogenic radioisotope contamination was ^{137}Cs. The maximum contamination level of this isotope did not exceed 10-15 Bq/kg. Furthermore, the activity of the cesium radioisotope in its localized zone in the soil at depths of 5-10 cm did not exceed these levels, indicating that no technogenic-origin radioisotopes were detected in the studied archaeological zone. This conclusion is supported by the fact that cesium isotopes were not found in any soil samples taken from the vertical profile. The next stage in studying the radiological parameters of soil profiles at various depths involved conducting gamma spectrometric analysis during the normal (horizontal) arrangement of the zones (Fig. 1-A). Additionally, the vertical placement of artifacts is one of the characteristics used for dating specific cultural layers. However, the specificity of the selected object does not exclude the possibility of horizontal shifts in the soil layers. This phenomenon is particularly characteristic of mountainous landscapes. Such horizontal displacement of archaeological zones is also observed in our object (Figure 1-B).

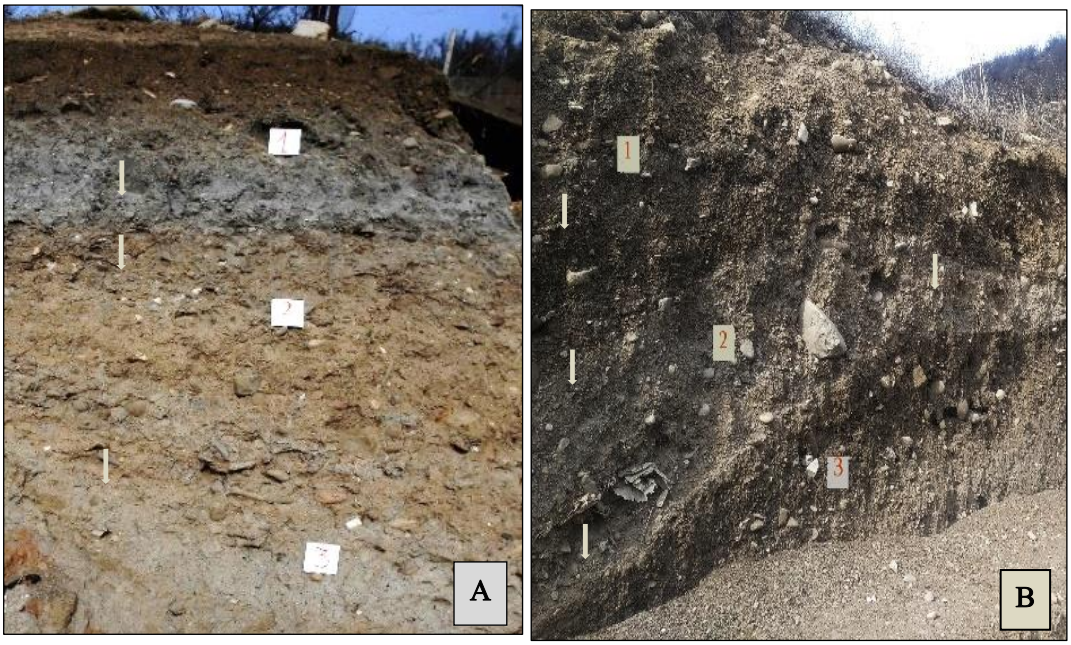

A - Soil profile of zone A in normal horizontal arrangement
B, C - Soil profile of zone B in case of horizontal arrangement disturbance
(The top three levels are marked with numbers; the boundaries of the soil horizons are indicated with arrows)

Based on the above, it is clear that the precise radiological characterization of the soils surrounding the discovered artifact can provide additional information regarding the duration of the artifact's presence at the site. For a model study of such situations, we selected specific archaeological locations based on the discovered objects and structures with various functional characteristics. "The following locations were selected for the study: 1- Vertical distribution of the natural soil zones (Fig. 1); 2- Agricultural zone (presumably a dairy production site) (Fig. 2-4); 3- Location of the residential building (Fig. 2.5); 4- Area designated for religious purposes (Fig. 2-6); and 5- Location adjacent to the clay furnace (Fig. 2-7).

Fig. 2. 4 - Agricultural zone (presumably a dairy production site); 5 - Location of the residential building; 6 - Area designated for religious purposes); and 7 - Location adjacent to the clay furnace

The results of the gamma spectrometric analysis of these locations are shown in Figure 3. Each sample has a distinct isotopic composition, represented by groups of isotopic families in the diagram. In the ^{238}U family, the isotope ^{226}Ra was detected only in the upper horizon of the soil vertical profile. At the same time, relatively high activity of this isotope was observed in the 4th**,** 5th**,** and 7th samples from the study area. This phenomenon can be attributed to specific agricultural practices in the areas studied. Additionally, the absence of the radium isotope in the sample from the sixth location, which is believed to have religious significance, may provide further evidence (Fig. 3-A).

The activity of isotopes in the ^{232}Th family is characterized by defined information content. This radioisotope was detected only in the upper horizon of the soil profile and was virtually absent in other locations of the studied zone. In this case, this fact can be interpreted as an indicator of the archaeological zone's stability, which may have been caused by the absence of mixing between the upper soil layer and the deeper layers (Fig. 3-B). Among the samples analyzed, the isotopes of the ^{235}U family exhibited the lowest activity (Fig. 3-C).

In terms of activity, ^{40}K occupies a particularly significant position. As shown in the diagram of Figure 3-D, in some samples, the activity of this isotope reached 450 Bq/kg, which is significantly higher than the activity of the other presented radioisotopes. Considering that the total activities of isotopes from the ^{238}U (^{234}Th, ^{226}Ra, ^{214}Pb, ^{214}Bi) and ^{232}Th (^{228}Ac, ^{210}Pb, ^{212}Bi) families do not exceed 60 and 38 Bq/kg, respectively, the radioactivity of ^{40}K emerges as the major component of the total radiation dose.

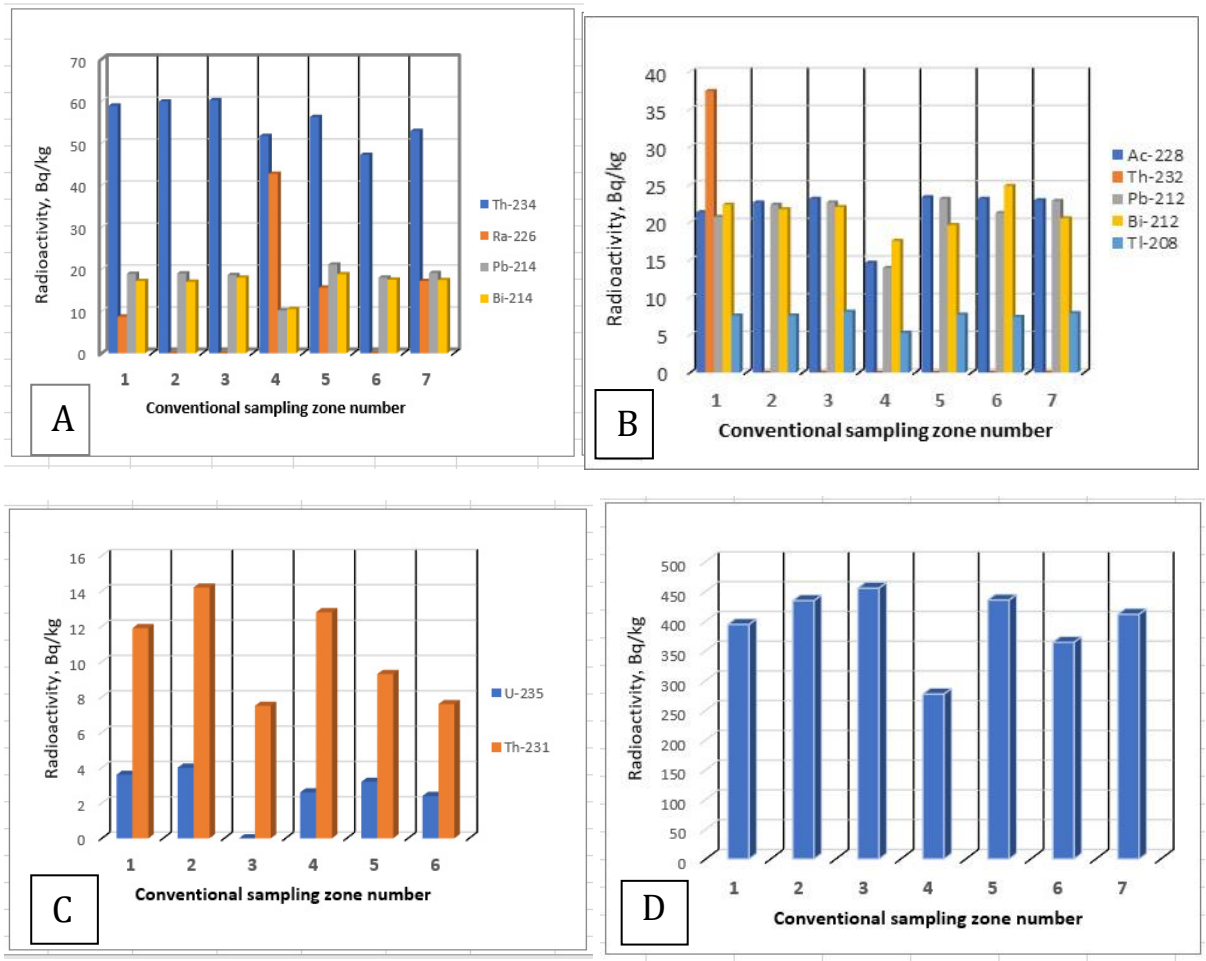

Fig. 3 Distribution of different family isotopes in the soil samples of the studied archaeological site

A-Family ^{238}U (^{234}Th,^{226}Ra,^{214}Pb, ^{214}Bi); **B**-Family ^{232}Th (^{228}Ac, ^{210}Pb, ^{212}Bi, ^{208}Tl); **C**-Family ^{235}U (^{231}Th,^{235}U); **D** – ^{40}K

(The numbering of the study zones in Figures 3 and 4 corresponds to the location in Figures 1 and 2

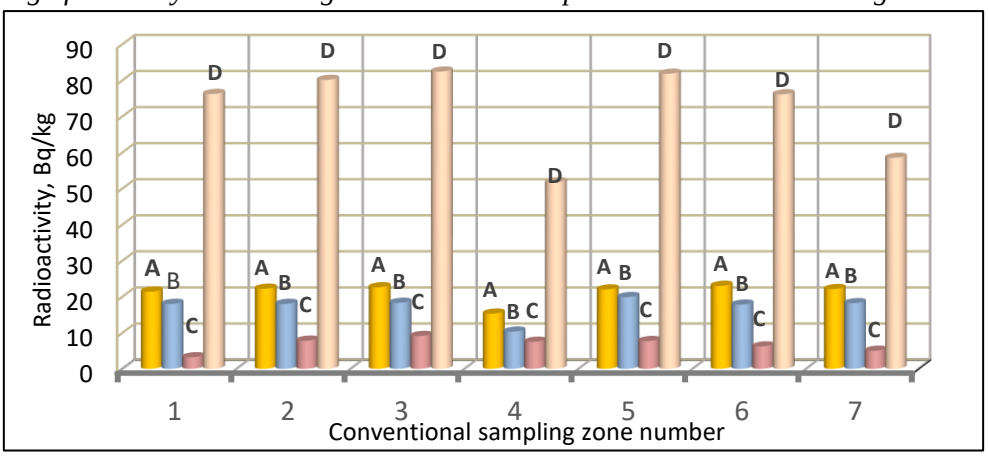

Fig.4. Radioactivity of uranium-thorium family radioisotopes in soil samples from different locations of the archaeological site

A-Family ^{232}Th (^{228}Ac, ^{210}Pb, ^{212}Bi, ^{208}Tl); **B**-Family ^{238}U (^{234}Th,^{226}Ra,^{214}Pb, ^{214}Bi); **C**-Family ^{235}U (^{231}Th,^{235}U); **D** - Radium equivalent activity

Thus, by analyzing the spectra of different isotopic families, it is possible to obtain additional characteristics of a multi-layered archaeological site. However, the key factor for dating through EPR analysis is determining the total radiation dose in the artifact's in situ fixed state. As shown in the data presented in Figure 4, the total radioactivity of the uranium-thorium family isotopes in each sample does not exceed 20 Bq/kg. To obtain the total values resulting from various types of radioisotopic irradiation, the equivalent activity of the radium isotope was used [14]. This criterion significantly improves the accuracy of the EPR signal analysis methodology for artifact dating.

Overall, the conducted research demonstrated that determining radiological parameters provides a relatively complete picture for characterizing multi-layered archaeological sites. Specifically, the radioisotopic spectrum from different locations during excavations justifiably reflects the potential for horizontal movement of soil masses. This is particularly relevant in cases where archaeological excavations are carried out in seismic and unstable landscape zones [15]. Furthermore, the increase in dosimetric parameters has the potential to significantly improve the accuracy of the EPR method in dating biogenic artifacts.

REFERENCES

[1]. Thilo Rehren, Efthymia Nikita. Archaeological Science. Encyclopedia of Archaeology (Second Edition). Volume 1, 2024, Pages 123-132.

[2]. Elisa Crabu, Caterina Fenu, Giuseppe Rodriguez, Giuseppa Tanda. Dating archaeological sites by seriation. Journal of Cultural Heritage. Volume 72, March–April 2025, Pages 42-47.

[3]. Grzegorz Piotr Guzik, Wacław Stachowicz, Jacek Michalik. Chapter 6 - Aspects of the EPR study on mineralized tissues as related to medicine, dosimetry, and dating. Experimental Methods in the Physical Sciences. Volume 50, 2019, P.115-127.

[4]. Öykü Ataytür, Cécile Gautheron, Adriana Horbe, Thierry Allard. Thermal stability of artificial radiation-induced defects in kaolinite: Enhancing EPR dating protocol. Applied Clay Science. Volume 252, 2024, 107349.

[5]. Shigueo Watanabe, Nilo F. Cano, Alvaro B. Carvalho-Júnior, Jorge S. Ayala-Arenas, Carlos D. Gonzales-Lorenzo, T.K. Gundu Rao. Dating of carbonate covering cave paintings at Peruaçu, Brazil by TL and EPR methods. Applied Radiation and Isotopes. Volume 153, 2019, 108847.

[6]. H.S. Sullasi, M.B. Andrade, W.E.F. Ayta, M. Frade, M.D. Sastry, S. Watanabe. Irradiation for dating Brazilian fish fossils by thermoluminescence and EPR technique. Nuclear Instruments and Methods in Physics Research Section B: Beam Interactions with Materials and Atoms. Volume 213, 2004, p.756-760.

[7]. Shuchen Wang, Zhenlin Jia, Hongshan Gao, Desheng Xue, Baotian Pan. Impact of microwave power on equivalent dose (De) evaluation in ESR dating. Radiation Measurements. Volume 177, 2024, 107231.

[8]. Anne R. Skinner. Electron Spin Resonance Dating. Encyclopedia of Geology. 2021, P.153-163.

[9]. Paola Fattibene, Freddy Callens. EPR dosimetry with tooth enamel: A review. Applied Radiation and Isotopes. Volume 68, Issue 11, 2010, Pages 2033-2116.

[10]. Alfredo Coppa, Rainer Grün, Chris Stringer, Stephen Eggins, Rita Vargiu. Newly recognized Pleistocene human teeth from Tabun Cave, Israel. Journal of Human Evolution. Volume 49, Issue 3, 2005, Pages 301-315

[11]. Vakhtang Licheli. The second stage of the Grakliani Culture. Wonders Lost and Found. A Celebration of the Archaeological Work of Professor Michael Vickers. Oxford: Archaeopress. P. 48-58.

[12]. Licheli V., Chikvaidze E.N., Gavasheli TA., Mamniashvili G.I. Gegechkori T.O., Gogebashvili M.E., Ivanishvili N.I. Electron paramagnetic resonance method for dating of archeological sites in Georgia. Journal of Radiobiology and Radiation Safety, Vol.1, No2, 2021, p.65-70.

[13]. Kiazo Nadareishvili at all. Effect of Chernobyl disaster on the radioecological situation in Transcaucasia. Radiation studies, Georgia, Tbilisi, 1991, Vol.VI, p.132-151.

[14]. Beretka, J., Mathew P.J. Natural Radioactivity of Australian Building Materials, Industrial Wastes and By-products. Health Physics 48(1), 1985, p. 87-95.

[15]. Iain Stewart. Archaeological and Cultural Records of Active Tectonics. Treatise on Geomorphology (Second Edition). Volume 2, 2022, Pages 13-33

"LOW" DOSES OF RADIOBIOLOGY

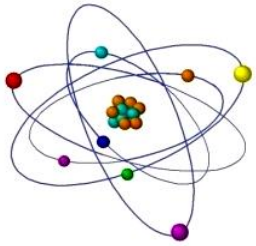

[1]Oleksandr Mikhyeyev[*], [2]Oksana Lapan
[1]Institute of Cell Biology and Genetic Engineering,
National Academy of Science of Ukraine
[2]National Aviation University, Ukraine

https://doi.org/10.63465/rrs520258989 *Corresponding author: Email: mikhalex7@yahoo.com

ABSTRACT*: The main radiobiological problems in the example of the Chernobyl accident are considered. It is pointed out that nowadays there is a paradoxical inconsistency between the relevance of radiobiological problems in the post-Chernobyl period and "low doses" of efforts that are made by radiobiologists to solve them. It is substantiated that at this stage of the development of the post-accident situation the existing experimental facts and theoretical provisions of radiobiology are quite sufficient to explain radiobiological and radioecological phenomena. Special attention is paid to the problem of "low" doses of ionizing radiation. The existence of "hot" particles of biological origin is experimentally proved. Special attention is paid to the inter-granular reactions of biological systems to irradiation in the example of gigantism of tree needles in the zone of the Chernobyl accident influence. The data on rating assessment of the degree of urgency of radioecology problems are presented. The role of radiophobia in psychosomatic diseases of the population in the zone of strict radiation control is considered.*

Key words: low dose, radionuclide, radiohormesis, radioadaptation, radiomodification.

INTRODUCTION

While during the Chernobyl era the staff of the Department of Biophysics and Radiobiology of the Institute of Plant Physiology of the Academy of Sciences of Ukraine had to deal mainly with the issues of "acute" radiobiology, studying deterministic effects of ionizing radiation (IR) in plants, after the Chernobyl accident the research focus changed sharply to the area of "dumb" radiobiology – studying the effects of low-dose and low-power ionizing radiation. Right now, on the eve of the 39th anniversary of the Chernobyl accident, the relevance of a number of practical and conceptual problems, the solution of which will allow us to "weigh" rationally the risks for human beings from all kinds of environmental stressors, is realized quite acutely. These are, first of all, the problem of the effect of acute IR doses on humans and, first of all, the consideration of the phenomenology and mechanisms of ARS, and, secondly, the complex of "Chernobyl problems". The relevance of the latter topic (scientific, economic, political, moral) is undoubted and gives a reason to consider the results of the effect of the so-called "low" radiation doses to which the population is exposed due to the Chernobyl accident. Nowadays there is a paradoxical discrepancy between the relevance of radiobiological problems in the post-Chernobyl period and "low doses" of efforts that are made by radiobiologists to solve them. It is necessary to bring all this into conformity, if only for the reason that more than 3 trillion US dollars have already been spent on radiation protection in the world, while in Ukraine in the post-Chernobyl period about 12% of the annual budget has been spent on liquidation of real and imaginary consequences of the accident. For this reason, radiobiology can be considered the most important biological science for Ukraine, as its development will significantly reduce the costs of "consequence management", based, in particular, on a more accurate assessment of radiogenic risk coefficients, which, in turn, will eliminate many scientific medical units parasitizing on the Chernobyl issue.

Let us consider the main radiobiological problems in the example of the Chernobyl accident. It is obvious that the Chernobyl accident could not have been overlooked by numerous radiobiological and radiological disciplines. The avalanche of publications generated by this interest makes us think about the emergence of a fundamentally new factual field, which requires additional research efforts on the part of radiobiological specialists. But is it really so? Did the accident at the Chernobyl NPP entail any

really unique (new or unusual) phenomena and processes from the radiobiological and radiological points of view, distinguishing them from the previously known phenomena? From our point of view, it is possible to speak about the uniqueness of the accident only with regard to its "technical" characteristics, mainly concerning the nature of radionuclide contamination of natural and man-made objects.

RANGE OF RADIOBIOLOGICAL PROBLEMS

In our opinion, at this stage of post-accident development, the existing experimental facts and theoretical concepts of radiobiology are sufficient to explain radiobiological and radioecological phenomena. Nevertheless, the Chernobyl accident caused essential changes in radiobiological science. This situation actually "saved" radiobiology, if not from "extinction", then from a significant reduction in funding.

If the totality of radiobiological problems is represented as a problem spectrum with its qualitative (many problem areas) and quantitative (human, financial, material and time resources spent on solving a particular problem) characteristics, it can be stated that in the post-accident period it has undergone only quantitative changes. In fact, there has been only a shift of research accents to the area of problems previously little studied and researched, for example, such as problems of radio-adaptation, radiation aging of organisms, aging of radionuclides, radiation-induced carcinogenesis and others. Insufficiently studied and developed remain in particular the following issues:

1. *Heterogeneity* (*tropicity*) of radionuclide (RN) distribution in plant structures and organs. Necessity to study ***"hot" particles of*** biological origin, the existence of which is indicated by the results of studies of radionuclide distribution on root structures in soil and water habitats of plants.
2. *Specificity of* action of incorporated radionuclides. There is an opinion that incorporated radionuclides in biological objects have an increased damaging effectivity. We believe that if the distribution of radionuclides in the biostructures under study is determined correctly (taking into account the tropism of distribution, starting with the intracellular level and ending at the community level), the specificity of such a specificity is absent. In fact, there is no reason to speak about a particularly high damaging effect of IR doses formed by incorporated sources.
3. Effects of "*low*" *doses of* IR. Firstly, "small" doses turn out to be not small at all (see point 2), and, secondly, considering "small doses" as subthreshold doses, any attempts to "demonize" them are excluded.
4. Phenomenology, mechanisms and significance (on-togenetic and phylogenetic) of *radiohormesis effects*, which are based on hyper-compensation of radiation-induced damage to biological structures of different levels of integration – from macromolecules to cenoses; in this state the object acquires increased resistance to subsequent stressing influences for a certain period of time.
5. The problem of *radioadaptation*, starting with phenomenology and ending with ontogenetic and phylogenetic mechanisms. Radioadaptation is based on the hormesis effect of IR (see point 4); radioadaptation should be considered not only as an increase in the initial level of radioresistance (hyperadaptation, "adaptive response"), but also as its decrease (hypo-radioadaptation) to a level still compatible with life activity; the necessity to take into account the phenomenon of *reverse* adaptation, when adaptive doses can act as radiotherapeutic doses, has been experimentally substantiated.
6. *Microevolutionary* processes in the 30-km zone of the Chernobyl NPP induced by IR. Most often there is no clear dosimetric "support" for this kind of research and the endogenous rhythm of values of biological parameters, for example, virulence or pathogenicity of microorganisms, is underestimated, that leads to radio-centrism in explaining the observed phenomena.
7. Effects of *combined* influence of IR with other stressors. There is no practice of using the methods of calculating non-additivity, for example, the methods of mathematical planning of experiment are insufficiently used; mistakenly all the effects of combined influences are assumed to be negative and synergistic.
8. Methods of *retrodosimetry.* Insufficient attention to the possibilities of biodesimetry; lack of development of equidosimetric approach as one of the bases of retrodosimetry.
9. The usage of *radiation sensitized* biological objects as test systems for controlling the level

of radiochemical, chemical and biological contamination of various artificial (man-made) and natural environments (the techniques are based on synergistic effects – see point 7).

9. *Integral* (remote, mediated, indirect) reactions of biological systems to irradiation. The dominance of unfounded ideas about the decisive role of direct IR action; reduction of indirect IR effects to the "witness effect"; underestimation of the modifying influence of biological structures of any level of integration.

10. *Epigenetic* effects of IR. There is a peculiar genocentrism in explaining the effects of IR, or the other extreme issue – explaining the effects of IR only on the basis of molecular mechanisms of gene activity regulation and underestimating the supracellular mechanisms, for example, the effects of positional information, correlative links of biostructures at different structural and functional levels.

11. Excessive attention to *deterministic* effects of IR in the period after the Chernobyl accident without sufficient “dosimetric” grounds, i.e. an attempt to study deterministic effects in the radiation environment (at doses and power of IR in a specific post-accident situation), in which they cannot manifest themselves in principle.

12. *Stochastic effects of* IR. Paradoxically, little attention is paid to the assessment of carcinogenic radiogenic risks (the levels of which, in our opinion, are overestimated by two orders of magnitude to assess the consequences of exposure) at the background of hyperdiagnosis and lack of proper statistics; experimentally unjustified adherence to the threshold-free concept of IR action.

13. *Fundamental radiobiological laws.* Excessive attention of academic institutes to applied aspects of IR, turning them into branch institutes.

14. ***Radiobiology as a methodological basis for*** theoretical stress-biology. The necessity to use methodical and methodological achievements of radiobiology and radioecology to develop general principles of stress-biology and theoretical biology.

PECULIARITIES OF RADIONUCLIDE CONTAMINATION

The uneven character of RN distribution in the territories adjacent to the accident zone (horizontal “spotting”), caused by fractionation of RN at the stage of their release from the destroyed reactor, the presence of vertical heterogeneity of RN distribution in the soil and the presence of “hot” particles in the habitat of plants and animals led to the fact that living organisms in the radionuclide contamination zone began to be exposed to the action of radiation sources of very heterogeneous composition and distribution. However, taking into account the fact that the actual radiobiological stage of interaction of a radiation factor with a biosystem starts with the moment of penetration of RN into the organism or with the moment of the beginning of a significant effect of external irradiation, the “prehistory” of RN migration at this stage is not important for the assessment of the radiobiological effect, being reflected only in the kinetics of the external irradiation effect or in the parameters of RN intake into the organism. At the same time, the power of radiation exposure and the character of RN distribution in tissues may change (a consequence of differential RN tropism), but from the “point of view” of dosimetry, it does not create new situations of interaction between radiation sources and biological objects and, consequently, cannot cause a qualitatively new radiobiological phenomenology.

THE PROBLEM OF “LOW” DOSES OF IONIZING RADIATION. “HOT” PARTICLES OF BIOLOGICAL ORIGIN

The most striking example of the “shift” of radiobiologists' research emphasis in the post-Chernobyl period is the increased attention to the problem of “low” IR doses. The radio-ecological situation created after the Chernobyl accident caused such characteristics of dose loads on organisms, which forced radiobiologists to proceed to a close study of the so-called “low” IR doses associated, as a rule, with conditions of chronic irradiation and causing mainly stochastic effects (mutagenic, carcinogenic, genetic).

In the radiobiological literature there is no consensus on the content of this concept [1, 2]. Probably,

the most practical definition of “low” doses would be to define them as poorly studied due to many methodological and methodological difficulties (difficulties of dosimetry, statistical processing of data, necessity to conduct large volumes of studies, the complexity of interpretation of the results obtained). It is obvious that most of the reactions under study have a certain threshold of sensitivity and/or resistance to irradiation. This applies, first of all, to deterministic effects. It is obvious that the only threshold-free reaction will be ionization and excitation of atoms and molecules of the irradiated object, since the energy of quanta or particles of the IR far exceeds the ionization energy of atoms or the energy of covalent bonds in molecules. In this connection, the issue about the threshold effect of radiation at the molecular level is removed and it is simply incorrect to speak about “small” doses with regard to these reactions. In fact, any absorbed dose of IR is capable of inducing a response at the molecular level, and the whole problem comes down to its detection.

There is experimental evidence that *stochastic effects* also *have dose thresholds.* Thus, the possibility of increasing the absorbed dose from background values, i.e. from the level of RB (radiation background), to a level that does not increase the background frequency of cytogenetic damage has been shown. The exceeding of this dose level leads to the emergence of a “*radio-adaptive response*”, when a lower (compared to background) frequency of cytogenetic damage is observed. Further dose increase leads to an increase in the yield of cytogenetic damages [3]. In this case, the concept of "subthreshold doses" includes the range of adaptive doses.

All reactions (stages of reaction) to irradiation develop within a specific structural and functional hierarchy of the studied biological system (potentially from the cell level to the level of ecosystems and the entire Biosphere). If reactions have a pronounced threshold character, the dose dependence has a true shoulder. Only for such reactions it is reasonable to speak about the existence of “small” doses, which are more correctly (more strictly and understandably) called subthreshold doses.

Of course, a subthreshold dose for one type of effect may simultaneously be above-threshold for another effect and vice versa. For example, subthreshold doses for insects with the respect to the effect of irradiation on their average life expectancy appear to sterilize or at least disrupt gametogenesis. In another situation, a subthreshold dose with respect to the inhibition of a function may turn out to be a suprathreshold dose with respect to the hormesis effect on the same or another function. In other words, we should speak about a complex potential structurization of any studied threshold, which, in general, has an area of indifferent influence (threshold proper) of irradiation and an area of radiation hormesis.

Thus, when studying the reactions of biological objects of any structural and functional level, one can always distinguish a range of doses called “small”, which are inherently subthreshold. Irrespective of the nature of the IR induced effect, i.e. whether it is stochastic or deterministic, from our point of view most of the doses absorbed by biological objects in the territories contaminated after the Chernobyl accident should be called “quasi-background doses”, by that emphasizing their proximity to the parameters of the natural radiation background (NRB). The problem of "low" doses has another important aspect, which reflects the effect of radionuclides predominantly incorporated in biological objects. It is about the existence of differential tropism of organelles, cells, tissues, etc. with respect to the accumulation of radionuclides. The calculation of doses from incorporated sources absorbed by biostructures without taking into account the heterogeneity of their endogenous distribution may give underestimated ratings and force researchers to make erroneous conclusions about the particularly high efficiency of low doses. In critical structures of biological objects there can occur rather high levels of RN accumulation (absorption coefficient up to 40000) and, consequently, high absorbed doses, which are commensurate with the corresponding doses of acute external irradiation of equal effectiveness. Such work was carried out by the author on plant seedlings, the results of which led to the necessity to conclude about the existence of “hot” particles of biological (in this case, plant) origin. This phenomenon was demonstrated in experiments with strontium-90 and cesium-137 salts. The observations were carried out on the roots of pea seedlings. Methodological details of this work are described in the monograph "Hyperadaptation. Stimulated ontogenetic adaptation of plants" [4].

Thus, the problem of low doses may be, on the one hand, a problem of not very strict scientific jargon, and, on the other hand, a problem caused by underestimation of the role of the heterogeneous tropism of radionuclides. The concept of “low” dose is actually a metaphor reflecting the aspiration of radiobiologists to study the reactions of the most fundamental structural and functional level of

organization of biological systems. From this point of view, this concept with all its vagueness fulfills an important function of concentration of radiobiologists' research efforts around such important problems as induction of new and modification of constitutive repair systems, mechanisms of radiation mutagenesis and carcinogenesis, the problem of radioadaptation and others. In order to work effectively in this field, radiobiologists had to go into the area of such doses that do not cause non-mediated visible changes at the organism level. Otherwise, it would be impossible to study “low-level” effects because they are masked by cell lethality. This is probably the origin of the practice of using the term “low” doses. However, on the other hand, it should be noted that this concept has a negative effect for distribution of researching radiobiologists' accents, distracting their attention from solving equally important problems of radiobiological objects of higher levels of integration (organisms, populations, communities etc.).

In addition, it is important to note that the research focus of radiobiologists is distracted from solving equally important problems of radiobiology of objects of higher levels of integration (organisms, populations, communities, etc.).

RADIATION HORMESIS. RADIOADAPTATION PHENOMENON

Dose loads on biological objects in the zone of influence of the Chernobyl accident determine a variety of radiobiological effects, among which radiohormesis effects are of the greatest interest. The term “*hormesis*” (from Greek “hormesis” – “rapid movement, striving”) was introduced to denote the positive effect on biological objects of certain ("small") doses of factors of practically any nature – from physical to biological [5-7]. For example, it can be expressed in the increase of reproductive capacity, growth and development rate, resistance to biogenic and abiogenic factors (survivability), speed and quality of recovery processes, etc. In real habitat conditions, organisms are subjected to the stressing effect of factors of diverse nature. According to the Arndt-Schultz law, weak irritants (doses of factors) stimulate organisms' vital activity, medium irritants enhance it, strong irritants strenthen it, and very strong ones paralyze or even cause their death. In fact, this rule clearly indicates the existence of a hormesis dose range. If IR acts as a factor capable of producing a hormesis effect, in this case we speak of *radiohormesis*. Radiohormesis effects (RHE) are observed at all levels of biological integration and for representatives of all systematic groups of organisms. It seems possible to consider RHEs as a kind of stress reaction – eustress according to G. Sellier. It is obvious that the primary mechanism of action of radiohormesis doses (RHD) is based on ionization of atoms and molecules of the irradiated object, i.e., a disintegrative process, the fact of which makes RHE paradoxical – the primary destructive factor eventually exerts a beneficial (radiohormesis) effect.

The mechanism of hormesis effects can be explained from the standpoint of Weygert's law of supercompensation, according to which the organism in response to “waste of substances or loss of tissues” (within known limits) reacts by forming new substances and tissues in an amount *exceeding* the lost ones. In other words, in the recovery period after a load (of a particular dosage of the factor) there is a peculiar “exaltation phase” – the phase of supercompensation, the presence of which indicates such a state of the biological object, in which it acquires additional capabilities to respond to the action of the stressor, i.e. indicates a state of increased compared to the initial stability. If every time after the stress the organism returned only to the initial state, the possibility of acquiring increased stability would disappear.

Previously, we showed a direct connection between the state of hyperadaptation of plants to the action of IR and the state of radiohormesis in growth parameters, which gave us grounds to reduce the study of the mechanism of radioadaptation to the study of the mechanism of radiohormesis (Mikheev et al., 2007). One of the mechanisms of hormesis (and hence adaptation) by growth parameters turned out to be stimulation of histo- logical parameters of the root apical meristem (proliferative activity of meristematic cells, meristem volume, and cell size), which was preceded by stimulation of cytokinin activity in the meristematic zone of the root apex.

The fact of hierarchical organization of biosystems provides for the study of RHE mechanisms in the form of a sequential description of reactions of all sublevels (subsystems) of the biological object for which it is described. We tried to realize this methodological approach by the example of studying RHE

in plants. We experimentally demonstrated the existence of a hierarchical system of radiohormesis mechanisms. The results obtained allow us to substantiate the hypothesis of the existence of supracellular mechanisms of radiohormesis detected at the organ level, which is based on the stimulation of cytokinin and, as a consequence, proliferative activity of cells forming critical plant tissues.

After exposure to an unfavorable factor (stressor), the organism can be in one of the following states for a certain period of time: a) at the initial level of adaptation, when its constitutive (current) level of adaptation is maintained – the state of *ordinary* adaptation; b) at the level of increased resistance, when the initial resistance of the object to the following effects of stressing factors increases – the state of *hyperadaptation* (eustress state according to G. Sellier); c) at the level of decreased resistance – the state of *hypoadaptation* (distress state according to G. Sellier). How can the degree of adaptability of an organism change? It is believed that the organism under the influence of a stressor undergoes a *transitional process*, which has a character of either incomplete recovery (under-recovery, *hypocompensation*) or over-recovery (*hypercompensation*) of structural-functional parameters characterizing the organism's vital capacity (growth and development rate, cell division rate, etc.). In fact, the transition to the state of hypercompensation is a consequence of inaccuracy *and inertia of biological* repair *systems* that function at all levels of integration of biological systems (enzymatic repair, cellular repopulation, regeneration, repopulation at the level of organism population).

RADIATION AND PHYLOGENY

It is not excluded that the increased attention to the problem of radionuclide concentration by certain biological structures will revive the interest in studying the role of the radiation factor in phylogenetic processes, which had died out. It is now becoming obvious that it is wrong to be guided only by averaged values of the natural radiation background in order to estimate dose loads on the organism. This is especially true for aquatic and soil organisms. Real dose loads may be significant enough for IR to act either as a factor of organismal variability, or as a selection factor, or both.

We would like to draw attention to some aspects of the problem “radiation and phylogeny”, which become especially relevant in the post-Chernobyl period, when the level of radiation background significantly increased.

Multilevel structure-functional organization of phylogenetic factors. Postulates: 1) phylogenetic factors can be of any nature, i.e. of any level of complexity; 2) in the process of progressive development, the phylogenetic factors are more and more organized factors, the action of which occurs against the background of the action of less organized factors.

Dosimetry of phylogenetic factors and their classification according to the produced effect. Indifferentiating, stimulating, inhibiting and lethal phylogenetic factors. Postulate: with progressive evolutionary development, the role of informational aspects of phylogenetic factors increases, while the role of energetic and material factors decreases.

Additivity, synergy and antagonism of phylogenetic factors. It is obvious that a complex of endogenous and exogenous phylogenetic factors has acted, is acting and will act on the developing systems that in the end forces us to solve the problem of studying the mechanism of their interaction. The lack of consideration of the need to solve this problem makes it impossible to obtain a reliable picture of phylogenetic transformations.

“Retrodosimetry” of phylogenetic factors, i.e., determination of qualitative and quantitative parameters of phylogenetic factors that *acted in the historical past.* Just as in radiobiology the “doza-effect” calibration curves obtained in an experiment are used for this purpose, a similar approach could be used to solve phylogenetic problems of retro- dosimetry. For this purpose, phylogeneticists need to establish a clear dependence between the parameters of a particular phylogenetic process and the doses of the phylogenetic factor. By the way, what is a phylogenetic factor in general? From our point of view, a phylogenetic factor is a factor of any nature (physical, chemical, biological), which acts in a series of

generations of a biological system and causes a persistent inheritance of its properties that have arisen due to interaction with this factor.

THE COMBINED EFFECT OF IONIZING RADIATION WITH OTHER FACTORS OF PHYSICAL, CHEMICAL AND BIOLOGICAL NATURE

The second major area of research, the attention to which increased in the post-accident period, was the study of the combined effect of IR with other environmental factors. The absence in the pre-accident period of a sufficient number of experimental and theoretical studies of the joint action of IR with factors of physical, chemical or biological nature led to the spread of the opinion that all possible types of interaction of environmental factors with IR are exclusively synergistic, i.e., reinforcing mutually negative influence of each other. At the same time, it is forgotten that, in general, factors can interact both additively and antagonistically, when they mutually reduce their negative effect, and synergism itself can be observed as a process of mutual strengthening of positively (hormesis) acting factors. In addition, attempts to study the combined effects are carried out without preliminary obtaining dose dependencies for individual factors, which would lead to the conclusion about the ambiguity of the influence (by sign) of factors on the object (process or structure) under study.

RADIOMODIFICATION PROBLEM

Ultimately, the problem of “synergism” is a particular case of the more general problem of modification of radiobiological reactions by a variety of factors acting before, during or after irradiation. From this point of view, the problems of protection against chronic exposure, radioadaptation, inducibility of repair systems, dose reconstruction, biodosimetry, etc. are aspects of either the problem of quasi-phonic (“low”) doses or the problem of synergism (modification). We would like to dwell especially on the last two problems, i.e. on the problem of dose reconstruction (the problem of retrodosimetry) and on the problem of biodosimetry. It seems to us that significant results in these areas can be achieved by using the methodology of modifying effects research. On the one hand, when it comes to retrodosimetry, by applying additional (“manifesting”) effects on the irradiated object, "hidden" radiation damage is revealed, or, more precisely, is transferred to a higher level. On the other hand, for the purposes of biodosimetry it would be advisable to use pre-sensitized objects, counting on the nonlinearity of interaction between sensitizing and radiation factors that will make the biodosimetric system more sensitive.

It is still important to consider one type of post- radiation positive modification of the effect of radiation factor in inhibitory doses. Positive post- radiation effects of incubation conditions (reduced temperature, “starvation environment”, etc.) are well known in radiobiology. In this case, the post-radiation factors create conditions for more efficient/effective work of intra- and supracellular repair systems. The peculiarity of our proposed approach is the idea of using IR by itself as a positively acting post-radiation factor. In other words, we tried to test the possibility to exert a “radiotherapeutic” effect (“treat”) on acutely irradiated objects by additional irradiation in the post- radiation period, i.e., to apply hormesis doses as "prophylactic" doses. In stress-biology, this possibility (in fact, radiation “homeopathy”) is not sufficiently studied. We have experimentally studied this type of modification, having called it "reverse adaptation", when as a therapeutic (“reversely adaptable”) influence, different impacts, including chronic IR, have been used for the therapeutic (“homeopathic”) effect on the plant object. The therapeutic (“homeopathic”) effect of post- radiation irradiation was observed in experiments with bean, evening primrose and pea seedlings. Probably post-radiation "radiotherapeutic" procedures modified the work of the recovery systems of irradiated plants, creating additional opportunities for more complete recovery at the intracellular (molecular) or cell-population levels. The results obtained are suggested to be considered as an experimental basis for the method of "low-dose radiotherapy" which may possibly find its application in the treatment of ARS.

INTEGRAL REACTIONS OF BIOLOGICAL SYSTEMS TO IRRADIATION

One of the radiobiological directions, the problems of which have acquired special urgency, is the study of integral (remote, mediated, indirect) reactions of biological systems to irradiation. Complexity, multilevel nature of biological systems, rapidity of functioning of their constituent elements and structures should inevitably be reflected in their radiobiological reactions. Most often the integrality of radiobiological reactions is manifested in the so-called remote (mediated, indirect) effects of irradiation. Let us illustrate the significance of integral reactions in the example of gigantism of needles observed after the Chernobyl accident at some sites in the Chernobyl Exclusion Zone.

The gigantism of needles and leaves observed in plants growing in some areas of the 30-km zone of Chernobyl NPP could be explained by considering it as a consequence of the direct effect of irradiation on needles [8]. However, strict adherence to the principles of system analysis, in particular, taking into account the necessity to describe the mechanism of the phenomenon at a specific structural-functional level, involving for this purpose information about the behavior or reactions of the elements directly forming this level, makes us look for another explanation of the gigantism of needles. From our point of view, irradiation at comparatively low (subthreshold) doses for differentiated cells (forming the bulk of photosynthetic tissue), but lethal for meristematic cells, led to massive but incomplete death of apical stem growth points. This led to the fact that a small number of surviving apices turned out to be acceptors of assimilation products, synthesized by the photosynthetic apparatus, which has a significantly higher level of radio resistance [9]. Thus, the limited number of stem apices (obesity meristems) and the needles laid in their structures were provided with an increased amount of nutrients, i.e., in fact, the effect of "fatness" of leaves and shoots well known in plant physiology, was observed. In other words, gigantism of needles was probably a consequence of the disturbance of correlative relationships in the irradiated plant. The validity of this explanation is confirmed by the data of N.I. Goltsova [10]. It turned out that complete or partial death of terminal and lateral buds led to an increase in the life span of the old, pre-accident needles of 1984–1985. Apparently, with the partial death of apical buds, apical dominance regulated by auxins and cytokinins decreased or completely disappeared, so that cytokinins transported upward from the root under the conditions of apical bud death stimulated the growth of the remaining adventive and dormant buds and had a juvenilizing effect on the already formed needles.

The removal of anthropogenic impacts (plowing, use of pesticides, mineral fertilizers, cattle grazing, etc.) leads to the recovery and even, in some cases, to the super-recovery of quantitative and qualitative parameters of populations, communities and cenoses. An illustration of this can be the fact of the super-recovery of wild boar numbers in the forests of Belarus, which were subjected to radio-nuclide contamination. In general, the 30-km zone of the Chernobyl NPP can serve as a huge reserve- polygon (paradoxical as it may sound) for studying succession processes.

Radiophobia and the *relief of anthropogenic pressure* (chronic and/or acute anthropogenic stress) on natural and artificial ecosystems are prime examples of radiation mediated effects. Even ardent supporters of the absolute threshold of radiation action do not take into account the possibility of radiation action mediated through the human psyche. In this case, people are affected not by IR itself, but by the fear of it, caused, on the one hand, by the lack of sufficient objective information about the degree of IR danger, and, on the other hand, by the availability of information about the real negative effect of IR in case of acute exposure, as it was in the case with the firefighters who put out the fire at the Chernobyl NPP.

DETERMINISTIC EFFECTS

We would not like to dwell in detail on deterministic effects in connection with the Chernobyl accident, as there is an extensive literature on this subject. We will only mention a few points. Firstly, the total number of the injured among the personnel working at the Chernobyl NPP on April 26, 1986, was 203 people, 115 persons among them were treated in a specialized hospital in Moscow from the second day and 19 persons in Kyiv. The subsequent change in the group size to 237 persons concerned only patients with acute radiation sickness (ARS) of the first degree (the mildest), who were treated in Kyiv. Isn't this where the myth about more effective treatment of ARS in Kyiv arose? Out of 499

hospitalized people, the diagnosis of ARS was confirmed in 134 people. According to official data, the number of people who died in different periods after irradiation from acute radiation sickness, aggravated by extensive thermal burns, amounted to 28 people. And, secondly, not a single case of chronic radiation sickness (CRS) has been registered for all the years after the Chernobyl accident. Let us now turn to the statistical data characterizing the natural mortality rate and compare them with the data on mortality among the liquidators [11]. There was no increased mortality among liquidators (for example, Robert Peter Gale, an American specialist in bone marrow transplantation, having arrived in Kyiv in June 1986, estimated the number of future fatalities at 80000) of 1990. On the contrary, mortality was naturally lower in all three republics compared to the controls, which included working-age men. Of course, there is still no reason to believe that there is a radiohormesis effect. Probably the most correct assumption at this stage would be that the effect is due to the selection of healthier men for the number of liquidators.

STOCHASTIC EFFECTS

What stochastic effects can cause “Chernobyl” (“small”) radiation doses in humans? Our interest in this problem arose due to a paradoxical situation – an extreme discrepancy between the importance of radiation safety and regulation on the one hand, and the number of relevant studies conducted in the countries of the former Soviet Union. Radiobiology, first of all, “serves” human interests, and it is very strange that the ICRP recommendations will play the role of a "sacred cow" of standardization. In fact, we can speak about one more “basic” radiobiological paradox. The problem of assessing the risk of stochastic consequences (first of all, carcinogenic) of IR has two aspects. First, it is a pre-dosimetric subproblem (adequate assessment of the IR dose, its distribution over critical tissues and organs, etc.), and, second, it is a subproblem of assessing the type and kind of relationship between absorbed doses and the probability of stochastic effects. As far as a cursory analysis of the Russian literature allows, the efforts of radiobiologists of the post-Soviet space are mainly focused on the first aspect.

We made an attempt to estimate (“reassess”) the carcinogenic radiogenic risk on the basis of data on spontaneous instability (thermodynamic, chemical) of DNA. However, let us first see how the carcinogenic risk coefficients recommended for use by the ICRP “work” in relation to the assessment of the Chernobyl accident consequences. Taking into account the value of the collective dose received by the inhabitants of the “affected” regions of Ukraine, Belarus and Russia (approximately 200,000 people according to the estimates of L. A. Ilyin and colleagues [12], and the ICRP proposed carcinogenic risk coefficient, the number of fatal cancers should be estimated at approximately 10000 (note, by the way, that the Chernobyl Forum estimates this value at 4000), which will be less than one percent of the spontaneous level of diseases of this type. The detection of such a relatively small "addition" to the spontaneous level is practically impossible, given the high level of annual fluctuations in the spontaneous level of carcinogenesis.

According to current estimates [13], the rate constant of DNA degradation due to spontaneous single-strand breaks is practically the same in different biological entities belonging to different radio-taxa and varies in the range $(1–9) \times 10^{-11} \times c^{-1}$, which is six orders of magnitude higher than the corresponding DNA degradation constant under the influence of radiation from an average RB ($2 \times 10^{-17} \times c^{-1}$. Based on this, we assumed that the incidence of spontaneous cancers (approximately 3000 cases per 1 million people per year) directly depends on the level of spontaneous DNA degradation and that the incidence of RB-induced cancers is in the same direct correlation with the level of DNA degradation induced by RB radiation. The proportion of RB-induced cancers should be 1×10^{-6} fraction of the spontaneous cancer rate, i.e., approximately 0.003 additional cases per year per 1 million people. Over the course of a year, 1 million people receive a collective effective dose from RB exposure of about 0.24×10^{6} cSv, which we hypothesize is likely to induce these 0.003 additional cases of cancer. Accordingly, there would be 0.012 additional cancer cases per 1 million people per year. Even over a 100-year lifetime, this risk will be equal to 1.2. Thus, the carcinogenic risk coefficient caused by IR may be at least two orders of magnitude lower than the generally accepted values of this parameter. It should also be taken into account that our estimates are obtained using the assumptions of threshold-free and linear dose-effect dependence and may be even overestimated for this reason.

It would probably be also appropriate to mention here the phenomenon of radiation hormesis, which, although still insufficiently studied to base irradiation regulation on it, is still significant evidence of the threshold effect of IR. At the same time, there are also sufficient grounds to consider a possible hormesis anticarcinogenic effect of irradiation, which, in particular, was observed in Japanese children affected by atomic bombings in 1945 – the number of spontaneous leukemia in children irradiated at a dose of 5-100 mSv decreased by 2/3 [14].

Based on the above-mentioned estimates of L. A. Ilyin and colleagues [9] and the carcinogenic risk factor calculated by us, it should be stated that the number of fatal cancers in the post-accident period should not exceed 20-30 cases, which is more than two orders of magnitude lower than the estimates of the Chernobyl Forum.

In general, a comparison of possible medical consequences (primarily deterministic effects) of the Chernobyl accident for the population with analogous consequences of other accidents shows that the Chernobyl accident ranks third in terms of the severity of medical consequences after the consequences of radioactive contamination of the Techa River and the Kyshtym accident [15]. The contamination of the Techa River was the largest radiation incident during the period when the nuclear industry functioned in the USSR. The Techa River region is the only area of the Soviet Union where the Techa River was contaminated. The Techa River region is the only place where the exposed population suffered medical consequences not only in the form of chronic radiation sickness and other radiation injuries, but also in excess infant mortality [16].

The Chernobyl accident was characterized by an exceptionally large area contaminated with radionuclides and an immeasurably larger population at increased radiation risk. However, after the Chernobyl accident, there was no increase in the number of cases of radiation sickness, no reliable increase in the incidence of leukemia and solid cancers, no increase in adverse pregnancy outcomes, no increase in mentally disabled children, and no congenital anomalies, and it has not yet been possible to identify a reduction in life expectancy. Moreover, a reduction in life expectancy by about 5 years occurred among the resettled residents of the Techa River region, but was not detected among those who remained living in their usual conditions [15].

Only insufficient surgical intervention to reduce radioiodine accumulation in the thyroid gland of children resulted in an “epidemic” of thyroid cancer. The same effects were observed in the timely unsettled Marshall Islanders exposed to radioiodine contamination in 1954. Dose levels from ^{131}I in the thyroid gland both after the contamination of the Marshall Islands and after the Chernobyl accident were significantly higher than 300 mSv, which caused an increased incidence of radiogenic thyroid cancers.

PROBLEMS OF MODERN RADIOECOLOGY AFTER THE ACCIDENT AT CHERNOBYL NUCLEAR POWER PLANT

The 39th anniversary of the Chernobyl accident is an important stimulus for analyzing the current state of radioecology. This accident sharply outlined and set before radioecology a whole range of theoretical and applied problems that required and to a large extent still require their solution. The main peculiarity of the accident is its scale and the degree of its impact on the environment, population and personnel employed in the 30 kilometers Exclusion Zone and beyond it. Of course, the main problem that has not been fully solved in Ukraine is the estimation and reconstruction of radiation doses to the population in the zone of influence of the Chernobyl accident in the most dangerous year of the acute period of the accident – 1986. According to a number of estimates, the radiation dose to people in 1986 may be from 60 to 99% of the total lifetime dose. It should also be noted that the radiation dose could be significant for the whole biota in the accident zone, which is also an important problem of modern radioecology.

As a result of the Chernobyl accident, the biotic component of ecosystems was and still is subjected to a significant dose impact from a few cGy to tens of cGy. This led, in particular, to the phenomenon of the "Red Forest" due to the death of the most radiosensitive coniferous species. Notable succession processes have occurred and are still occurring in the Exclusion Zone and surrounding areas. For instance, the number of some wild mammals increased tenfold after the accident; even red-listed species (black stork) appeared. Despite the fact that many of these phenomena are due to a significant decrease

of anthropogenic pressure (for example, reducing the level of "doses" of the anxiety factor of wild animals), one should still expect radioecological consequences, since the period after the accident is insufficient for the manifestation of long-term environmental consequences (in particular, population genetic ones). In addition, due to continuous processes of radionuclide redistribution along trophic chains and ecosystem components (biota, bottom sediments, forest litter, etc.), further changes in absorbed doses in biotic components of ecosystems should be expected, and hence new consequences of them.

More than 200 different countermeasures were implemented during the Chernobyl accident consequences elimination, which formed a multitude of actions different in their effectiveness and consequences. These efforts deserve to be fully analyzed in order to assess their effectiveness and to build a universal system of countermeasures suitable for use in dealing with other types of environmental accidents (chemical, biological).

At one of the seminars of the Ukrainian Section of the International Union of Radioecologists (IUR), 30 expert participants compiled a list of almost 100 unresolved problems of modern radioecology and ranked them in terms of importance and relevance (see table). The experts rated the degree of importance and/or unresolved problems in scores from 1 to 10.

PSYCHOSOCIAL ASPECTS OF THE ACCIDENT AT CHERNOBYL NUCLEAR POWER PLANT

We are convinced that the main consequences of the Chernobyl accident for human beings are social and psychological. For example, in post- accident Europe, as a result of pregnancy termination and/or refusal to plan childbirth, more than 300,000 additional children were not born. This situation is largely due to the prevalence of radiophobia – excessive fear of possible or imaginary effects of IR. The cause of the so-called psychosomatic diseases that in their turn should be considered as mediated (in this case by the human psyche), is the nature of information perception regarding the action of IR. In this case, the human organism is affected not by the IR itself, but by excessive mental tension, which is predetermined, on the one hand, by the absence of sufficient objective information regarding the degree of threat from the IR and, on the other hand, by the presence of real information regarding the negative effects of the IR in case of acute exposure, for example, information about the death of firefighters (extinguishing big fire at the fourth block of Chernobyl NPP) from ARS. Radiophobia is considered to be a type of neurosis, namely information neurosis, predetermined by informational uncertainty (lack of information or its inadequacy), which manifests itself variously in the appearance of excessive mental stress feelings (frustrations). Even ardent supporters of the absolute threshold of the IR action do not always take into account the possibility of its mediated somatic (deterministic) influence through the human psyche. It is known that more than a half of human somatic diseases are of psychosomatic nature [17], and it is likely that some of such diseases will increase in the process of human social evolution. Of course, a person who is ill on "radiophobic grounds" is also entitled to the status of Chernobyl victim.

Table.1 Unresolved radioecological problems

Problem (task) formulation	Sum of points
Monitoring of radioecological, phyto- and zoosanitary condition of biocenoses of 30-km Chernobyl NPP Exclusion Zone	121
Development of technologies for long-term **disposal of** radioactive waste	118
Environmental **standardization of** radiation exposures	107
Environmental radiation **risks** (genetic and somatic)	106
Criteria for **criticality of landscapes** and individual components (subsystems) of ecosystems	106
Financing of radioecological research. Determination of optimal proportions of financing of fundamental and applied research	104
Ecological capacity and radio-capacity **of** ecosystems	104

Methods of **equidosimetry and dosimetry of** radiation due to elevated levels of radionuclide contamination	103
Identification of critical pathways **for radionuclide migration** beyond the Exclusion Zone boundaries	103
Development of criteria (selection of parameters) for **ecosystem sustainability**	102
Peculiarities of **"Chernobyl" radioecology** and its importance for general radioecology	102
Harmonization of risks from exposure to radiation and other factors	101
Monitoring of **uranium tailings**	101
Cooperation of radioecologists at local and global levels	100
“Destiny” of the Chernobyl Exclusion **Zone**	99
Methodological and methodological **significance of radioecology (RE)** for general ecology (radionuclides as tracers for the study of fundamental properties of ecosystems)	98
Adaptation of biota to radiation loads against the background of other factors unfavorable for ecosystems	98
Scientific support of works on further **stabilization of the ecosystems of** the Exclusion Zone.	98
Experiment (control) in radioecology	97
Self-cleaning of ecosystems from radionuclide contamination	97
Contribution of radioecology to solving the problem of "**low dose**" exposure to ionizing radiation	97
Scientific support of works on **radioactive waste** management	97
Development and application of **benefit-harm** analysis in shelter-2 construction, countermeasures and decision making	96
Selection and organization of **industrial sites** for NPP construction (organization of radionuclide- release systems)	96
Popularization of radioecological knowledge	95
Development of environmentally safe NPP **decommissioning** technology	95
Radionuclide **contamination of underground water horizons**	95
Application of **generalized parameters of** ecosystem state under conditions of chemical and radionuclide contamination	94
Teaching RE. Preparing ready-made research groups	94
Health and social RE	94
Retrodosimetry (retrofactory dosimetry)	93
"Critical **("marker")** human foodstuffs in the practice of assessment of human background radiation (BR) doses. Objective assessment of the structure and dynamics of human nutrition under conditions of radioactive contamination	93
Application of analytical geographic information technologies **(GIT)** in radioecology	92
Migration characteristics of radionuclides in ecosystems	92
Comparison of **radioecological risks** with other radiation and non-radiation risks and threats. Approaches to risk management based on assessment of their relative importance	92
Study of physicochemical mechanisms of radionuclide **migration**	91
Development of a register of **countermeasures** with recommendations for their **adaptation** to specific levels and conditions of radionuclide contamination	91
Assessment of applicability of average and maximum estimates of **radioecological risks** in conditions of uncertainty (fluctuations) of factors forming them. Standardization of approaches (algorithms) for establishing maximum estimates of radioecological risks	91
Relative Environmental Effectiveness of Ionizing Radiation (REEIR)	90

Adapting the experience of Russia and Belarus in solving agricultural RE problems (experience in applying countermeasures)	90
Relation of resistance to **chronic and acute exposure.** Predictive value of parameter estimates of **deterministic effects** for similar estimates of **stochastic effects**	90
Design (engineering) of ecosystems with specified radioecological parameters in the zone of NPP influence	89
The problem of anomalous values of **the transfer coefficient** (K_t) and accumulation coefficient (K_a) of radionuclides in the "soil-plant" system	89
Statistical aspects and specificity of RE research. The problem of extra- and interpolation in RE epidemiology	89
"Radioecological thermometer"	88
Development of a unified **radioecological terminology**	88
Creation of a unified **information base**	87
Pairing of samplers during experimental work in a real environment	87
Enhancing **ecosystem barrier functions** and optimizing the performance of water protection structures	87
Role of **isotopic and non-isotopic carriers** in radionuclide migration along trophic chains	85
Mathematical models of radionuclide behavior in the environment	84
Management of radionuclide **self-cleaning** of ecosystems	84
Development of criteria for assessing existing and prospective directions of organizing **nature reserve activities** in the Zone	84
Publishing activities, conferences, conventions, etc.	83
Methods and models for estimating **the airborne transport of** radionuclides in radiation accidents	83
Radioecological assessment of western, bog and other overwatered landscapes. Role of **landscape depressions** in radionuclide migration	83
"**Prevention" and "therapy" of ecosystems** under conditions of increased levels of radiation loads	82
Radiation and evolution. Role of radionuclide anomalies for ontogenesis and phylogeny	82
Role of **transboundary** radionuclide **transport** in ecosystems	81
Assessment of **ontogenetic radiation risks** from natural background radiation (BR)	80
Radioecology of **ultra-long-lived radionuclides** (^{36} Cl,^{99} Tc,^{129} I, Transuranic elements)	80
Landscape passportization (including retrospective) of monitoring grids, sampling points, experimental sites, plots, stations, etc.	80
The applicability of average and maximum estimates of **radioecological risks** under conditions of uncertain division (fluctuation) of forming factors. The standardization of approaches (algorithms) for setting maximum estimates of radioecological risks.	80
Successional processes in biota of ecosystems under radionuclide contamination	79
Precise **optimal agriculture** ("Precise agriculture") on radioactively contaminated soils	79
Ratio of **direct to indirect (e.g., social-psychological) RE effects** nuclear disasters	79
Relation of RE to general radiobiology, to related sciences	77
Influence of ionizing radiation in 30-km zone of Chernobyl NPP on **pathogenicity of viruses and microorganisms** for plants, animals and humans	77
Nanotechnology in RE (e.g. selective sorption of r.n.)	77
Role of **the active response function of biota** under conditions of increased radiation exposure	76

Passportization (including retrospective) of hydrothermal conditions of experimental works in real environment	76
Influence of radiation in 30-km zone of Chernobyl NPP on pathogenicity of viruses and microorganisms for plants, animals and humans. **Microbial communities** in conditions of increased RF	75
Comparability of **autoradiological and synradioecological** data	74
Optimal **organization of work** according to the RE	74
Development of systems for biodecontamination of ecosystems from radionuclide contamination	74
Radioecological **hormesis** (radioecostimulation)	74
Coordinate georeferencing (including retrospective) **of monitoring** grids**,** sampling points, experimental sites, plots, stations, etc.	73
Study of dependence of **radionuclide transfer to plants** on soil solution parameters	73
Use of the **non-interference principle** to assess total damage and pure benefit in radioecological situations	72
Study of dependence of **soil solution parameters** on physicochemical and biological parameters of soil	72
Objectivity and universality of **dose "prices"** (coefficients)	70
Assessment of **radioecological situation parameters** during different time phases of the accident (formation of post-accident radioecological situation)	67
Use of the **non-interference principle** to assess total damage and pure benefit in radioecological situations	60
Defining the **subject of radioecology** as a scientific discipline, integrating and distinguishing it from frontier disciplines, identifying the fundamental core of the discipline and it's applied aspects.	52

Let us see what psychic and psychosocial factors could influence the qualitative and quantitative dynamics of diseases of liquidators and evacuated population, as well as the rest of the population exposed to the powerful informational influence of mass media. In the post-accident period, there was one of the neurosis varieties – *hypoinformation neurosis*, caused by information uncertainty (lack and rotation of information), which manifested itself in the emergence of mental tension (frustration). The cause of such a neurosis can also be conscious informational deprivation, as was the case, for example, with Samuil Petrovich Yarmonenko, a well-known but, unfortunately, now dead radio biologist. The author personally encountered the fact that his article in one of the library issues of a radiobiological journal, in which Samuil Petrovich gave a not very favorable assessment of Ukrainian radiobiologists, was torn out. Only 38% of newspaper articles about the post- Chernobyl situation belonged to specialists (it is not known what the percentage of really professional specialists was among them). Critical ("intimidating") character was in 76% of publications.

The reactions of eyewitnesses to the accident or liquidators of its consequences were typical for people in any other extreme situation: apathy in some, euphoria in others, fear and anxiety in others. In non-professionals, group or individual infantilism, pseudo-heroism, mastery and aggressiveness were noted.

A characteristic manifestation of chronic stress is a high level of anxiety (more than 70% of those surveyed), low self-esteem of their mental and somatic health (more than 83% of people considered themselves unhealthy). There was also an exacerbation of latent somatic diseases, somatoneuroses, worsening of the course of so called stress diseases (hypertension, peptic ulcer disease, ischemic heart disease, diabetes mellitus, neurodermatitis ("stigmata"), decreased immune status of the organism, etc.). The following behavioral deviations were recorded in liquidators: dominance of psychasthenic and anxiety-phobic reactions, predominance of passive-defensive reactions to the post-ex-treme situation. Anxiety among women in the area of strict radiation control was higher than among men (90.6 and 86.3% respectively). Among women, only 5.9% felt unhealthy (which is not identical to the proportion of actually ill) compared to 21.7% of men. In liquidators (dose level from 0.2 to 1.0 Gy), no dose-

dependent changes in the state of the nervous system were found, i.e. no direct effect of IR was detected.

It is interesting (useful and extremely important) to note that more people with higher education or specialized secondary education (teachers, doctors, nurses), who probably had more opportunity to adequately assess the situation, felt healthy.

It has long been known that the higher the anxiety, the lower the level of positive self- assessment of health. Thus, among those who considered the situation dangerous for their health, 8.6% felt healthy, and among those who did not feel anxious – 45.4%. In the control area the level of self-assessment of health (32.9%) is 2.5 times higher than the analogous indicator for the residents of the strict radiation control. In the conditions of chronic psychological traumatic effects of the anxiety factor, one of the mechanisms of psychological defense – the defense of affect denial – was activated, which was typical for adolescents in 1987. For example, the life expectancy of adolescent schoolchildren from the Narodichesky District of Kyiv Oblast was more "shortened" (56.2 years) (about 60 years – average life expectancy of Ukrainian men) compared to the same life expectancy of their peers from Kyiv and Poltava Oblast, whose life expectancy averaged 76.4 years. Among adolescents living in areas of strict radiation control, 77.7% had health complaints. The data of in-depth examination of these adolescents revealed deviations in somato-neurological health only in 16% of those examined. The state of chronic mental stress actualizes previously existing problems of the personality, which become pathogenic for it. The population of the "affected" areas continues to experience socio-psychological discomfort, while the doses of general radiation exposure for the overwhelming majority do not exceed 0.5 cGy. This stress is exacerbated by the hard pressing of the media and the real difficulties of life.

REFERENCES

[1] Lucky, T. D. (1991). Radiation Hormesis. Boca Raton Publisher, CRC Press, 239 p.
[2] Buldakov, L. A. (2002). Medical consequences of radiation accidents for the population. Medical Radiology and Radiation Safety, (2), 7–18.
[3] Vilenchik, M. M. (1987). DNA instability and long-term consequences of radiation exposure. Energoatomizdat, 192 p.
[4] Geraskin, S. A. (1998). Regularities in the formation of cytogenetic effects of low doses of ionizing radiation: Abstract of dissertation for the degree of Doctor of Biological Sciences. Obninsk, 50 p.
[5] Geraskin, S. A. (1995). Concept of the biological action of ionizing radiation on cells. Radiation Biology. Radioecology, 35(5), 571–580.
[6] Goltsova, N. I. (1990). Influence of radioactive contamination on the structural features of Scots pine (*Pinus sylvestris L.*) (Chernobyl). Chernobyl-90: Proceedings of the 1st International Conference “Biological and Radioecological Aspects of the Consequences of the Chernobyl Accident”, 1, 74–89.
[7] Grodzinsky, D. M., Bullakh, A. A., & Kolomiets, O. D. (1991). Anthropogenic radionuclide anomaly and plants. Lybid, 160 p.
[8] Ilyin, L. A. (1996). Realities and Myths of Chernobyl. ALARA Limited, 474 p.
[9] Ilyin, L. A., Kirillov, V. F., & Korenkov, I. P. (1999). Radiation hygiene. Medicine, 384 p.
[10] Keirim-Markus, I. B. (2002). Unconstructive radiation hormesis. Medical Radiology and Radiation Safety, (2), 73–76.
[11] Mikheev, A. N. (2015). Hyperadaptation: Stimulated ontogenetic adaptation of plants. Phytosociocenter, 423 p.
[12] Petin, V. G., & Pronkevich, M. D. (2012). Radiation hormesis under the action of low doses of ionizing radiation. IATE NRNU MEPhI, 73 p.
[13] Savin, V. N. (1981). The effect of ionizing radiation on an integral plant organism. Energoatomizdat, 120 p.
[14] Saurov, M. M. (2002). Estimation of the probability of lethal effects under the action of ionizing radiation on the population. Medical Radiology and Radiation Safety, (5), 5–16.
[15] Spitkovsky, D. M. (1992). Concept of the action of low doses of ionizing radiation on cells and its possible applications to the interpretation of medical and biological consequences. Radiobiology, 32(3), 382–400.
[16] Topolyansky, V. D., & Strukovskaya, M. V. (1986). Psychosomatic disorders. Medicine, 384 p.
[17] Calabrese, E. J., & Baldwin, L. A. (2000). Radiation hormesis: Origins, history, scientific foundation. Human & Experimental Toxicology, 19(1), 41–75.

Requirements for Authors

- The article should be submitted to the A4 format in the text editor Microsoft Office Word;
- Areas: upper - 20 mm; Left - 30 mm; Right -20 mm; Bottom - 20 mm
- Font: Times New Roman. Interval -1,0
- In the article formulas must be typed in the formula's editor Equation
- Drawings and illustrative materials should be inserted in the JPEG or TIFF format
- Write the article title (14 Pt, Bold) on the first line
- Bypassing the line - the surname and first name of the author(s) (11 Pt, Bold)
- One of the authors will need to be identified as the corresponding author (*), with their full name and email address displayed.
- Full name of the organization on the next line, with indicating the country or residence (11 Pt, Bold, in case of participation of different organizations in the article should be used "[1]")
- Skipping of two lines - abstract (11 Pt, Italics, not more than 500 words)
- Maximum 5 Key words (11Pt)
- Contents of the article (11Pt) by skipping the line
- Bypassing two lines – references (10 Pt). Used literature should be numbered according the sequence it is used in the main text (when citing inside the text, the number of the source should be written in square brackets). Use the following example while creating the reference list:

  [1] Author(s') surname(s) and initial(s). (Year of publication). Article name. *Journal in which the article is published*, *issue*, pages.

  [1] Derwing, T. M., Rossiter, M. J., & Munro, M. J. (2002). Teaching native speakers to listen to foreign-accented speech. *Journal of Multilingual and Multicultural Development*, *23*(4), 245-259.

- Electronic version of the article must be sent to the e-mail: radiobiologia2020@gmail.com
- The file must be named by the last name of the author

The editorial board is responsible for the topics of the materials submitted for publication in the journal, and the authors' responsibility relies on the content of the article, the results and conclusions. The publisher is not responsible for possible damages, which could be a result of content derived from this publication and any liabilities arising from them remain the responsibility of the authors. Articles incompatible with the above-mentioned requirements or incompatible with the theme of the article are not considered for publication. Materials are published by the author's editorship.

Editorial office: 14 Levan Gotua St, Rooms-913; 931, Tbilisi, Georgia, 0160

Tel: (+995) 032 237-03-00/911, **Mob**. (+99532)555-10-17-90
E-mail: radiobiologia2020@gmail.com

Website:https://radiobiology.ge